Downloaded from orbit.dtu.dk on: Dec 20, 2017

Technical University of Denmark

High quality ion channels recordings on an injection molded polymer chip

Tanzi, Simone; Kutchinsky, Jonatan; Taboryski, Rafael J.

Publication date:
2013

Document Version
Publisher's PDF, also known as Version of record

Link back to DTU Orbit

Citation (APA):
Tanzi, S., Kutchinsky, J., & Taboryski, R. J. (2013). High quality ion channels recordings on an injection molded polymer chip. Kgs. Lyngby: Technical University of Denmark (DTU).

DTU Library
Technical Information Center of Denmark

General rights
Copyright and moral rights for the publications made accessible in the public portal are retained by the authors and/or other copyright owners and it is a condition of accessing publications that users recognise and abide by the legal requirements associated with these rights.

- Users may download and print one copy of any publication from the public portal for the purpose of private study or research.
- You may not further distribute the material or use it for any profit-making activity or commercial gain
- You may freely distribute the URL identifying the publication in the public portal

If you believe that this document breaches copyright please contact us providing details, and we will remove access to the work immediately and investigate your claim.

DTU

High quality ion channels recordings on an injection molded polymer chip

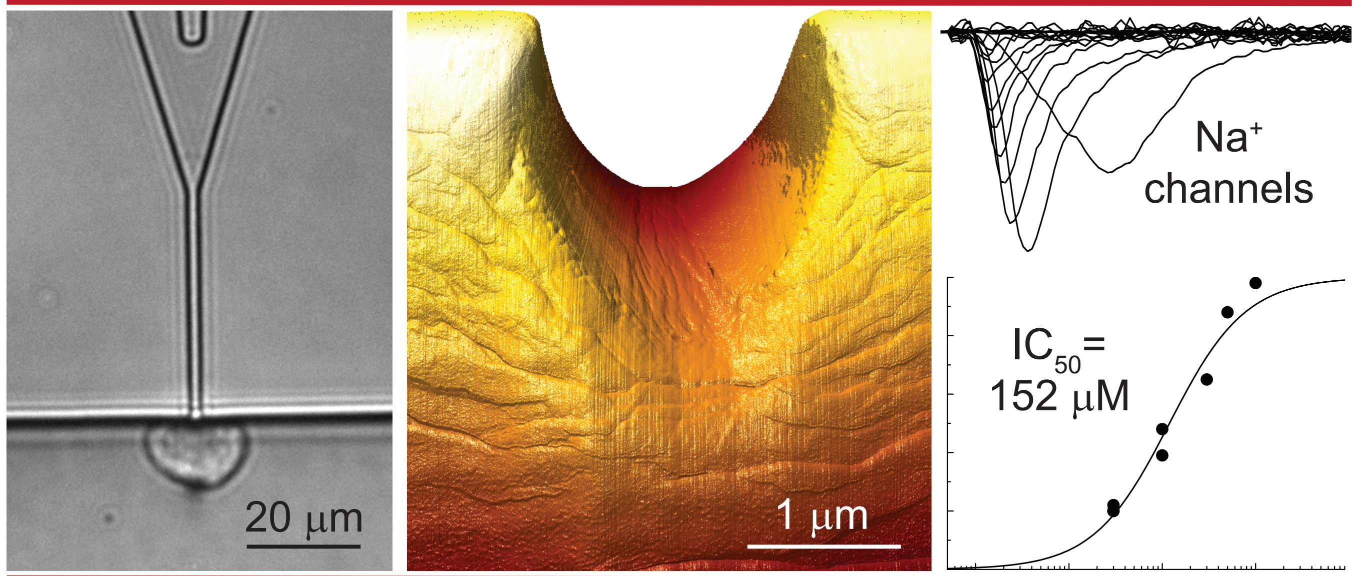

Simone Tanzi

Ph.D. Thesis

DTU Nanotech

Department of Micro- and Nanotechnology

High quality ion channels recordings on an injection molded polymer chip

Simone Tanzi
DTU Nanotech, Dept. of Micro- and Nanotechnology
Technical University of Denmark

A thesis submitted for the degree of
Philosophiæ Doctor (Ph.D.)
June, 2013

Supervisors: Rafael J. Taboryski and Jonatan Kutchinsky

A Sergio e Stella...

Abstract

In this thesis we demonstrate high quality recordings of the ion channel activity across the cell membrane in a biological cell by employing the so called patch clamping technique on an injection molded polymer microfluidic device. Such recordings are traditionally made using glass micropipettes, or in recent years using consumable microfluidic chips of high costs. The patch clamping method is widely used both in fundamental studies of electrophysiology of living cells and tissue and in drug discovery.

The findings of this work will allow direct recordings of ion channel activity to be made using the cheapest materials and production platform to date, and with the potential for very high throughput. The employment of cornered apertures for cell capture allowed the fabrication of devices without through holes via a process comprising master origination by dry etching in a silicon substrate, electroplating in nickel, and injection molding of the final part. A thorough characterization of the patching orifices by means of SEM and AFM showed high replication accuracy through the fabrication process.

The most critical device parameters were identified as the length of the patching capillaries and the very low surface roughness inside of the capillaries. The cross-sectional shape of the cornered apertures was found to be less critical, as apertures with different profiles were tested with cells and showed the same ability to form tight seals with cells with negligible leak currents. The ability to form high resistance seals in the GOhm range, the so called gigaseals, is demonstrated with a success rate of 15 %. The devices were functionally tested with Human Embryonic Kidney (HEK) cells expressing voltage-gated sodium channels and benchmarked against a commercial state-of-the-art system for automated ion channel recordings. These experiments considered current-voltage relationships for activation and inactivation of the sodium channels and their sensitivity to a local anesthetic, lidocaine. Both IVs and lidocaine dose response curves obtained from the injection molded polymer device were in excellent agreement with data obtained from the commercial system.

Dansk resumé

I denne afhandling demonstreres højkvalitets målinger af ionkanalaktiviteten igennem cellemembranen i en biologisk celle ved anvendelse af den såkaldte "patch clamp"teknik på en sprøjtestøbt polymer mikrofluid chip. Sådanne målinger udføres traditionelt ved hjælp mikropipetter af glas, eller i de seneste år ved hjælp meget dyre microfluide chips til engangsbrug. Patch clamping metoden anvendes til både grundlæggende elektrofysiologiske studier på levende celler og i cellevæv og til "drug discovery".

Resultaterne af dette arbejde vil gøre det muligt at direkte målinger af ionkanalaktivitet kan foretages på den billigste materiale- og produktionsplatform til dato, og med potentiale for meget højt throughput. Valget af et chip-design med brug af sidekanaler til indfangning af cellerne tillod at chips kunne fremstilles uden gennemgående huller og ved hjælp af en proces bestående af master-fremstilling ved brug af tør-æts i et silicium substrat, elektroplattering af en nikkel støbeform fra siliciummasteren, og endeligt sprøjtestøbning af plastikchips ved brug af nikkelformen. En grundig karakterisering af de kritiske mikrokanallysninger blev udført ved hjælp af SEM og AFM og viste høj replikationsnøjagtighed i hele produktionsprocessen.

De mest kritiske chipparametre blev identificeret som længden af de kapillære sidekanaler til patching af cellerne og den meget lave overfladeruhed på indersiden af disse kaneler. Profilen af sidekanalerne fandtes at være mindre kritisk, da lysninger med forskellige profiler testet med celler viste den samme evne til at danne tætte forseglinger mod cellerne med ubetydelige lækstrømme. Evnen til at danne forsejlinger med høj elektrisk lækmodstand i omegnen af GOhm, de såkaldte "gigaseals", påvistes med en succesrate på 15 %. Chips blev testet funktionelt med humane embryonale nyreceller (HEK), som udtrykte spændingsafhængige natriumkanaler og blev sammenlignet med et kommercielt state-of-the-art system til automatiserede ionkanalmålinger. Disse eksperimenter vedrørte strøm-spænding karakteristikken for aktivering og inaktivering af natrium kanaler og deres følsomhed over for et stof til lokalbedøvelse, lidocain. Både IV karakteristikkerne og lidocain dosisresponskurverne optaget med de sprøjtestøbte plastikchips var i fremragende overensstemmelse med resultaterne opnået på det kommercielle system.

Preface

The Ph.D. thesis presented here is the result of a 3 year PhD project carried out at the Department of Micro- and Nanotechnology, Technical University of Denmark at the research group of Rafael Taboryski from 2010 to 2013. A four month external stay at AgResearch in New Zealand took place during the winter of 2011.

The project was supported by the Danish Advanced Technology Foundation through the Advanced Technology Project PILOC (grant no 061-2010-1) and from the Danish Council for Strategic Research through the Strategic Research Center PolyNano (grant no 10-092322/DSF). This research center is aimed at the development of high-volume low-cost lab-on-a-chip technologies for different bioanalytical applications.

The Ph.D. project has been supervised by Rafael J. Taboryski, Group Leader of the Polymic group, as main supervisor and by Jonatan Kutchinsky, Vice President and head of the Development at Sophion Bioscience A/S, as co-supervisor.

The application targeted in this project is the recording of ion channel currents from biological cells. The main tool and golden standard in this field of research is the so called patch clamping technique. Traditionally, this method requires a highly skilled staff and has a very low throughput. Within the last decade, microfabricated devices for automated patch clamping have been presented and introduced in the market, but none of these are low-cost devices aimed at high-throughput experiments.

The goal of this work was to propose an alternative method for mass production of cheap chips for automated patch clamping without compromising functionality by employing cutting edge clean room based polymer replication techniques. In order to fulfill this goal, injection molding of thermoplastic polymers was chosen as fabrication technology.

In the introduction, a general background about ion channels, conventional patch clamping, and an overview of the up to date devices for automated patch clamping is given. In Chapter 2, the fabrication method developed in this project for the fabrication of all-polymer microfluidic devices is described. The method was presented in the peer-reviewed journal Micromechanics and Microengineering in September 2012. In Chapter 3, the electrophysiological results obtained from patch clamping measurements on the polymer micro devices are reported. This work was done in collaboration with Sophion Bioscience A/S. A manuscript about this work is ready to be submitted. In Chapter 4, as a short de-

tour, the results on the characterization of the inhibitor effect of two toxin peptides are presented. This work was achieved during the stay at AgResearch in New Zealand. In Chapter 5, we present a study on the manufacturing costs of the polymer device and a discussion on how the device may be implemented into a more standard format for a future commercialization. Finally, Chapter 6 concludes this thesis and gives a future perspective.

The technology presented in this thesis was protected by an international patent application that was filed in May 2013 by DTU with the author of this thesis and Rafael J. Taboryski as the inventors.

Kgs. Lyngby, June 14, 2013

Simone Tanzi

Acknowledgements

I sincerely thank my supervisors Rafael Taboryski and Jonatan Kutchinsky for inspiration, motivation, encouragement and support during the project work. I thank also Julie Dalziel for giving an enthusiastic insight into patch clamping and giving the possibility to spend some time in New Zealand. I would like to thank all my colleagues and friends at Nanotech. In particular, I thank Marco Matteucci for keeping me up with the motivation when things were not working. I would like to thank people at Sophion Bioscience for the fruitful collaboration, especially Søren Friis and Anders Lindqvist for inspiring discussions.

I also want to thank all my friends in Copenhagen, in Italy, in New Zealand, and all around the world where they are continuously moving. A special thank goes to Tony and Jacopo and to my lovely flatmates.

Finally and most importantly, I want to thank my parents for their continuous support and love, without them this thesis would not have been possible. A special hug to Mattia, Michale and Cinzia.

Abbreviation list

The abbreviations and acronyms used in this thesis are explained in the following. New abbreviations have only been introduced where they contribute to readability or clarity; otherwise terms commonly found in the literature have been used.

AFM	Atomic Force Microscope
AOE	Advance Oxide Etching
APC	Automated Patch Clamping
COC	Cyclic Olefin Copolymer
DEEMO	Dry Etching, Electroplating and MOlding
DKK	Danish krone
DMSO	Dimethyl Sulfoxide
DRIE	Deep Reactive Ion Etching
HEK	Human Embryonic Kidney
HF	Hydrofluoric acid
HMDS	Hexamethyldisilazane
KOH	Potassium hydroxide
LIGA	LIthographie, Galvanoformung and Abformung[1]
LOC	Lab-On-a-Chip
MEMS	MicroElectroMechanical Systems
PDMS	Polydimethylsiloxane
RIE	Reactive Ion Etching
S.E.M.	Standard Error Deviation
SEM	Scanning Electron Microscope
T_g	Glass transition temperature
TEOS	Tetraethyl Orthosilicate
UV	Ultra Violet

[1]German acronym for lithographie (lithography), galvanoformung (electroplating), abformung (molding).

Contents

1 Background **1**

1.1 Ion Channels and channelopathies 1

1.1.1 Ion movement in excitable cells 1

1.1.2 Ion channels 2

1.1.3 Channelopathies and drug discovery 2

1.2 The patch clamp technique 3

1.3 Automated Patch Clamping (APC) 5

1.4 Future perspective 7

1.5 The PILOC project 7

2 Fabrication of polymer devices **9**

2.1 Polymer microfabrication methods 10

2.1.1 Dry Etching, Electroplating and MOlding (DEEMO) 10

2.2 Chip Design 12

2.2.1 Operation principle 13

2.2.2 Through holes and cornered apertures 14

2.2.3 Device layout 15

2.3 Experimental details 17

2.3.1 Masks 17

2.3.2 Fabrication of the silicon master 18

2.3.3 Electroforming of nickel inserts 23

2.3.4 Injection molding of polymer chips 25

2.3.5 Thermal bonding 26

2.4 Results and discussion 28

2.4.1 Characterization of the patching channels 28
2.4.2 Development of the silicon master 31
2.5 Conclusions 33

3 Ion channels recordings 35

3.1 Recording set-up and cells 35
3.1.1 Cell culture 35
3.1.2 Solutions and compounds 36
3.1.3 Instrumentation 37
3.1.4 Experimental settings 39
3.1.5 Voltage protocols 40
3.1.6 QPatch^{TM} settings 40
3.2 Chip resistance and chip capacitance 41
3.3 Sealing properties 42
3.3.1 Lenght of the patching capillaries 43
3.4 Gigaseal 43
3.4.1 Gigaseal frequency 44
3.5 Factors for high seal formation 45
3.6 Patch clamp recordings 46
3.6.1 Voltage-gated sodium channels 46
3.6.2 Whole-cell recordings 47
3.6.3 Current-voltage relations 47
3.6.4 Leak subtraction 52
3.6.5 Inhibition 53
3.6.6 Perfusion of blocking compounds 54
3.7 Conclusions 57

4 Characterization of toxin peptides 59

4.1 Peptide toxins 59
4.2 BK potassium channel 60
4.3 Cells and solutions 60
4.4 Electrophysiological recordings of BK channels 60
4.5 Functional characterization of peptides #9 and #10 on BK channels 61
4.6 Conclusions 63

5 Manufacturing cost **65**

5.1 Background 65

5.2 Manufacturing cost: three important factors 66

5.3 Production cost estimate 67

5.4 Standard format 72

5.5 Conclusions 73

6 Conclusions **75**

Bibliography **79**

List of publications **91**

Chapter 1

Background

This chapter will provide a general background for the main topics of this thesis: Ion channels, conventional patch clamping, and automated patch clamping. More background information specific to the following chapters will be provided in their respective introductory sections.

1.1 Ion Channels and channelopathies

1.1.1 Ion movement in excitable cells

All biological cells are enveloped by a thin (∼10 nm) plasma membrane that acts as a barrier between intracellular space (cytoplasm) and the extracellular space [1, 2]. The cell membrane is semi-permeable to ions and capable to regulate transport in and out of the cell. The cell membrane is formed by phospholipids which embeds transmembrane proteins. The phosphorlipid membrane by itself does not allow the passing of ions. Specialized transmembrane proteins facilitate the flow of ions across the membrane. Ions are not uniformly distributed and their different concentrations inside and outside the cell establish the concentration gradients for the various ion species across the cell membrane. The concentration gradients across the cell membrane are regulated by two types of maintenance mechanisms, active transport of ions and passive distribution of ions [2].

Pumps and co-transporters are the most important proteins capable of actively pumping ions against their concentration gradients. Ions passively flow down their electrochemical gradients through aqueous pores formed by proteins. These pores are called ion channels. The net ion movement depends on the interplay of active and passive mechanisms. The charges on the two sides of the membrane are also not in balance; in most circumstances the inside is more negatively charged than the outside, and the difference between the two establishes an electrical transmembrane potential. At equilibrium, the membrane is polarized and exhibits a constant potential called resting potential, typically -50 to -80 mV for all excitable cells [3].

1.1.2 Ion channels

Ion channels facilitate ion diffusion across the cell membrane by forming an aqueous pore [2]. They have high transport efficiency, allowing up to 10 million ions to flow through a single open channel each second. This flow generates a current signal of a few picoamps (10-12 A) [4]. Their number per cell is relatively small, corresponding to a few thousand of a given type. The function of ion channels is thus to allow specific inorganic ions to diffuse down their electrochemical gradients across the cell membrane. The ability to control ion fluxes through these channels is vital for many cell functions. Ion channels underlie the heartbeat, muscle contractions and brain activity as well as many other basic physiological actions [1]. Two important properties characterize ion channels, where the first property is the ion selectivity, permitting some ions to pass, but not others. The narrowest part of the channel, which is called the selectivity filter, limits the passage according to their size and charge. Ion channels are named after the specific ion species they allow to pass, the most common being sodium, potassium, calcium, and chloride. However, some ion channels can conduct a few or several different ions and they are called non-selective cation channels. The second important property of the ion-channels is their ability to open and close. Ion channels are gated, which allows them to open briefly and then close again in response to a stimulus. They are classified according to their gating mechanism; voltage-gated ion channels activate in response to changes in membrane potential and ligand-gated channels activate in response to binding of ligands (hormones or neurotransmitters) [1]. The two gating mechanisms are shown in Figure 1.1. The opening of the channels is a thermal stochastic event with a different open probability in each of the different states in which the ion channel can be found (open, closed or inactivated). Each channel type follows a different mechanism of activation [5].

1.1.3 Channelopathies and drug discovery

Because ion channels are heavily involved in many physiological operations of cells, they are also involved in a diverse range of disorders and pathological conditions, called channelopathies [7, 4]. Mutations in ion channel genes have been associated with diseases such as cystic fibrosis, hypertension, long-QT syndrome, ataxia, arrhythmia as several types of epilepsy and many others [4]. Therefore, ion channels also represent highly attractive therapeutic targets for treating these pathologies and they are already in the top five gene families targeted by available drugs [8] with a recently estimated market of US$12 billion [9]. Furthermore, since 2006, the U.S. Food and Drug Administration has mandated the assessment of cardiac ion channels, such as human Ether-à-go-go-Related Gene (hERGs), making ion channels part of the standard safety screening for all new drug candidates [10]. This increased further the interest in studying ion channels and therefore the interest in the available technologies for doing it. The only direct way of validating the effect of drug candidates on ion channels is to measure the ionic current and determine whether the

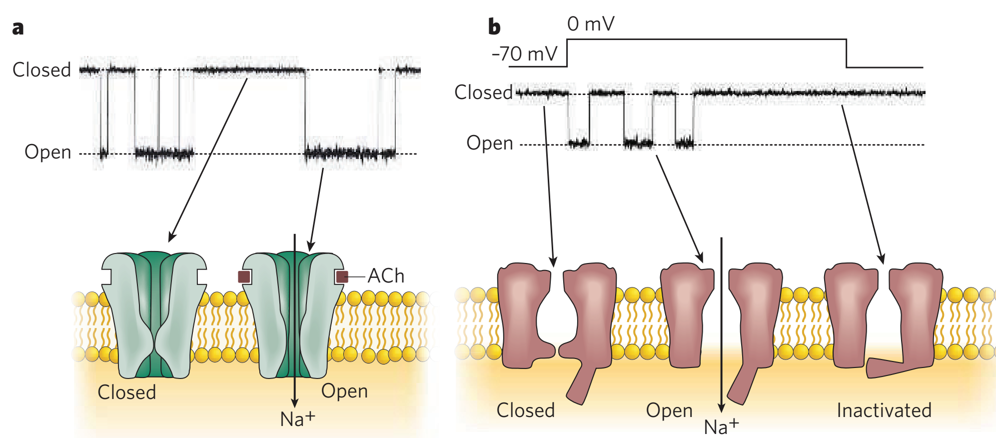

Figure 1.1: Schematics illustrating how ion channels open and close, with associated single-channel recordings. Opening and closing of the channel are random events, but the frequency with which they occur is influenced by, for example, ligand-binding (a) or transmembrane voltage (b). The transition rate between open and closed states is <10 µs. Following opening, some voltage-gated channels enter an inactivated (non-conducting) state in which they are refractory to subsequent depolarization (b). Adapted from [6].

compound causes a change in this current.

Despite their enormous potential as druggable targets, the use of ion channels for drug discovery has been well behind expectation, mainly due to the lack of adequate screening technologies [10]. Developing a new drug is a complex process which can take 15 years to be completed and can cost more than US$ 1 billion [11]. The process typically starts with a primary screening of entire libraries of compounds (hundreds of thousands) that leads to a number of "hits" showing some kinds of interactions with the targeted ion channel. This screening requires high throughput capabilities and is normally performed via indirect methods, such as fluorescence or radioligand assays [12]. Unfortunately, those techniques suffer from low specificity and thus the associated risk of generating false negative or false positive results [10, 13]. Therefore, a secondary screening by higher information-content methods such as patch clamping is employed in order to validate the hits from primary screening before they will reach the lead optimization phase, in which their composition is optimized. Finally, compounds need to be tested for unwanted side effects. Ideally, in order to obtain better information about drug candidates, patch clamping should be employed as early as possible in this screening cascade, but because of its extremely low throughput and associated high costs, this is not possible today [14].

1.2 The patch clamp technique

Patch clamp is the accepted standard method for studying ion channel function. It allows direct measurement of single channel currents as well as of the total current across the

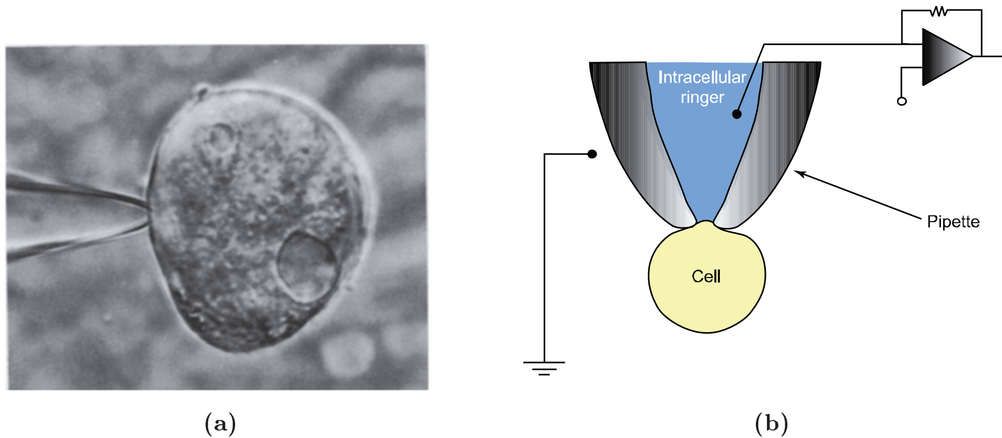

Figure 1.2: (a) The micrograph shows the tip of a patch micropipette in contactc with a rat myoball. Adapted from [16]. (b) Patch clamp technique. A glass micropipette with a tip diameter of ∼1 µm is moved onto the cell to form a high resistance seal with the cell. The micropipette is manually controlled, on an inverted microscope, by a three-axis micromanipulator. Suction is applied and a gigaseal is obtained between the pipette and cell. The membrane underlying the pipette aperture is then broken to enable whole-cell configuration.Adapted from [17].

entire cell membrane. In this technique, a fire-polished glass micropipette containing an electrolyte and an electrode, is pressed against the membrane of a cell, forming a tight electrical seal, as shown in Figure 1.2. A tiny piece of membrane, so called patch, is sucked into the pipette tip and the movement of ions across the ion channels contained in this patch is recorded. The high resistance of the seal ensures that most of the currents flow into the pipette and not through the seal.

The patch clamp method was first introduced by Erwin Neher and Bert Sakmann, in 1976, when they demonstrated current recordings from single ion channels [15]. But a real breakthrough for the patch-clamp method was reported few years later, in 1981, when they observed that clean glass pipettes, with suction applied to the pipette interior, can result in a seal with resistances of 10-100 GOhms [16]. They called the seal a "gigaseal" from the order of magnitude of the electrical resistance. Gigaseals also showed unexpected mechanical stability, even allowing the cell membrane to be partly disrupted and in some cases pulled off without destroying the gigaseal. Neher and Sakmann were awarded the Nobel Prize in Physiology and Medicine "for their discoveries concerning the function of single ion channels in cells".

When the pipette is sealed to the cell membrane and a gigaseal is formed, the initial 'cell-attached', also termed 'on-cell', patch mode is established. Activity of the ion channels in the tiny patch of membrane isolated by the tip of the pipette can be monitored. This configuration leaves the cell intact and it does not require physical manipulation of the membrane. When the patch contained in the pipette tip is ruptured with a pulse of suction or voltage, the 'whole-cell' configuration is achieved. This provides a direct access to the cytoplasm which establishes low-resistance electrical and physical continuity between the

cell and the electrode in the pipette. This allows control of the voltage of the whole cell via a voltage clamp and recording of ensemble currents from all the ion channels in the cell membrane. The access to cell interior also permits control of the chemical composition on both sides of the cell membrane.

With the discovery of gigaseals, patch clamping became the accepted standard for fundamental studies of ion channel proteins in electrophysiology, and the whole-cell configuration became one of the most popular methods for the biophysical and pharmacological study of ion channels and their effectors. Unfortunately, patch clamping has one main drawback, being a very complex and low throughput technique. It is time-consuming and demands the presence of skilled personnel. Obtaining the necessary seal between the glass pipette and the cell is not easy in practice. Typically only 10 cells can be clamped on a "good" day.

1.3 Automated Patch Clamping (APC)

In order to remove the existing trade-off between high-throughput and high-sensitivity and to transform patch clamping from a delicate yet powerful method into a higher throughput assay, the approach of replacing glass micropipettes with systems able to perform patch clamping recording on a chip with higher throughput was proposed [18]. After some years of product development, the first automated parallel patch clamping system (APC) was made available in 2003 [19]. Since then, 7 companies (Molecular Devices, Sophion Bioscience, Nanion, Cytocentrics, Cellectricon, FlyIon and Fluxion) have entered the market, establishing APC as an essential technology for secondary screening, lead optimization and cardiac safety testing in the drug discovery process [20]. APC systems replace the use of conventional glass micropipettes with single-use, disposable devices fabricated in materials such as quartz [18] and silicon/silicon-dioxide [21]. The majority of the available platforms share the so- called planar approach, where cells in suspension are blindly positioned by suction onto micro apertures made as through holes in thin membranes [18]. Alternatively, a lateral approach has been proposed, where suspended cells are trapped at lateral apertures generated at the junction of two microfluidic channels [22]. In both cases, the automated approach reverses the traditional sequence of patch clamping where the cell is stationary and the patching micropipette is navigated and carefully placed against the cell. In this way, the process of patch clamping is 'de-skilled' and some of the time-consuming operations are removed [17]. The trade-off is that cells cannot be selected by the operator on size or other selection criteria, and thus the quality of the cell suspension needs to be high and uniform [23].

In the late 90's , when APC systems started to be developed, first in university and then in industry, micromachining of silicon was a well-established technology and therefore became the natural choice for fabrication of such micro sized through holes in thin substrates.

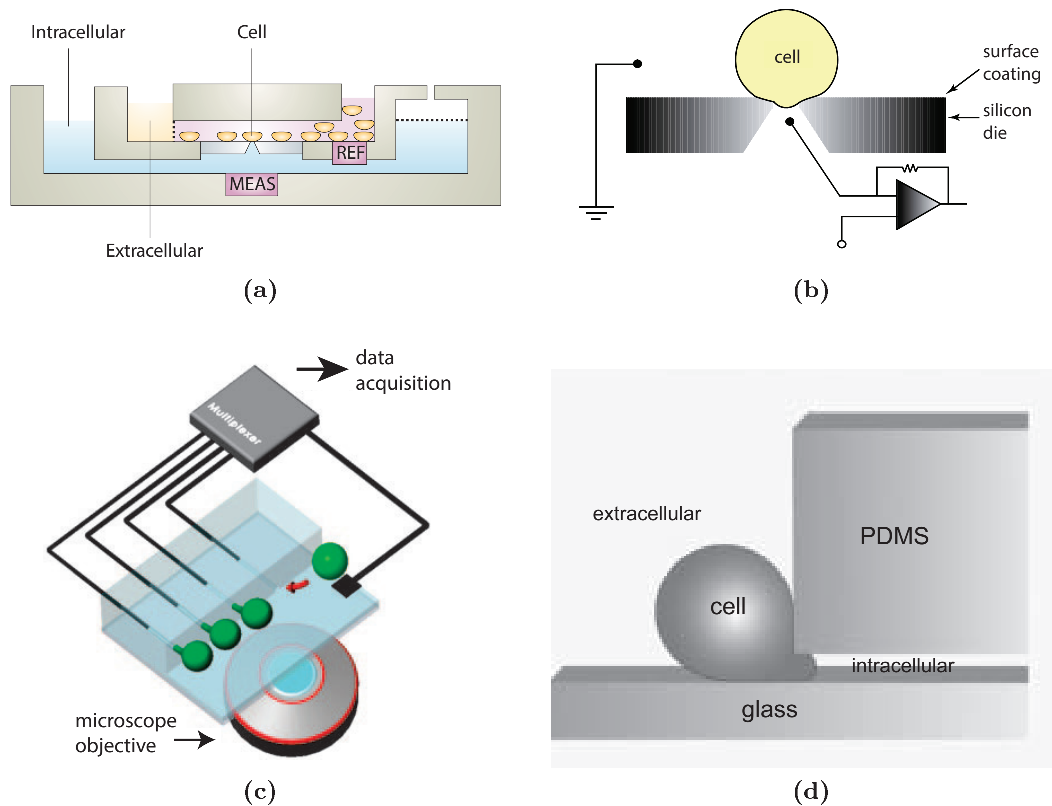

Figure 1.3: (a) Cross-sectional illustration of chips and flow channels used in automated APC system QPatchTM from Sophion Bioscience. Adapted from [20]. (b) A hole is etched or micromachined into a silicon-based substrate. Suction brings one of the cells close to the hole and the gigaseal is formed. This removes the need for an operator skilled in 3D manipulation to bring patch pipette in contact with a cell. Adapted from [17]. (c) Patch clamp array based on lateral apertures.Cell trapping is achieved by applying negative pressure to recording capillaries, which open into a main chamber containing cells in suspension. Attached cells deform, protruding into the capillaries. Patch clamp recordings are obtained by placing electrodes in each of the capillaries, as well as in the main chamber. The PDMS device is bonded to a glass coverslip for optical monitoring. Adapted from [22]. (d) Cross-sectional illustration showing how the cell is trapped. Adapted from [24].

However, silicon is a semiconducting material and therefore not ideal for providing electrical insulation during the patch clamping recordings. The problem was overcome by employing silicon oxide coatings or using quarts instead of silicon as the substrate material. The use of polymeric substrates, which have better dieletric properties, has also been widely investigated, and planar microfluidic chips have been demonstrated in hybrid poly(dimethylsiloxane)-polyimide (PDMS-PI) [25], polyimide [26], oxygen plasma treated PDMS [27, 28, 29] and poly(ethylene glycol) (PEG)/SU-8 mixture [30]. Unfortunately, all the afore-mentioned polymer devices have so far failed to deliver relevant electrophysiological results. Most likely, this lack of success in using polymer was due to the complexity on the fabrication of through holes in thin polymer substrates.

In 2005, Zanetti *et al* [22] overcame this problem by proposing a radical change in the geometry of the patching apertures. In their approach lateral apertures replaced the vertical

through holes. These lateral junctions were successfully implemented into a microfluidic device fabricated by casting of polydimethylsiloxane (PDMS) [22, 31]. In 2009, this device was eventually commercialized by Fluxion, and it remains the only APC system relying on cornered apertures to date [32]. This approach considerably improved the microfluidic integration of the orifices and the packaging into portable chips.

1.4 Future perspective

In the last decade, the advent of Automated Patch Clamp (APC) arrays has revolutionized ion channel screening, enabling faster and more accurate drug discovery. Unfortunately, present APC systems are based on expensive production technologies and the manufacturing cost per device is still prohibitive. This prevents the establishing of APC as a technique used in all aspects of ion channel drug discovery, including high throughput screening [33]. However, there is a strong market demand to extend this screening method to primary screening. In order dramatically to reduce the price per data point, this demand calls for innovative materials and solutions in the fabrication of chips.

1.5 The PILOC project

The PILOC (Polymer Ion-channel Lab On a Chip) project is an ongoing collaboration between DTU Nanotech and Sophion Bioscience A/S, a danish company which develops, manufactures and sells automated patch clamping systems on a commercial basis. This three and a half year project (September 2010 – January 2011) aims to develop an APC device for primary screening of compound libraries for possible effects on ion-channel functioning. The system may reduce drug development times by 2 years (average). It will facilitate orphan drug development by reducing cost and will reduce need for animal testing through improved in-vitro capabilities. Ambitious success criteria have been set for the project: Substantial reduction of cost per data point (-90%), and an increase of the throughput (20 times) maintaining unchanged the data quality. Those factors were recognized as the key to the outcome of the customer decision-making process.

The very critical requirement for cheapness of the final device calls for the use of polymers as substrate material. There is a high likelihood that any other materials suitable for micro fabrication, such as glass or silicon, could not fulfill this condition. The project is composed of 4 work packages: Fabrication of the microholes (WP1), the study of surface chemistry (WP2), chip and system integration (WP3) and cell testing (WP4).

This Ph.D. work was part of WP1 with the aim of fabricating well-defined through-holes of sub cellular scale dimensions in polymers, with a rim of sufficient quality to form a tight seal with the cells, and part of WP4 with the aim of testing the fabricated devices with biological cells.

from

Chapter 2

Fabrication of microfluidic polymer systems using a multilevel dry etching, electroplating and molding process

In this chapter, the method employed for fabrication of the polymer microfluidic device is presented. The process was first demonstrated for multi-level all-in-polymer chips for single-cell capture and reported in Tanzi *et al* [34]. This method consists of deep reactive ion etching (DRIE) of a silicon substrate, nickel electroforming and injection molding of cyclic olefin copolymer (COC). UV-assisted thermal bonding was found to provide a strong seal of the microstructures in the molded part without altering the channels geometry. Different dry etching processes and masking layers have been investigated for origination of the silicon masters in order to avoid defects during demolding. The combination of a modified Bosch process and an isotropic polysilicon etch was found to facilitate demolding by resulting in slightly positively tapered side walls with negligible undercut at the mask interface. Moreover, an additional layer of tetraethyl orthosilicate (TEOS) oxide was deposited in order to smooth the surface around the patching orifice where the cell is captured. The conceptual design and the chip layout are also presented. Part of the experimental work was done during the Master thesis project of DTU Nanotech student Thomas L. Christiansen [35], where the author of this thesis was co-supervisor. Some of the results and figures are therefore shared with [35]. The UV-assisted bonding process was optimized by Dr. Marco Matteucci.

2.1 Polymer microfabrication methods

In recent years, polymeric materials [36, 37, 38, 39] have gradually replaced glass and silicon [40, 41] as the preferred production platform for microfluidic devices in general. Polymers exhibit a broad range of appealing chemical, mechanical, electrical and optical properties [36]. Moreover, the multitude of different methods to manufacture microstructures in polymers make polymeric materials suitable for almost any given application, ranging from fast prototyping methods such as polydimethylsiloxane (PDMS) casting, laser milling or micromachining [42, 43, 44] to high volume mass production. In terms of physical parameters and thus technological pathways to fabrication, polymers can be classified into thermosets, thermoplastics and elastomers [36]. While PDMS have become a primary choice for fast prototyping and low-volume manufacturing in the academic environment [45], technical thermoplastic polymers are employed by commercial replication methods like injection molding [46, 47] and hot embossing [46]. However, polymer mass replication methods are poorly compatible with the requirements for design flexibility and fast turnaround times in the research environment. In fact, traditional injection molding tools are expensive and very time-consuming to fabricate, especially if they have very small features and narrow tolerances.

2.1.1 Dry Etching, Electroplating and MOlding (DEEMO)

In this work we propose a technology that aim to bridge the gap between methods and materials used in academic and industrial environments. The method consists of a versatile prototyping technology directly applicable to mass production. A nickel electroform is produced from a micro structured silicon master to transfer micrometer features to a substrate suitable for injection molding by using a commercial molding machine, as shown in Figure 2.1. Origination of a master having the inverse structures of the final part is the underlying principle of any replication technology [36]. The relatively expensive step requiring microfabrication is only done once on a single master and identical polymer substrates can be produced in large quantity [36]. Due to the high pressure regime inside the mold during the injection of the polymer, hard metal inserts are preferred over brittle silicon substrates.

For origination of the metal inserts many techniques have been used in the past such as micromachining methods and electroplating methods [48]. Among those methods, the most commonly used are LIGA[1] [49], and LIGA-like techniques, depending on the source of radiation employed [50, 51]. Although LIGA remains the best choice for high aspect ratio microstructures [52], it suffers from serious drawbacks when required facilities and the associated costs are considered. LIGA-like processes, in particular the well established UV-LIGA, then becomes the low cost alternatives. UV-LIGA employs the use of a thick layer

[1] German acronym for lithographie (lithography), galvanoformung (electroplating), abformung (molding).

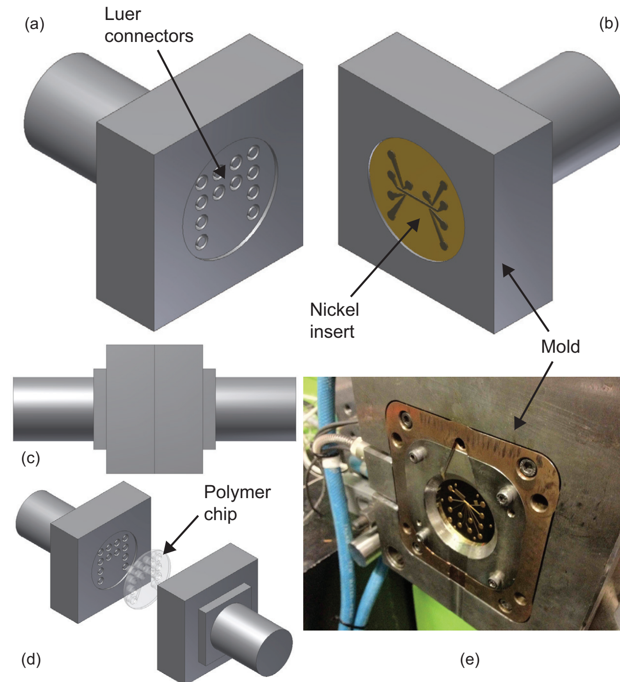

Figure 2.1: The figures illustrate the principle of the injection molding process. (a) Mold shaped with the Luer connectors. (b) Mold containing the microstructured nickel insert. (c) Mold is closed in order to form the cavity where polymer is injected. (d) Mold is pulled apart and the polymer chip can be removed. (e) Pictures of the mold with the nickel insert.

of polymer photoresist, typically SU8, in which the microstructures are defined. Unfortunately those materials have two major drawbacks: the difficulty of structuring multi-level channels and the high surface roughness that is transferred to the final device and can compromise the quality of the bonding. Therefore an alternative fabrication process needed to be evaluated.

A method where micro channels are not made in thick photoresist but directly in silicon using wet etching was first described by McCormick *et al* [53]. Elwenspoek *et al* [54] proposed a process in which the X-ray lithography step of the LIGA process was substituted by dry etching. The process was called DEEMO, which is the acronym for Dry Etching, Electroplating and MOlding [54, 55]. The very low surface roughness of the silicon wafers guarantees optimum flatness of the final chip surface and so optimum bonding conditions. The state of the art in dry etching techniques makes it possible to design advanced microfluidic systems, where the intersection between channels with heights in broad ranges from micrometers to tens of micrometers are required [56]. Moreover, this method exploits the advantages of dry etching in terms of directional freedom and high selectivity with respect to the mask material [57, 58, 59].

Because of the stated reasons, we decided to employ a DEEMO process. A multi-level fabrication scheme was adopted where first shallow channels and then deep channels were etched in the silicon wafer via photolithography using photoresist and oxide as masking

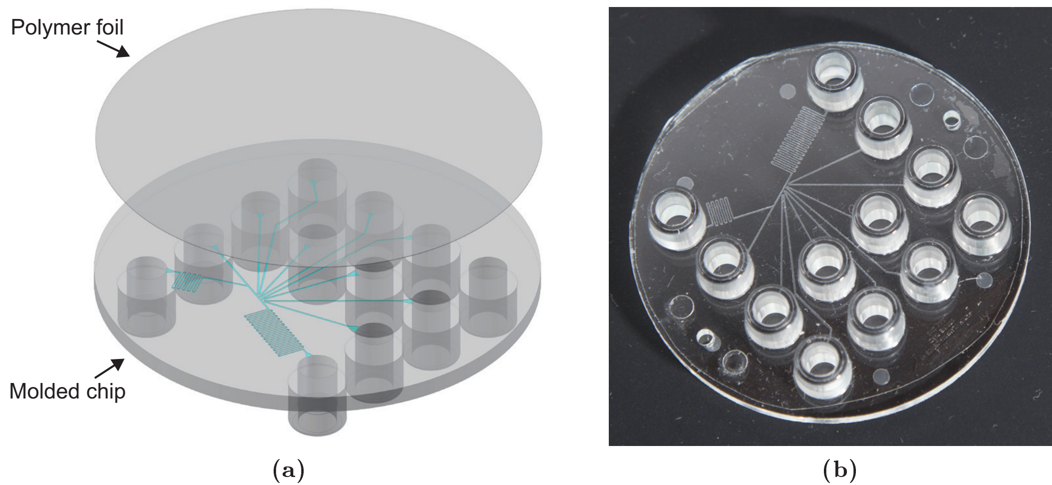

(a) (b)

Figure 2.2: (a) 3D illustration of the polymer device concept. The final device results from UV-assisted thermal bonding between an injection molded polymer part and a 100 µm thick lid. The blue color shows the microfluidics open system for conducing the cells to the patching orifices. (b) One of the molded device used in the experiments.

materials. The next step was to grow a 300 µm thick layer of nickel on top of the silicon master by first sputtering a thin metal seed layer to promote adhesion to the silicon surface and then afterwards electroforming the nickel layer. The entire silicon master was eventually removed by dipping the stack of silicon and nickel into a KOH bath, leaving only the nickel plate. A nickel insert was then punched out from this plate and inserted into the molding tool. Parts were molded from cyclic olefin copolymers (COCs) [60, 61].

As reviewed by Nunes *et al* [62] COCs are increasingly popular as substrates for microfluidic applications. They have promising properties such as high chemical resistance, low water absorption, good optical transparency and ease of fabrication by injection molding [48]. Devices in COCs have already been implemented for a multitude of applications, including capillary electrophoresis [63], electro chromatography [64] and mass spectroscopy [65]. Therefore COC was an obvious choice for the device. The chips were sealed by UV-assisted thermal bonding to a thin polymer foil from the same material, as shown in Figure 2.2a. Thus the complete device resulted from only two parts bonded together. The use of the thin polymer foil, only 100 µm thick, addresses the requirements of short working distance for microscopy. Integrated inlet/outlet ports designed according to the Luer fitting standard [66] for practical fluidic interconnects were defined by the traditional machined part of the injection molding tool and therefore included in every device during the molding. One of the molded device used in the experiments is shown in Figure 2.2b.

2.2 Chip Design

Manipulation of single-cells is basic for cell-related studies, such as cell impedance analysis and drug screening. For applications in automated patch clamping, we needed a microflu-

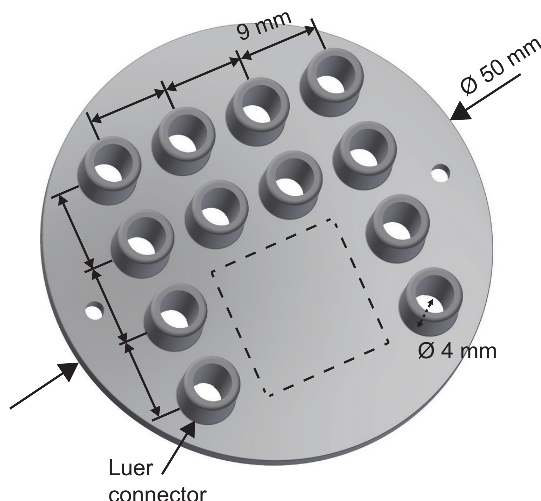

Figure 2.3: 3D illustration of the polymer device with all the specifications and geometrical constrains.

idic system capable of both trapping a single-cell to a micro sized hole and forming a tight seal between the cell and the substrate. Any device intended for automated patch clamping is therefore primarily a device for single-cell capture, and this was the case here. Since patch clamping on polymer injection molded devices has not been reported before, there were not previous studies on how cells form tight seals on hard polymer substrates.

The overall shape of the presented device was determined by the standard geometry of the custom designed mold available at DTU Danchip. The used mold forms 50 mm diameter and 2 mm thick polymer chips that contain 12 integrated inlet/outlet Luer ports used to connect the microfluidic channels on the chip to external flow or air pressure controls. The Luer connectors terminated with a diameter of approximately 4 mm [67] in the side structured with the microfluidic channels. The distance between two consecutive connectors was 9 mm (center – to – center). Luer ports had advantages of ease to use with standard syringes and leak-free connections with a male-taper fitting when applying pressure or suction. The presence of Luer connectors limited the actual usable area to 4 cm^2 where the patching sites were located. However, this is not seen as a limitation for the channel design. The device with all the specifications is illustrated in Figure 2.3. The layout is further described in Section 2.2.3.

2.2.1 Operation principle

A suspension of cells is inserted in one of the inlets, which functions as cell reservoir. By applying pressure to the microfluidic channel connected to this cell reservoir inlet, cells are transported in the proximity of the capturing site where a single cell is captured at one of the apertures by suction. Once one of the cells is trapped, a tight seal is expected to form between the cell membrane and the substrate and electrical recordings on the cell can be

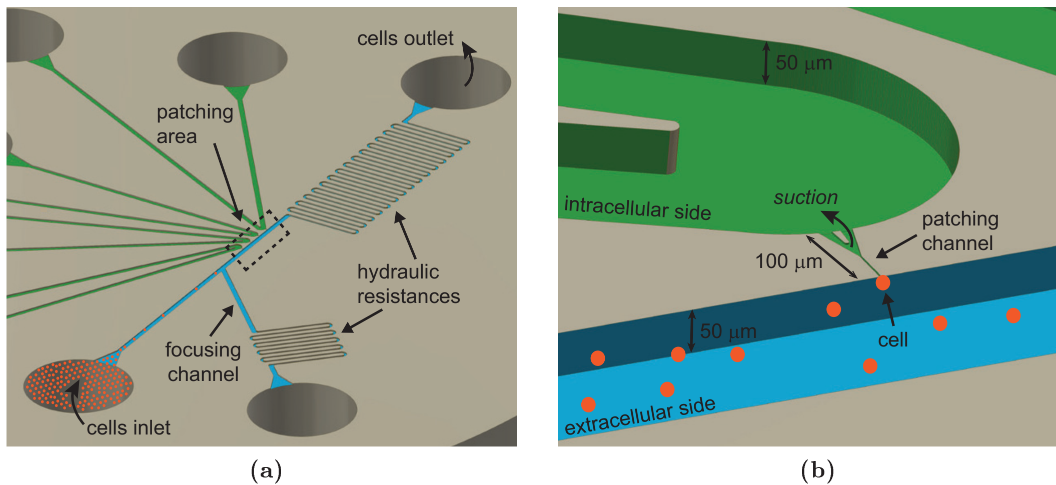

(a) (b)

Figure 2.4: (a) An illustratation of the main channel geometry. (b) An illustration of the capturing principle in the presented device. A cell flowing in the main carrier channel is captured at one of the apertures by applying suction to it. The two compartments across the patching channel contain extracellular and intracellular solution.

performed through electrodes inserted into two of the inlets. This is described in details in Chapter 3. More specifically, two main compartments, at the two sides of the micro sized apertures, are filled up with the electrolyte solutions: extracellular solution in the side where cells are flowing and intracellular solution in the side with no cells. This is also the side that will be connected to the interior of the cell after the cell will be perforated in whole-cell mode. An illustration of the capturing principle is presented in Figure 2.4.

2.2.2 Through holes and cornered apertures

Two types of capturing geometries have been demonstrated and are nowadays employed in commercially available systems: vertical apertures or through holes in this substrates, and lateral (or cornered) apertures. Both geometries rely on the same principle, where a cell flowing in a carrier channel is captured to a micro channel by suction and only differentiate for the position of this micro channel in respect to the carrier channel. The two type of capture geometries are illustrated in Figure 2.5.

If we look at the way these two capturing apertures could be fabricated, cornered apertures are easier to obtain, especially on polymer substrates. Cornered apertures, in fact, require only two layers: a structured half that contains the microfluidics and a half being only flat. Furthermore, the two halves can be bonded with no needs for alignment. On the other hand, through holes require at least three layers which all need to be structured and carefully aligned during bonding. Moreover, fabrication of the through micron sized holes in the middle thin layer is not a trivial process. These type of apertures have been successfully demonstrated in thin membrane made of glass [18] or silicon [23] and are employed in some of the commercial APC systems. However, through holes would not be

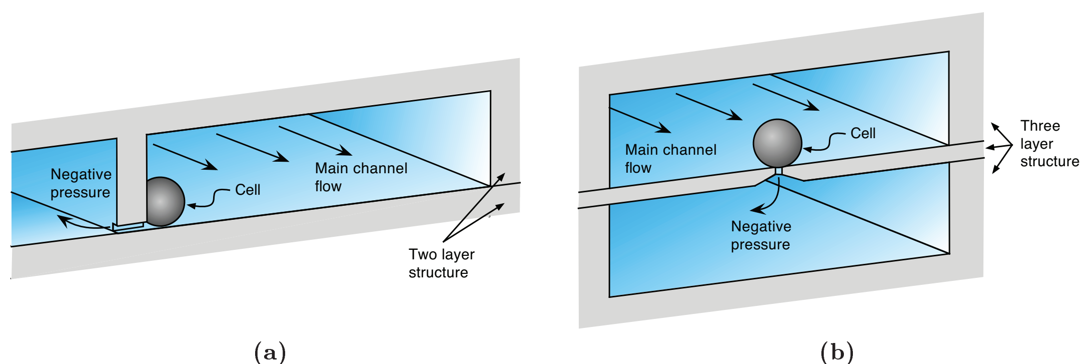

Figure 2.5: Two concept designs for single-cell capture and patch clamping. a) Capture by means of 'cornered' apertures based on microfluidic junctions between a large chamber for cell delivery and a lateral capillary for cell trapping. b) The most common approach employed for single-cell capture in patch clamping devices based on vertical apertures [35].

easy to fabricate in thin polymer substrates. The use of injection molding is limited by the fragility of pins that should be employed in the mold for originating the apertures in the final parts, while alternative methods such as laser ablation are under investigation but have not yet delivered successful results [68]. From this analysis, it seems obvious that we chose cornered apertures to be employed in the present device. Seo *et al* [31] and Zanetti *et al* [22] were the first authors to report on lateral apertures in a PDMS microfluidic device for electrophysiology recordings. Similar to these works, the present device enables to capture a cell flowing in a carrier channel close to a small microhole, as shown in Figure 2.4. The silicon master and thus the final COC chips contain both patching channels (circa 2 µm wide and 2 µm deep) and carrier deep channels (200 µm wide, 50 µm deep).

2.2.3 Device layout

The mask layout contains four independent lateral apertures 600 µm apart which are aligned along a straight channel reserved for transportation of cells, as shown in Figure 2.6. The side channels are connected at the other end to four separate inlet channels that contain intracellular electrolyte solution. As shown in Figure 2.7, the patching channel is Y shaped and consists of a straight capillary with a rectangular profile and rounded corners at the end where the cell is captured and a wider opening at the opposing end for the reduction of the total hydraulic resistance of the shallow channel, making the cell capture easier. In addition, a second type of device with a semicircular profile was molded and tested. In the following, the two groups of devices will be called type A device (rectangular profile) and type B device (semicircular profile). Details about these two devices are given later in this chapter. Moreover the patching channel includes a structure which extends from the wider opening to prevent collapse of the shallow channel during the bonding.

In order to find the optimal length of the patching channel capillaries, we made the four channels with different lengths of the straight capillary fraction, respectively 15 µm, 25

µm, 35 µm and 45 µm. The four patching capillaries are shown in Figure 2.8. The distance between channels dedicated for intracellular and extracellular was kept fixed and equal to 100 µm. Conveniently, one of the unused patching capillaries could be used for perfusion of compound into the main channel. Further details are given in Chapter 3. The design also contains a hydraulic resistance and a lateral focusing channel, respectively downstream and upstream the capturing site, as shown in Figure 2.4a. Those two elements were introduced in order to control the flow rate of the cell in the carrier channel more efficiently. The additional hydraulic resistance, consisting in a meander shaped channel with halved width, was inserted to increase the total hydraulic resistance of the carrier channel and therefore reduce the velocity regime of the cells in suspension. The lateral focusing channel was introduced upstream the capture site in order to focus the cells toward the capturing aperture. During the experiments there was no need for focusing the cell and therefore this feature was never employed.

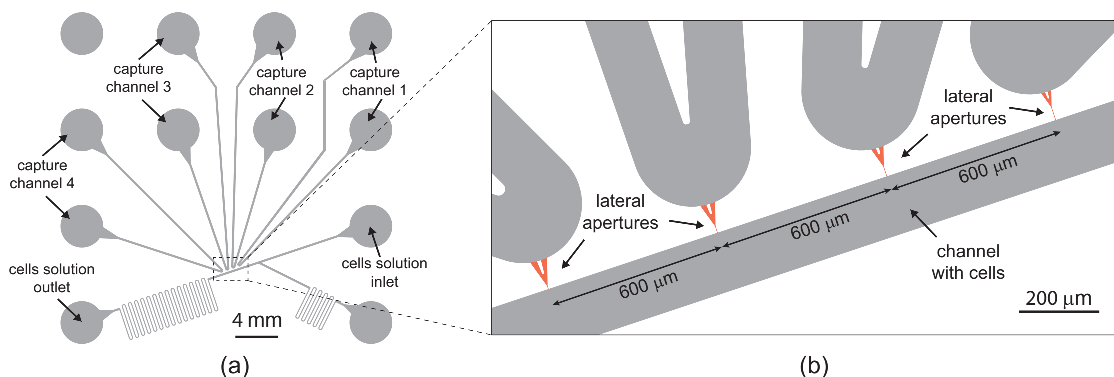

Figure 2.6: (a) Layout of the microfluidic device with a channel reserved for transportation of cells and 4 capture channels. (b) Close-up of the key part of the design with four independent lateral apertures 600 µm apart aligned along a straight channel with cells.

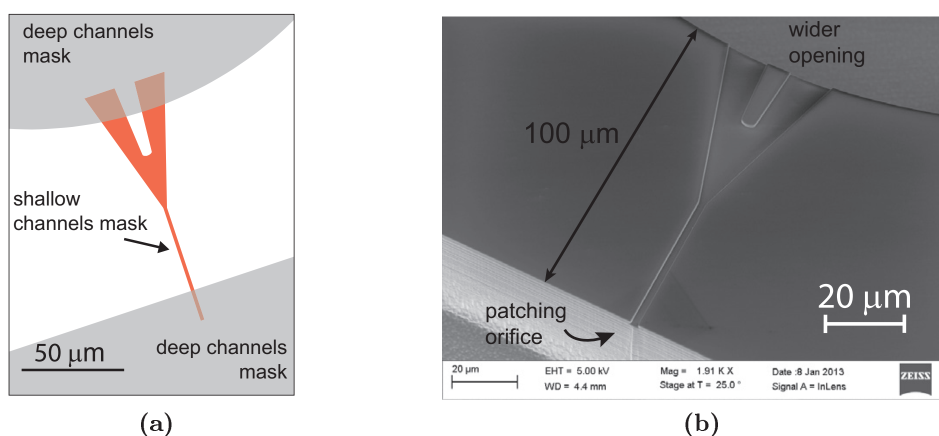

Figure 2.7: (a) Overlap between the Y shaped patching channels and the deep channels for intracellular and extracellular solutions in the two masks. (b) SEM micrograph of the Y shaped patching channel in the silicon master.

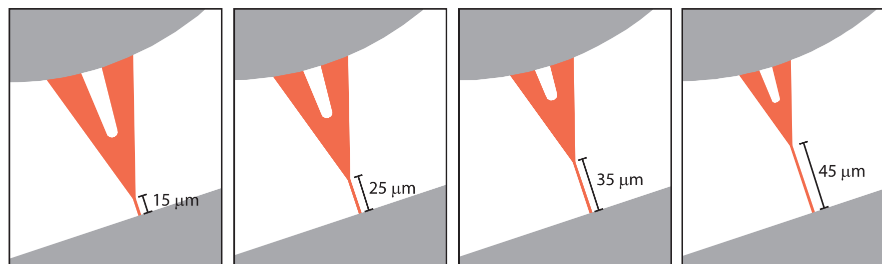

Figure 2.8: The four patching capillaries with different lengths of the straight part, respectively 15 µm, 25 µm, 35 µm and 45 µm.

2.3 Experimental details

Each phase of the fabrication scheme, from the shaping of the silicon master to the bonding of the final patch clamping device is described in the following paragraphs. The patterning of the silicon wafer is reported as it was employed for the final patch clamping device. However, during the development of it, we observed problems due to the demolding of the polymer parts during the molding process. The polymer chips presented scratched material from the sidewalls of the deep channels that, in the worst case, sealed off the orifices and made the devices useless. Therefore, several types of etching and masking methods for the origination of the silicon masters were investigated. One of these methods was eventually employed to make a device for single-cell capture. The fabrication of such a device was a fundamental milestone achieved in the project. It was important in proving that the device had the potential to work. Development and a brief description of the fabrication process for the fabrication of the silicon master employed for the single-cell capture device will be discussed at the end in this chapter.

2.3.1 Masks

In order to structure the silicon with channels to have different heights, two UV masks were used: the first one containing the Y shaped shallow patching channels and the other one containing the deep channels and the connections to the Luer ports. We used hard chrome coated soda-lime glass masks for high dimensional accuracy and long service life. The smallest dimension in our design corresponds to the width of the patching capillaries and is equal to 2 µm. After a first iteration it was observed how the width of the patching channel slightly increased at the end of the first lithography. Because of this, a nominal width of 1.5 µm was chosen in the mask. Masks were designed so there was an overlap between the Y shaped patching channels and the deep channels for intracellular and extracellular solutions, as shown in Figure 2.7a. This was introduced to ensure that the shallow and the deep channels intersect creating the patching orifices. The purpose was to overcome the possible misalignment of 1-5 µm during the UV-photolithography.

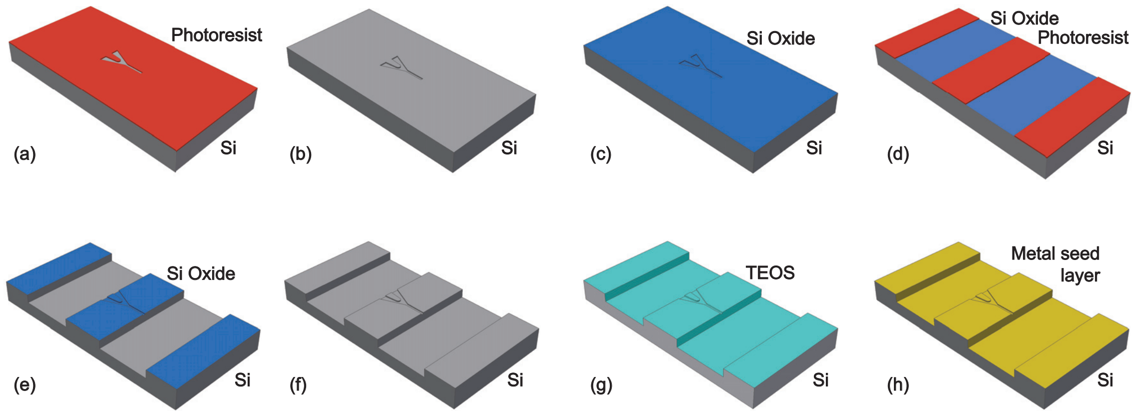

Figure 2.9: Schematics of the fabrication process for shaping the silicon master, after the main steps: (a) UV-photolithography; (b) silicon etching of the shallow patching channel; (c) oxidation with 50 nm thick thermal silicon oxide; (d) UV-photolithography; (e) oxide and silicon etching of the deep channels; (f) oxide removal; (g) TEOS oxidation; and (h) sputtering of metal seed layer.

2.3.2 Fabrication of the silicon master

First step in the process was to create a positive copy of the final chip in the silicon wafer that is referred to as the silicon master. The fabrication scheme employed positive photolithography, dry and wet etching, deposition of silicon oxide and various cleaning steps, as shown in Figure 2.9. All details are presented in Table 2.1. The only difference between type A and type B was the etching process employed to form the patching capillaries: Bosch reactive ion etching was chosen for sample type A while a continuous reactive ion etching was chosen for sample type B. Beside this, the silicon masters for device type A and type B were fabricated identically.

Silicon wafers. Since we had no special requirements for the silicon substrate, standard 100 mm, $<1\ 0\ 0>$, single side polished, 525 µm thick silicon wafers were used. Before the first spin coating of photoresist, the wafers were dipped into buffered hydrofluoric acid (HF) bath for 60 seconds at room temperature and rinsed in water in order to remove native dioxide layer and thus promote the resist adhesion on the silicon substrates. The treatment renders the silicon surface more hydrophobic leading to better wettability by the photoresist during the spinning phase.

First photolithography. A 1.5 µm thick layer of AZ5214E photoresist from MicroChemicals was applied to the substrate using a SSE Maximus 804 cluster system and baked at 90 °C for 90 seconds. The wafers were then exposed in hard contact mode for 6.7 seconds using a Karl Süss Mask Aligner MA6 (exposure wavelength 365 nm) and developed in AZ351 for 63 seconds in a positive process where only the exposed resist was removed. The optimal exposure and development time was found by using test wafers. The wafers were etched with $C_4F_8/SF_6/O_2$ plasma in a Deep Reactive Ion Etching (DRIE) Pegasus system from SPTS Technologies in order to create the Y shaped patching channels for type A device. Alternatively, the wafers used to generate type B device were exposed to $C_4F_8/O_2/CHF_3$

Table 2.1: Process parameters for origination of the silicon masters for both devices A and B type.

Process	Parameters
Oxide removal	HF bath; t = 60 sec
Spin coating	1.5 µm AZ5214E; pre-bake: 90 °C for 90 sec
Photolithography	- hard contact mode, front side alignment W/A= 7 mW/cm^2; t = 6,7 sec - AZ351 developer; t = 63 sec
Device type A Si DRIE (shallow channels)	$C_4F_8/SF_6/O_2$ = 150/275/5 sccm; 11 cycles; t = 24.2 sec
Device type B Si RIE (shallow channels)	SF6/O2/CHF3 = 30/29/5 sccm; t = 24 min; WRF = 20 W; P = 80 mTorr
Wafer cleaning	RCA1: H_2O:NH_4OH:H_2O_2(5:1:1); RCA2: H_2O:HCl:H_2O_2 (5:1:1); HF bath
Oxide deposition	1050 °C dry oxidation ; t = 40 min + 20 min annealing
Spin coating	- HMDS vapor deposition - 2,2 µm AZ5214E; pre-bake: 90 °C for 90 sec
Photolithography	- hard contact mode, front side alignment W/A= 7 mW/cm^2; t = 8 sec - AZ351 developer; t = 70 sec
Oxide etch AOE (deep channels)	C_4F_8/H_2 = 5/4 sccm; t = 25 sec; WRF = 200 W; T = 0 °C; P = 4 mTorr
Si DRIE (deep channels)	$C_4F_8/SF_6/O_2$ = 150/275/5 sccm; 215 cycles; t = 552 sec
Polysilicon etch	H_2O:HNO_3:BHF (20:20:1); t = 8 min; T= 20°C
Oxide removal	BHF bath; t = 3 min
Wafer cleaning	RCA1 : H_2O:NH_4OH:H_2O_2(5:1:1); RCA2 : H_2O:HCl:H_2O_2 (5:1:1); HF bath
Oxide deposition	1100°C dry oxidation ; t = 150 min + 20 min annealing
Oxide removal	HF bath; t = 15 min
TEOS deposition	T = 725 °C; t = 17 min; P = 190 mTorr; TEOS/O_2 = 50/30 sccm

plasma in a Reactive Ion Etching (RIE) system from SPTS Technologies. Two etching processes were chosen here in order to originate different profiles for the orifices, rectangular and semicircular respectively. Micrographs of the two orifices are provided in Section 2.4.

While the RIE process is performed in a single step, the DRIE process, also known with the name of the inventor Roberts Bosch, relies on many repetitions of alternating etch and passivation cycles. First, a mixture of oxygen and SF_6 gas bombards the silicon surface and chemically etches the silicon substrate. Then SF_6 gas is replaced by polymer-producing gas C_4F_8 that forms a protective polymer layer. In successive etching step, the same mixture of etching gases is applied, oxygen ions remove the bottom polymer, and fluoride ions etch the silicon at the bottom while the sidewalls remain protected by polymer. The continuous repetition of such etching and passivation cycles results in a scalloped sidewall, as shown in

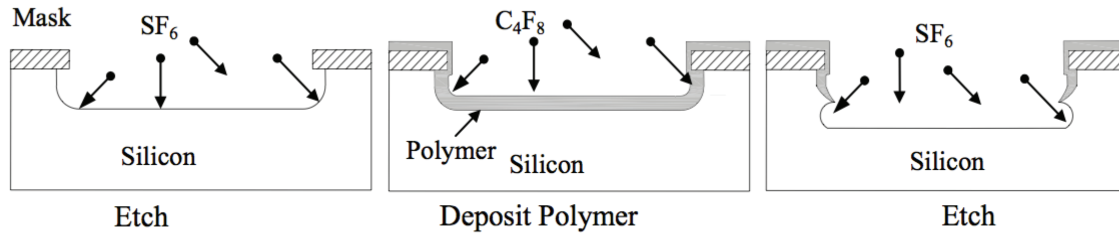

Figure 2.10: Principle of deep reactive ion etching (DRIE- Bosch) process. Adopted from [69].

Figure 2.10 [69]. The process is anisotropic and generates almost straight sidewalls giving a substantially rectangular cross section. In contrast to this, in a continuous etching process the passivation step is not employed and therefore the process results are more isotropic and consequently profiles tend to be semicircular. The recipe for continuous etching employed for device B type was specifically adapted to accentuate this effect. A mask with an initial width of only 1 µm was employed in this case. Removal of photoresist after the etching processes was performed by using a PVA 300 Plasma asher from Tepla with an O_2/N_2 at 1000 W for 20 minutes.

RCA and oxidation. After the etching of the Y shaped channels, a protective oxide layer was applied to the wafers in order to avoid damages at the bottom of the patching capillaries during the rest of the process. The wafers were cleaned with a standard RCA clean before the oxidation. This process is a standard cleanroom procedure always employed when wafers partially processed require further processing in a furnace that is considered a clean environment. It comprises three steps: RCA1 removes organic films, RCA2 removes alkali ions and metal hydroxides, hydrofluoric acid (HF) removes the thin oxide film grown during RCA1 and RCA2. The wafers were then oxidized for 40 minutes in a Tempress horizontal furnace at 1050 °C with an oxygen flow of 5 slm[2] and 20 minutes annealing at the same temperature, with a nitrogen flow of 3 slm. During heating and cooling, a nitrogen flow of 3 slm was used. Thickness of the oxide layer was measured to be 50-65 nm.

Second lithography. A second photolithographic step was performed for the patterning of the deep channels. Before the second spin coating of photoresist, the wafers were treated with hexamethyldisilazane (HMDS) to promote the adhesion of the resist on the oxide. This was performed in a STAR2000 HMDS/vapor prime oven from IMTEC. As an alternative to a HF bath when the oxide layer want to be maintained, the treatment increases the hydrophobicity of the substrate surface leading to better wettability by the photoresist during the spinning phase.

Subsequently a 1.5 µm thick layer of AZ5214E photoresist was applied, and the wafers were exposed in hard contact mode and developed as described for first lithography. The oxide layer was etched to form the deep channels in the silicon oxide layer and then further etched to form them in the silicon wafer. To remove the oxide layer, the wafers were exposed to a C_4F_8/H_2 plasma in an Advance Oxide Etching (AOE) from SPTS Technologies. Without

[2]Standard liters per minute

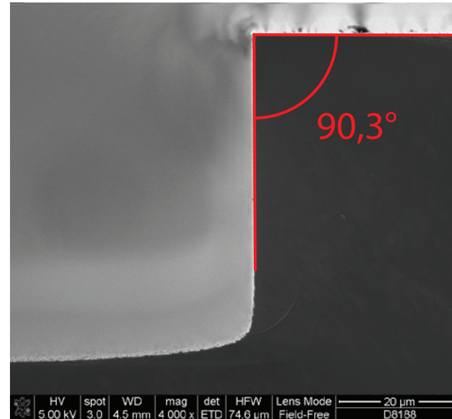

Figure 2.11: SEM micrograph of the cross-sectional profile of the deep channel from a cleaved wafer processed with ramped Bosch etching process in the Pegasus system. The sidewall slope is 90.3° and the underetching at the surface of the wafer is almost non-existing [35].

removing the photoresist, wafers were then transferred into the DRIE Pegasus system and deep channels (200 µm wide, 50 µm deep) were etched into the silicon with a ramped Bosch process. This process consisted of an alternation between a deposition phase and an etching phase, as described previously. The etch depth is controlled by adjusting the number of cycles. In addition to the scalloped sidewalls, in case of deep etching, the process tends to deliver a slightly negative slope, since ions are increasingly deflected from the bottom and sidewalls of the channel, thereby degrading the passivation layer and allowing a slight lateral etching [69]. In order to correct this effect, the etch/passivation cycle time over the duration of the process was ramped. The slope of the ramping of the passivation cycle was set to be lower than the slope of the etch cycle time, hence resulting in an increase in the passivation to etch ratio. Over the entire duration of the process (215 cycles), the deposition phase was ramped from 2 to 1 seconds and the etching phase was ramped from 2.4 to 0.1 seconds. As shown in Figure 2.11, this was found to counteract the lateral etching and improve the sidewalls slope (90.3°) compared with a standard Bosch etching ($< 90°$). The process showed almost no taper deviation ($<$0.2 µm).

However, the passivation layer was not sufficiently removed, due to the high passivation to etch cycle time at the end of the etch creating substantial grass formation at the bottom of the channel, Figure 2.12a. As can be seen from Figure 2.13, showing the etched depth for varying numbers of etch/passivation cycles, the etch depth starts to stagnate around 160–180 cycles, indicating that the grass formation is dominating for higher cycle numbers. This could potentially become a problem during the molding process, as the polymer would fill up many small cavities in the nickel shim created by the grass, hence compromising the de-molding process.

Removal of photoresist after the etching processes was performed by using a PVA 300 Plasma asher from Tepla with an O_2/N_2 at 1000 W for 20 minutes.

Polysilicon etch. In order to avoid such demolding issues, we decided to remove the grass

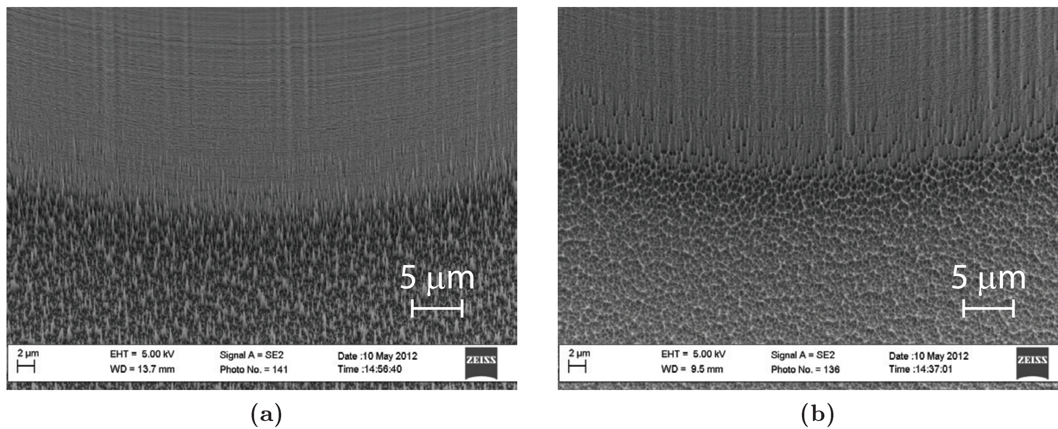

Figure 2.12: (a) SEM micrograph of the grass developed in the bottom of the channel due to the high passivation to etch cycle time in the end of the etch process. (b) SEM micrograph of the same detail after the polysilicon (mixture of HNO3, BHF and H2O) wet etching process.

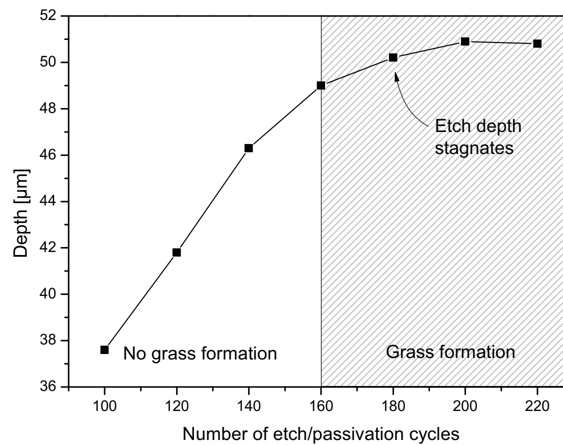

Figure 2.13: A plot of the etched depth as a function of the number of cycles in the modified DRIE Bosch process for the deep channel etches. It is seen that for high numbers of cycles, the etched depth stagnates, which is consistent with the observation of grass formation in the bottom of the etched channels [35].

using a wet etching process. A polysilicon etch mixture of HNO_3, BHF and H_2O in the ratio 20:1:20 was found to remove the grass successfully. The silicon wafers were dipped in polysilicon etch mixture at room 20 temperature for 8 minutes and then rinsed in water. Wet etching agents have previously been used to smoothen rough silicon surfaces [70]. Well-known etchants such as potassium hydroxide (KOH) and tetramathyl ammonium hydroxide (TMAH) can be used to smoothen surfaces, but both KOH and TMAH are anisotropic silicon etching agents, while the polysilicon etch is a completely isotropic etch [71]. Figure 2.12b shows how the wet isotropic etching successfully reduced the grass and partially smoothened the scallops.

Smoothing. The remainder of the oxide mask was stripped in a buffered HF solution for 3 minutes at room temperature and then rinsed in water. Smoothing of the sidewalls by thermal oxidation was performed in a horizontal furnace; the wafers were oxidized for 150

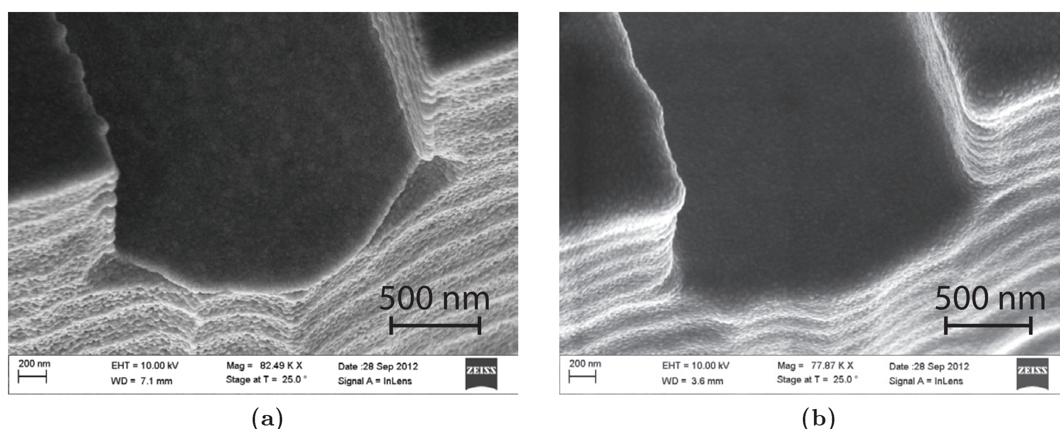

Figure 2.14: SEM micrographs show the effect of the smoothing steps. (a) SEM micrograph of one of the patching orifices type A in the silicon wafer before the smoothing steps were performed. (b) SEM micrograph of the same detail after the smoothing steps.

minutes at 1100 °C with an oxygen flow of 5 slm and 20 minutes annealing at the same temperature, with a nitrogen flow of 3 slm. During heating and cooling, a nitrogen flow of 3 slm was used. The thickness of the oxide layer was circa 200 nm. The oxide layer was then stripped in a buffered HF solution for 15 minutes at room temperature. The use of sacrificial oxidation is a well known effect for smoothing of silicon sidewall surfaces. It simply consists of first growing a silicon dioxide on the silicon surface and then removing it in wet etchants [72]. After the oxide was stripped, the wafers were transferred into a low pressure chemical vapor deposition (LPCVD) furnace from Tempress and an additional layer of tetraethyl orthosilicate (TEOS) oxide was deposited at 725 °C. The thickness of the TEOS oxide layer was circa 180 nm. Figure 2.14 shows one of the patching orifices in the silicon wafer before and after the smoothing steps were performed.

2.3.3 Electroforming of nickel inserts

The second step in the process was to produce a negative copy of the shaped silicon master such that this would comprise a relief pattern corresponding to the pattern of microfluidic channels etched into the master, as shown in Figure 2.15. This copy was electroformed in hard metal (nickel) and was used for the polymer injection molding, as shown in Figure 2.16. In electroforming, a layer of nickel is electrodeposited on a conductive surface and perfectly replicates the structures. A hole or a channel in the silicon will originate a pillar or a protrusion respectively in the nickel plate. Electroforming is a galvanic process where the silicon master works as a cathode. Since silicon is a semiconductor, in order to achieve a uniform metal growth, the wafers needed to be covered with a conductive seed layer.

For the deposition of the metal seed layer, sputtering provided an even layer both on the bottom and on the sidewalls of the microfluidic channels due to its relatively high sputtering angle. In the chamber, the wafer was held face down and rotating during the

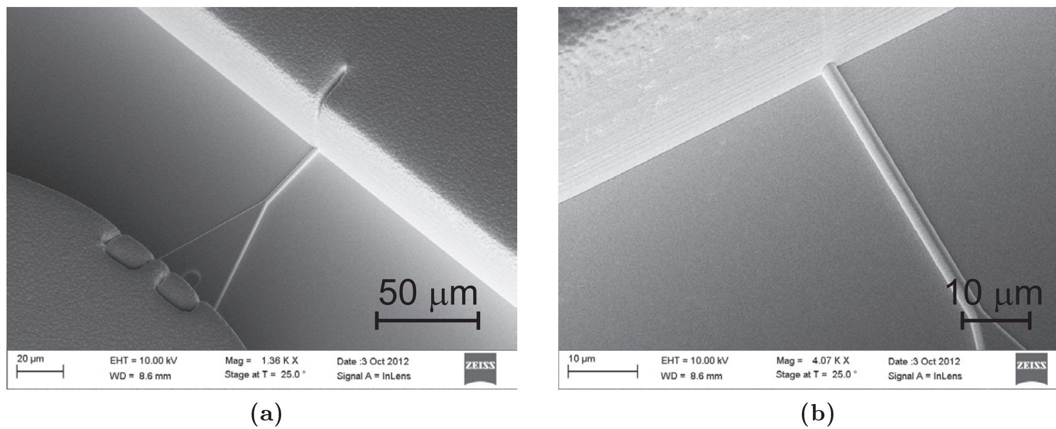

(a) (b)

Figure 2.15: SEM micrographs of the negative copy of patching channel in on of the nickel inserts.

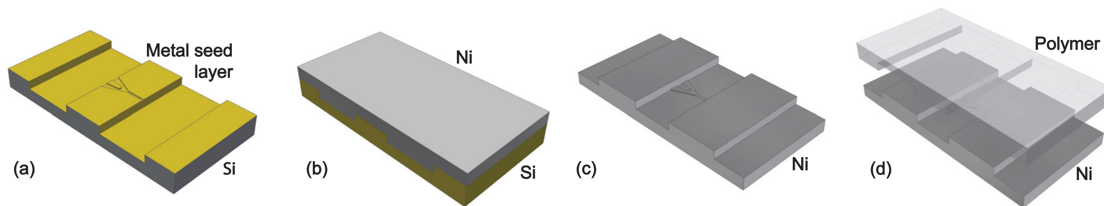

Figure 2.16: Schematics of the electroforming process: (a) deposition of a conductive metal seed layer; (b) nickel eletroforming; (c) etching of the silicon in KOH; (d) injection molding of the polymer part.

sputtering while the metal targets were positioned underneath and tilted with an angle of approximately 45 degrees. For this reason it was preferred to other deposition methods such as e-beam evaporation or thermal evaporation. The silicon masters were sputtered with approximately 10 nm of titanium and 50 nm of gold with a sputter system from Lesker. The two depositions took place consecutively while the wafers were kept inside the sputtering system avoiding oxidation of the intermediate titanium layer. The thin layer of titanium was applied to enhance the adhesion between gold and silicon [73].

Electroforming was performed in an electrochemical bath Microform 200 from Technotrans and resulted in a nickel coverage with a thickness of about 300 μm. The current was increased linearly from 0 to 0.5 A during the first 15 minutes, and from 0.5 to 1.5 A for the next 15 minutes. Then the current was constantly raised up to 17 A for a total process time of about 12 hours. In order to release the nickel plate from the silicon master, the latter was dissolved in a KOH bath at 80 °C for 8 hours. From the yellow color of the electroformed plate after the etching process, we could see that the seed layer remained almost entirely attached to the nickel plate. In fact, the thin titanium layer might have been removed in the KOH bath [73]. However, the presence of gold was not considered harmful for the injection molding phase and the gold was not removed.

The resulting nickel-electroformed plates were punched into an 85 mm diameter shim by using a hydraulic press fitted with a customized punching tool. The inserts had two

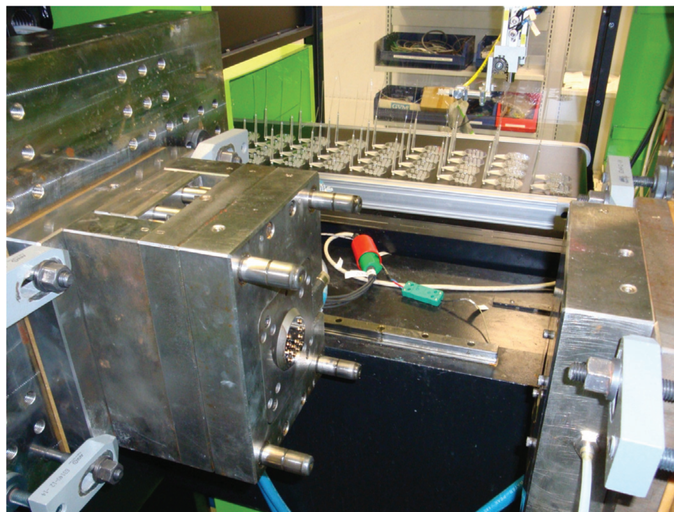

Figure 2.17: Injection molding of polymer parts.

flat parts to ensure rotational direction definition when the inserts were mounted into the injection molding tool. Two alignment marks replicated into the nickel and positioned outside the 85 mm area were used to align the plates in the punching tool. Before punching, a layer of blue adhesive tape was applied to the front side of the nickel plates in order to protect the microstructures during the operation. The inserts were then transferred into the molding tool.

2.3.4 Injection molding of polymer chips

The third step in the process was the injection molding of the polymer parts. Replicas of the original structures were molded with a Victory 80/45 Tech injection molder from Engel, a machine typically used for mass production. Figure 2.17 shows the machine during the molding process. The mold assembly consists of two halves: one fixed half anchored to the injection unit and one moving half anchored to the clamping unit. The nickel shim was inserted into the fixed half of the mold. The presence of centering metal pins allowed the shim to be in the correct position. The other half included the ejector pins and the cavities that originated the Luer fittings on the unstructured side of the chips. As shown in Table 2.2, chips were molded with a variotherm process with a nozzle temperature of 280 °C, mold temperature of 130 °C and demolding temperature below 60 °C. The holding pressure was 1700 bar and decreased to 0 bar in 0.75 seconds. Chips were molded from COC TOPAS grade 5013 (glass transition temperature, T_g of 135 °C) from TOPAS Advanced Polymers GmbH.

When injection molding involves micron and sub-micron scale structures, exact replicas are achieved through variotherm [36, 74] process, where the cavity is heated to a temperature close to the glass transition temperature of the polymer to facilitate the polymer to flow into the microfeatures of the mold insert. The parts are ejected when the mold is cooled

Table 2.2: The process parameters for injection molding of the polymer chips.

Parameters	
Nozzle Temperature	280°C
Mold Temperature	130°C
Demolding Temperature	< 60°C
Holding Pressure	1700 bar to 0 bar in 0.75 sec
Clamping Force	450 kN
Injection Speed	52 cm^3/sec
Shot Volume	12 cm^3

down below a suitable release temperature (in our case 60 °C) to release the molded part well after freeze of the polymer. This process substantially increases the total cycle time, which here was 3 minutes including ejection of the polymer parts. The machine was run in fully automated mode. It was equipped with a robotic arm and a conveyor belt so that the polymer parts were automatically picked up from the open mold and placed onto the belt. The machine was programmed to form rows of 4 chips. The parts were collected at the exit of the conveyor belt. The sprue attached to each chip was manually removed using a scalpel and then a layer of blue adhesive tape was applied to the front side of chips in order to protect them from dust particles. This was employed after particles of dust were revealed blocking the channels during the bonding process. Once the blue tape was applied, the chips were stored and were ready for the bonding.

2.3.5 Thermal bonding

In order to create a closed microfluidic device able to withstand the required pressure, the chips need to be tightly sealed. In recent years, several techniques for bonding of thermoplastic polymers have been proposed, such as micro laser welding [75], microwave welding [76], solvent-assisted bonding [77], chemical-assisted bonding [78], or thermal bonding [79]. Amongst all these, thermal bonding is considered the most suitable for large scale production of microfluidic chips for the following reasons. It does not require expensive equipment, it does not give substantial chemical modification of the surfaces, it avoids the introduction of potentially hazardous chemicals (such as solvents) and enables the use of the same material for both the sealing layer and the actual chip. This assures uniformity in chemical and physical behavior of the microfluidic chips. For all these reasons, thermal bonding was chosen as bonding method for this work.

The bonding was performed with a conventional press (P/O/Weber) with decoupled internal temperature control of both plates and external force (P/O/Weber Presstronic) control. A 100 µm thick extruded polymer film TOPAS 5013F-04 from Advanced Polymers Extrusion Lab was used as a cover lid. Prior to bonding, both the foil and the molded chip surface were exposed to UV radiation from a lamp (DYMAX mercury UV-bulb F/5000)

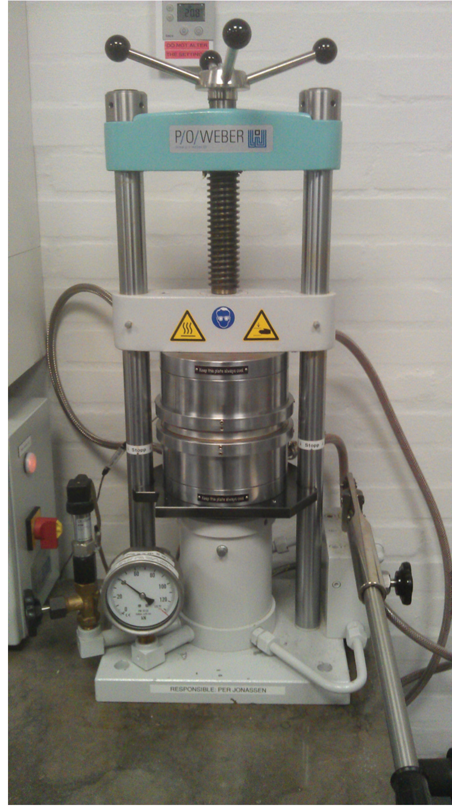

Figure 2.18: Bonding press employed for the bonding.

Table 2.3: The process parameters for thermal bonding of the polymer devices.

Parameters	
UV radiation time	30 sec
Piston Force	40 kN
Plate Temperature	115 °C
Process Time	10 min

emitting over the full unfiltered Hg line spectrum with a power of 44.5 W/cm^2 measured at the wavelength 365 nm. All samples were kept under the UV light for 30 seconds. In order to ensure uniform pressure all over the chip surface, an aluminum holder was built in which the Luer fitting protrusions could be inserted. Since the area of the press allowed more than one chip at the time and in order to speed up the bonding process, a special holder was designed for 7 chips, so they could be bonded at the same time. In addition, to preserve the flatness and the optical quality of the chip intact, the chips were covered with nickel disks and a thin PDMS layer to compensate possible non-uniformities in flatness. Before inserting the samples, both plates of the press were heated up to 115 °C which was maintained during the bonding. The process did not require alignment between the chips and the foil. Once the samples were inserted, the clamping force was increased to 40 kN and applied for 10 minutes. Then the samples were released and removed from the press in order to cool down to room temperature.

The bonding parameters were adapted after the bonding procedure was optimized on a single chip for maximum bonding strength while still preserving the integrity of the nano and micro channel geometry. This was reported in Matteucci *et al* [80]. X-ray photoelectron spectroscopy (XPS) indicated that the UV treatment did not alter the surface chemistry of the parts. Rather the UV treatment seemed to have an annealing effect on the surface [80].

2.4 Results and discussion

2.4.1 Characterization of the patching channels

The replication quality of the injection molded microstructures, especially the patching orifices, was investigated by scanning electron microscopy (SEM). Figure 2.19 and Figure 2.20 show SEM micrographs of the entrance of the capturing orifices after the main three steps of the DEEMO process for type A and B devices: Silicon master, nickel insert, and replicated polymer part. In order to make the surface conductive and improve the resolution, the polymer chips were coated with a 10 nm gold layer from a Hummer sputter coater. All details were faithfully replicated from the silicon to the nickel copy and so into the thermoplastic chip. Moreover, the topography of the orifices and of the inside of the patching capillaries was thoroughly characterized by atomic force microscopy (AFM). AFM data from channels with rectangular and semicircular profiles are presented in Table 2.4.

As expected, the profile taken across the patching channels revealed the presence of scallops with an average periodicity of approximately 180 nm for type A profile chips with scallops generated by Bosch type reactive ion etching process employed for master mold origination [81]. The amplitude and periodicity of the scallops defined the waviness of the surface and dominates the calculated roughness value. To overcome the dominating effect of the scallops and evaluate the surface roughness R_q between the scallops, images were filtered with a cut-off wavelength shorter than the average periodicity between the scallops. After

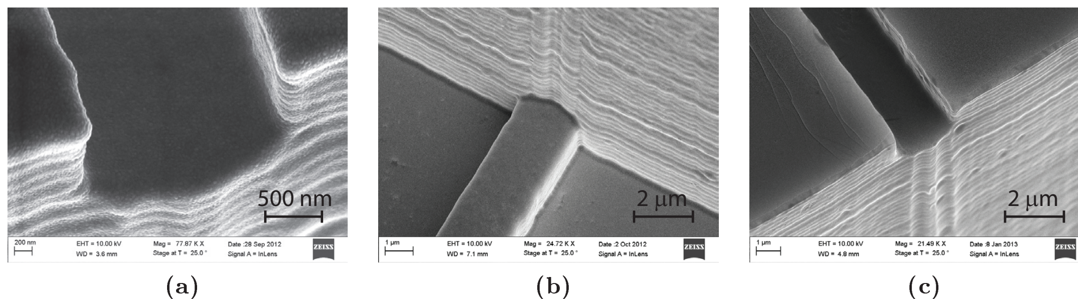

Figure 2.19: SEM micrographs of the patching orifice with rectangular cross-sectional area after the main three step of the fabrication process: Silicon master (a), nickel insert (b) and replicated polymer part (c).

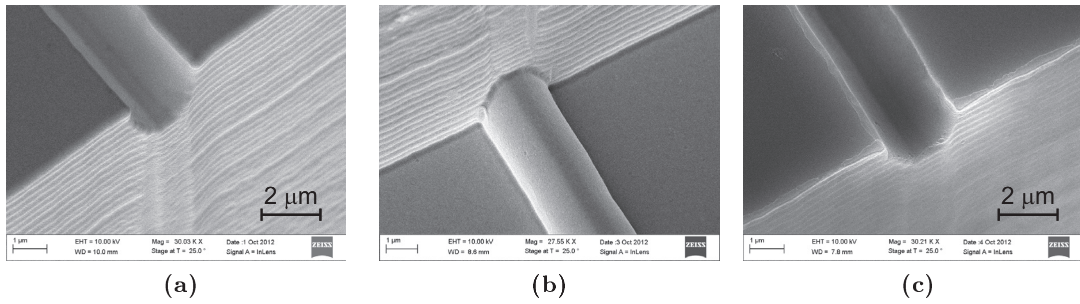

(a) (b) (c)

Figure 2.20: SEM micrographs of the patching orifice with semicircular cross-sectional area after the main three step of the fabrication process: Silicon master (a), nickel insert (b) and replicated polymer part (c).

Table 2.4: The root mean square deviation R_q of the assessed profiles for injection molded polymer parts inside the patching capillaries for the two geometries and for the one without smoothing steps. [a]The image was line wise corrected by a second order least mean squares fit in order to remove the (semicircular) shape of the profile. [b]The surface roughness R_q was calculated from an image after it was filtered so that only short wave profile components with a cut-off wavelength of λ = 0.18 μm is included. The filtering was done to avoid the influence of the Bosch process induced scallops on the calculated surface roughness (only relevant for devices with the rectangular profile).

Device	**R_q [nm] Bottom patching capillary**	**R_q [nm] Sidewall patching capillary**	**R_q [nm] Foil**
Rectangular profile	2.0 ± 0.3	6.5 ± 1.3[a] (2.4 ± 0.4)[b]	1.2 ± 0.2
Semicircular profile	0.7 ± 0.2	1.0 ± 0.2[a] (0.8 ± 0.1)[b]	1.2 ± 0.2
Rectangular profile (no smoothing steps)	3.9 ± 0.6	8.0 ± 1.2[a] (4.2 ± 0.6)[b]	1.2 ± 0.2

filtering, the surface roughness of the sidewall of the rectangular and semicircular channel are comparable and in the range of 1 to 2 nm. Therefore, the surface roughness R_q of the sidewall for both samples seems to be determined primarily by the smoothing steps that were the same for both. In general, the inside of the patching channel, including the bottom of the channel and the foil, exhibits very low surface roughness, with $R_q$in the range of 1-2 nm. For comparison, a device molded from a silicon master with rectangular profiles for the patching channels but not treated with smoothing steps was also characterized with the AFM, results are shown in Figure 2.21 and in Table 2.4. Both the bottom and the sidewall of the patching channel, after filtering, exhibit R_q about 4 nm. This confirmed the smoothing effects of the sacrificial oxidation and TEOS deposition. The side length of the images were 1.3 μm. This length was determined by the depth of the patching capillaries, being approximately 2 μm. In order to avoid edge effects 1.3 μm was the largest area that could be considered on the sidewall. Consequently, all the other images were also evaluated on the same side length. All measurements were carried out with a MultiMode 8 atomic force microscope from Bruker in intermittent contact mode using single crystal silicon cantilevers with spring constants of approximately 40 mN and radius of curvature

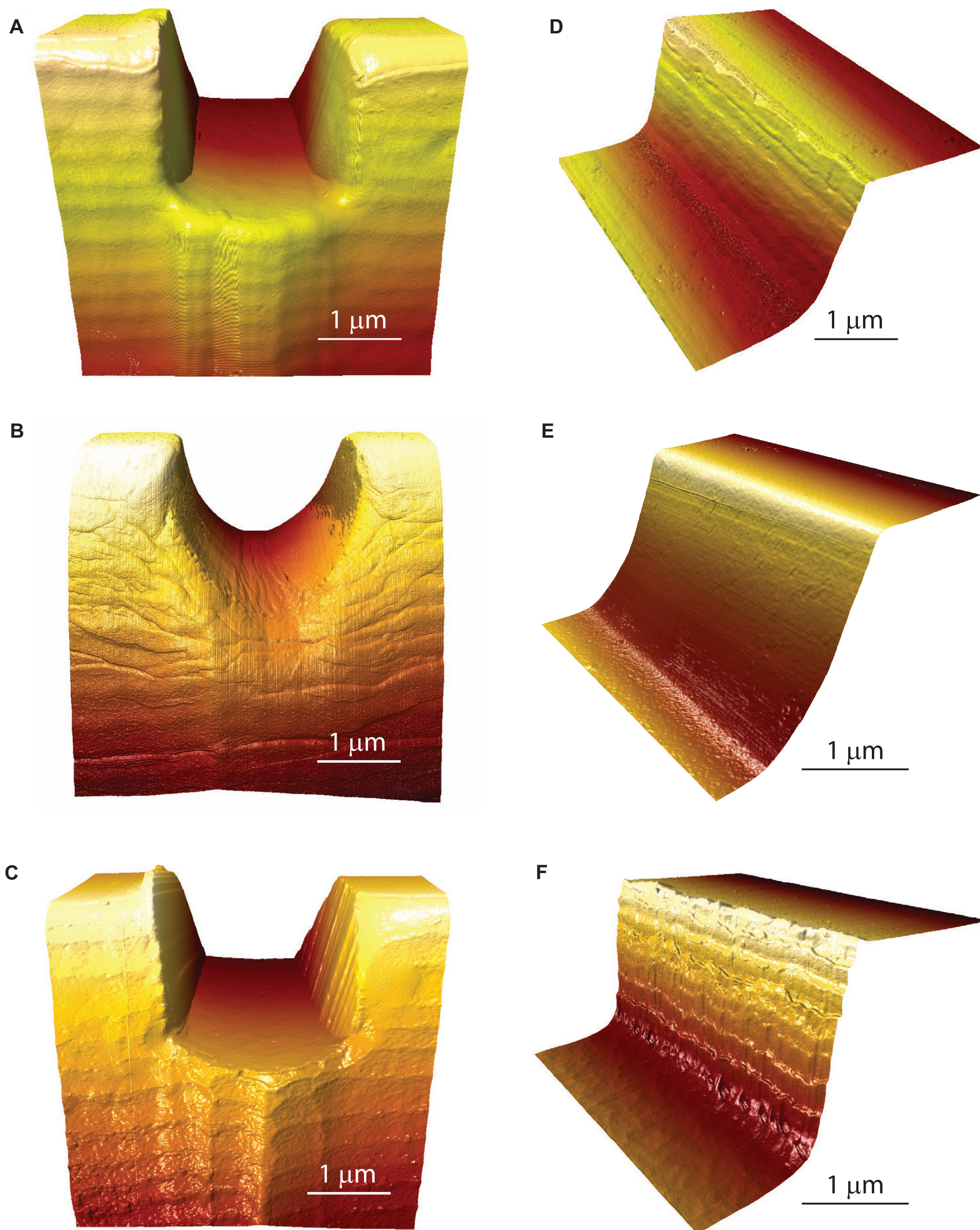

Figure 2.21: AFM images of the patching orifices from three different polymer devices. (a) 3D AFM image of the patching orifice and of the sidewall (type A). (b) 3D AFM image of the patching orifice and of the sidewall (type A). (c) 3D AFM image of the patching orifice and of the sidewall (type A without smoothing steps).

of 5 nm to 10 nm. Measuremetns were carried out by Dr. Jørgen Garnaes at the Danish Institute for Fundamental Metrology (DFM). A customized aluminum holder was designed and machined in order to keep the sample in tilted position during the scan. The angle of tilting was 50 degrees. The images taken across the patching channel were line-wise corrected by a second order least mean squares fit in order to remove the (semicircular)

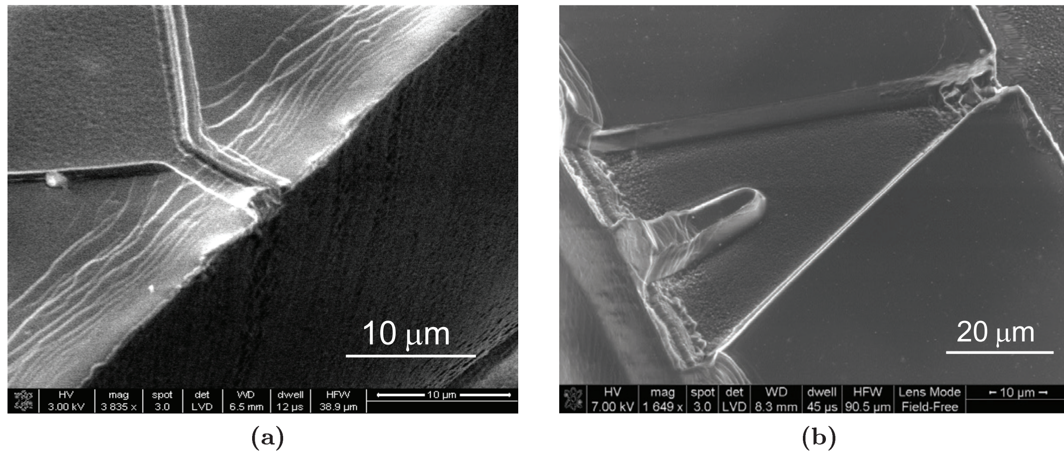

(a) (b)

Figure 2.22: SEM micrographs of the capturing channel in the molded polymer chip. (a) In earlier samples, the orifice was blocked by accumulation of material during the demolding. (b) A circa 5 µm wide patching channel was successfully molded but many defects were present.

shape of the profile. This effect was particularly noticeable for type B devices, for which the roughness before the correction was largely dominated by the overall semicircular shape. The images on the bottom of the channel were taken along the channel and so they were not corrected.

2.4.2 Development of the silicon master

Initially the fabrication process for the shaping of the silicon master was designed to be as simple as possible and it enrolled a standard Bosch process for etching of the deep channels. Photoresist could be used as masking material and no hard masks were required, making the process flexible and much faster. Unfortunately, the polymer parts replicated from this master showed scratches of material from the sidewalls of the carrier channels that partially or totally blocked the lateral patching apertures, as shown in Figure 2.22a. After this, we performed the etching experiments with a continuous process by using the gases SF_6, O_2 and Ar, and the etching of the shallow channels was postponed to the end of the process by using a 300 µm thick oxide layer as mask. The orifices were successfully replicated from this master but defects were reported at the bottom of the shallow channels due to the very long etching times required by the thick oxide, see Figure 2.22b.

Therefore we employed a thinner oxide layer and this gave a smooth tapered sidewall (>90°) and a mask undercut of about 4 µm, see Figure 2.23. The result was a perfect replica of the microstructures without any damages during the molding. The entire process is reported in Table 2.5. The taper deviation at the interface between the oxide mask and the etched substrate considered to be mainly caused by the difficulty of the etch gas to reach regions close below the mask [82]. This curvature generated challenges in terms of demolding when structures shallower than 4 µm had been structured. A device for capturing of single cells with 4 µm deep apertures was made from these polymer chips [34]. SEM micrographs

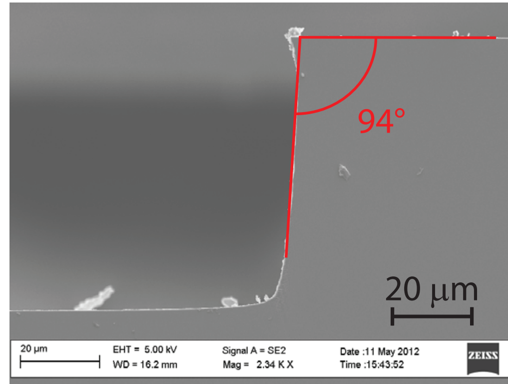

Figure 2.23: SEM micrograph of the cross-sectional profile of the deep channel from a cleaved wafer processed with continous $SF_6/O_2/Ar$ plasma isotropic etch process. The sidewall is positively tapered with an angle of 94°, while the underetching is about 4 µm.

Table 2.5: The table shows the process parameters for origination of the silicon master for the single-cell capture device.

Process	Parameters
Oxide deposition	1050°C dry oxidation ; t = 90 min + 20 min annealing
Spin coating	- HMDS vapor deposition - 2.2 µm AZ5214E; pre-bake: 90 °C for 90 sec
Photolithography	- hard contact mode, front side alignment W/A= 7 mW/cm2; t = 9 sec - AZ351 developer; t = 90 sec
Oxide etch (shallow channels)	CF4/CHF3= 14/26 sccm; t = 210 sec; WRF = 60 W; P = 100 mTorr
Spin coating	- HMDS vapor deposition - 6.2 µm AZ5214E; pre-bake: 100 °C for 100 sec
Photolithography	- hard contact mode, front side alignment W/A= 7 mW/cm2; t = 30 sec - AZ351 developer; t = 300 sec
Oxide etch (deep channels)	CF4/CHF3= 14/26 sccm; t = 210 sec; WRF = 60 W; P = 100 mTorr
Si DRIE (deep channels)	SF6/O2/Ar = 180/160/100; P = 246>>91mT, coil 2.8kW, platen (HF) 170>>215W, t = 2:40 min
Si RIE (shallow channels)	SF6/ O2 = 32/8 sccm; WRF = 30 W; t = 4 min; P = 80 mTorr
Oxide removal	BHF bath; t = 3 min

of the capturing orifices are shown in Figure 2.24. To achieve smaller and in particular shallower (2 µm) apertures needed for patch clamping, the process was modified as it was presented in this chapter.

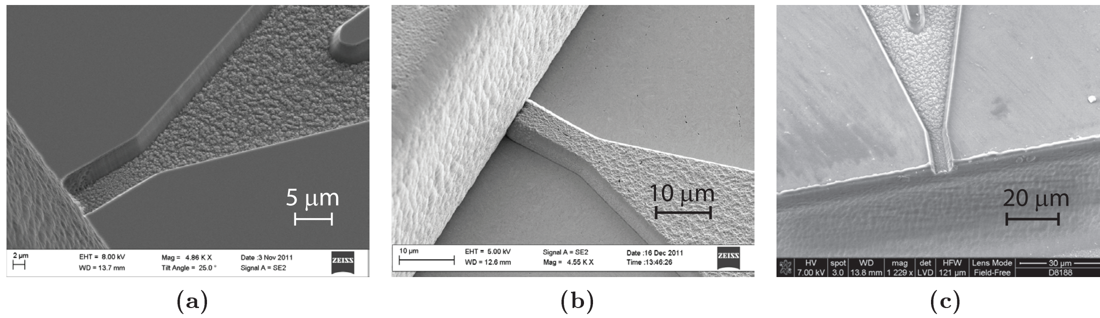

(a) (b) (c)

Figure 2.24: SEM micrographs of the micro sized apertures in the single cell capture device. Silicon master (a), electroplated nickel insert (b) and molded polymer part (c).

2.5 Conclusions

We have developed and demonstrated a method for thermoplastic materials replication that we believe is suitable for prototyping, and also directly applicable to a large-scale production. We used a standard commercial injection-molding machine to demonstrate it. This method, termed DEEMO, was employed to produce multi-level all-in-polymer devices for capturing of single cells. It enables the direct etching of the silicon substrate, and exploits the large MEMS tool box for Si microfabrication. Using dry etching techniques, multi-level microfluidic systems can be structured in silicon and then replicated in thermoplastic polymers with high accuracy. We have also proposed technical solutions to challenges during molding by achieving slightly positive tapered sidewalls. Smoothing oxidations were employed in order to reduce the surface roughness in the inside of the channels after the etching processes. An effective reduction was confirmed by AFM investigation. UV-assisted thermal bonding was found as a good process to ensure strong seals of the microfluidic channels in the molded parts.

Chapter 3

Ion channels recordings on an injection molded polymer chip

Chips fabricated as described in Chapter 2 were used for cell testing. After packaging into chips, they were tested with HEK cells expressing $Na_v1.7$, a voltage-gated sodium channel appropriate for benchmarking studies. The experiments were carried out at Sophion Bioscience A/S, Ballerup. The experiments were designed to explore current-voltage (IV) relationships for the activation and the inactivation of $Na_v1.7$ channels and their sensitivity to a local anesthetic, lidocaine. Both IVs and lidocaine dose response curves obtained from the injection molded polymer device were benchmarked against the commercially available QPatch^{TM} system from Sophion Bioscience A/S. In this chapter, we provide the description of the device functionality and results of benchmarking tests against existing state-of-the-art method. A manuscript about this work is ready to be submitted.

3.1 Recording set-up and cells

For the experiments shown in this Chapter, the cells were prepared by technicians at the cell laboratory at Sophion Bioscience A/S. In patch clamping recordings, the quality of the cells is equally important for successful results as is the fabrication of a fully functional device. Therefore, we decided to commint the cell harvesting to skilled people.

The set-up used for the experiments was modified from a set-up for manual patch clamping, where micropipette and micromanipulator were removed and replaced with the recording box containing the polymer device. The set-up consisted of an inverted microscope, an amplifier and a pressure controller connected to a computer.

3.1.1 Cell culture

Over the past years, scientists at Sophion Bioscience A/S have developed a way to culture cells to be specifically used for patch clamp recordings. The culture procedure is reported

here with the courtesy of Mette T. Christensen. We tested voltage gated sodium channel $Na_v1.7$ were expressed in Human Embryonic Kidney 293 (HEK293) cells. The cells were provided by SB Drug Discovery, Scotland. The cells were grown and maintained under standard culture conditions at 37 °C and 5 % CO2. The cells were cultured in T175 culture flasks (Nunc A/S) to maximum 80 % confluence in high glucose Dulbecco's Modified Eagle Medium (DMEM, Sigma-Aldrich D0819) supplemented with 10 % fetal bovine serum (FBS, Sigma-Aldrich F2442), 2 µg/ml blasticidin S (Sigma-Aldrich 15205) and 600 µg/ml geneticin (Sigma-Aldrich G8168). The cells were sub-cultured for two weeks before reaching a stable growth pattern and then used in the experiments. For sub-culture, the culture medium was removed and the cells washed with phosphate buffered saline (PBS) without calcium chloride and magnesium chloride (Sigma-Aldrich D8537). Trypsin/EDTA (Sigma-Aldrich T4174) was added to the culture flask and the flask incubated at 37 °C for 2 minutes. Medium was added to the flask and the cells re-suspended and placed in a new mother flask. The day of the experiments, the cells were treated differently. The culture medium was removed and the cells washed with PBS without calcium chloride and magnesium chloride. Detachin (VWR) was added to the culture flask and the flask incubated at 37 °C for 5 minutes or until the cells showed a round shape indicating detachment from the flask surfaces. The cells were re-suspended in serum-free CHO medium (Sigma-Aldrich C5467) supplemented with 25 mM HEPES (Sigma-Aldrich H0887), 100 ug/ml penicillin/streptomycin (Sigma-Aldrich P4333) and 0.04 mg/ml soy bean trypsin inhibitor (Sigma-Aldrich T6522). Cell density and viability was determined by diluting an aliquot 1:2 in Trypan Blue (Sigma-Aldrich T8154) and performing a cell countusing the dye exclusion method in a hemocytometer. Cell concentration in the suspension was 2-3 M/ml. After being harvested, cells were maintained on a rocking table in order to avoid formation of clusters. Cells rested for at least one hour before being used in the experiments.

3.1.2 Solutions and compounds

The intracellular electrolyte solution contained (in mM): 135 CsF, 1/5 ethylene glycol tetraacetic acid (EGTA)/CsOH, 10 mM HEPES and 10 NaCl. The pH was adjusted to 7.3 with KOH and osmolarity to 320 mOsm with sucrose. The extracellular electrolyte solution contained (in mM): 1 $CaCl_2$, 1 $MgCl_2$, 5 HEPES, 3 KCl, 140 NaCl, 0.1 $CdCl_2$ and 20 TEA-Cl. The pH was adjusted to 7.3 with NaOH and osmolarity to 320 mOsm with sucrose. All chemicals were purchased from Sigma Aldrich. Both solutions were stored in the fridge at 4 °C and vacuum degassed for 20 minutes before use. Lidocaine hydrochloride monohydrate (Sigma Aldrich L5647) was dissolved in dimethyl sulfoxide (DMSO) to give a 100 mM stock solution kept in the freezer. Subsequent dilutions were performed in extracellular electrolyte solution and store in the fridge.

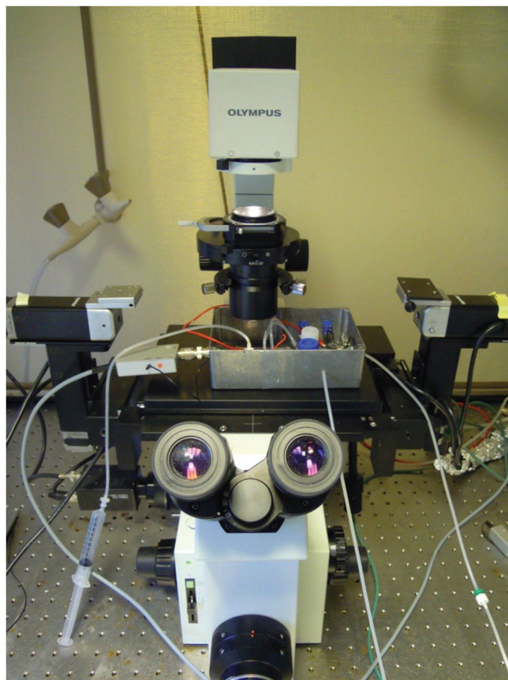

Figure 3.1: Inverted microscope with the recording box in place during the experiments.

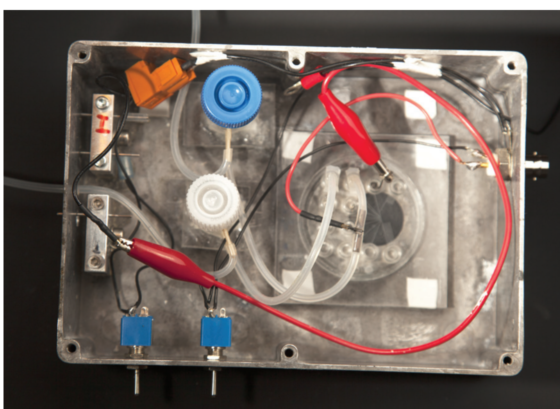

Figure 3.2: Polymer device inserted into the recording box with electrodes and connections to the two reservoirs.

3.1.3 Instrumentation

The device was mounted into a customized aluminum box and positioned on the stage of an Olympus IX70 inverted microscope located inside a Faraday cage, as shown in Figure 3.1. The recording box, shown in Figure 3.2, was set-up with two reservoirs that contain intracellular solution and electrodes and wires for connecting the device to the head of the amplifier. To start, the device was primed with the electrolyte solutions. This operation was done on a laboratory bench before inserting the device into the recording box. An illustration of the layout of the microfluidic device with numbered inlet/outlet ports is shown in Figure 3.3.

First, a 1 ml syringe was plugged into port 8 and a gentle pressure was applied until

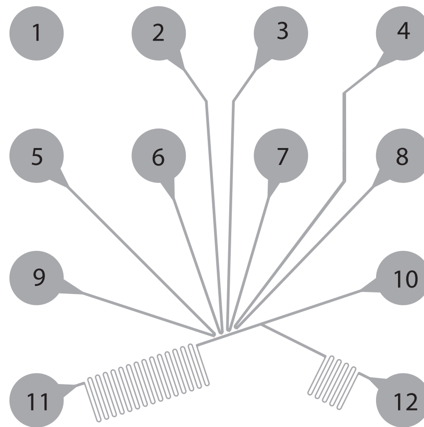

Figure 3.3: Layout of the microfluidic device with numbered inlet/outlet ports.

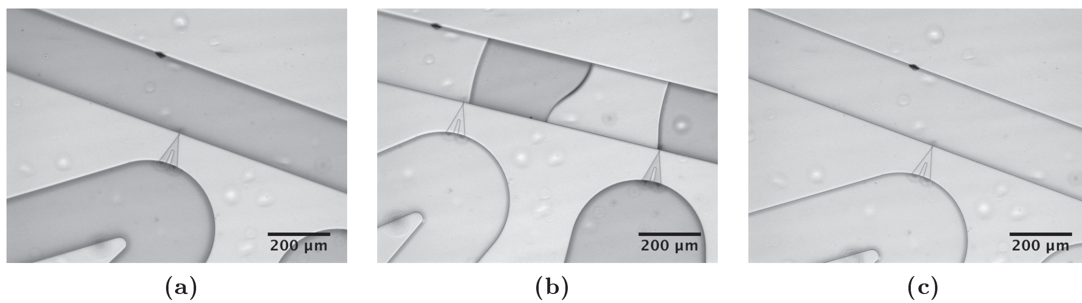

(a) **(b)** **(c)**

Figure 3.4: Sequence of images showing the priming of the polymer device with electrolyte solution before experiments with cells. (a) All channels are empty before priming. (b) Intracellular channel is completly filled and extracellular side partially filled after priming with intracellular solution. (c) Also the carrier channel on the extracellular side is filled.

the solution filled up the connected port 4. Then a second 1 ml syringe was plugged in port 4 and pressure was applied to both syringes at the same time. This operation was carefully repeated for the other three capturing channels (syringe in port 7 and 3, 6 and 2, 5 and 9). Then the device was moved under the microscope in order to verify that some of the intracellular solution could be found in the extracellular channel, indicating that the solution had successfully perfused through the patching capillaries. Finally, the cell carrier channel was filled with extracellular solution by using a 1 ml syringe plugged in Luer 10. Figure 3.4 shows a sequence of images for the priming of one of the patching channels: all channels are empty before priming (Figure 3.4a), the intracellular channel is completely filled and the extracellular side is partially filled after priming with only intracellular solution (Figure 3.4b), and both channels are filled (Figure 3.4c).

The device was mounted into the aluminum box and the box relocated on the microscope stage. The channel chosen as recording channel (port 8 and 4) was connected through the reservoirs to an external custom-made pressure controller build from a piezo-valve terminal from Festo and controlled with Labview software (National Instruments). A slight positive pressure of 4 mbar was applied from both port 8 and 4 to the patching channel to prevent

contamination of the aperture when cells were introduced. The reservoirs were employed because a first series of experiments showed formation of air bubbles when suction was applied. Air bubbles must be avoided in these experiments and once they have formed, they are very difficult to eliminate and the chip must be discarded. The use of reservoirs prevented the formation of the air bubbles. The possibility of monitoring what happens in the device during the priming and the suction is one of the major advantages of the lateral approach and the transparent polymer substrate. When planar apertures in silicon substrate are used, the only way to monitor what is happening at the apertures is measuring the variation of electrical resistance across the hole. Thus, in silicon devices the detection of air bubbles is difficult and this can lead to false results.

Chlorinated silver wires (Ag/AgCl) served as the recording and reference electrodes. They were located across the orifice and connected to the headstage unit of the patch clamp amplifier, as shown in Figure 3.6. Specifically, the sensing electrode was inserted into the tube connecting port 4 to the reservoir while the reference electrode was directly inserted into the bath in port 10. An illustration of the set-up is shown in Figure 3.5. Only when everything was ready and while maintaining slightly positive pressure at the aperture intended for patching, the cells were taken with a 1 ml syringe from the flask, they were introduced into the inlet port 10 and transported by convective flow applied by a 10 ml syringe connected to the other end (port 11). After waiting a few seconds, a single cell was captured at the hole by applying suction (negative pressure of 400 mbar from port 8, +4 mbar from port 4) to the patching channel, Figure 3.7. Conveniently, one of the unused patching capillaries was employed for perfusion of lidocaine by using a 1 ml syringe connected to the corresponding Luer port 6.

3.1.4 Experimental settings

Recordings were carried out using a HEKA Patch Clamp EPC 9 amplifier (HEKA Electronics) at room temperature. Pulse software (v 8.53, HEKA Electronics) was used for data acquisition. Electrodes were electrically connected to the EPC9 head stage mounted on the customized aluminum box and the chip resistance was monitored by applying a 10 mV test square pulse for 10 ms. The amplifier offset potential was zeroed before patching the cell and the holding potential held at -90 mV. Response currents were sampled at 10 kHz and filtered at 2,9 kHz with a 4 pole Bessel filter.

Once one of the cells was trapped, the suction of -400 mbar was maintained for about 20 seconds and then reduced to -30 mbar. The resistance across the aperture was continuously monitored by applying a 10 mV pulse for 10 ms. At this stage, the resistance was typically between 100 and 200 MΩ. Some of the cells showed whole-cell configuration immediately after patching. Otherwise the whole-cell configuration was achieved by applying suction pulses (from -30 mbar to -400 mbar) and electrical pulses combined. The achievement of whole-cell configuration was verified by depolarizing the cell. Eventually the cells reached

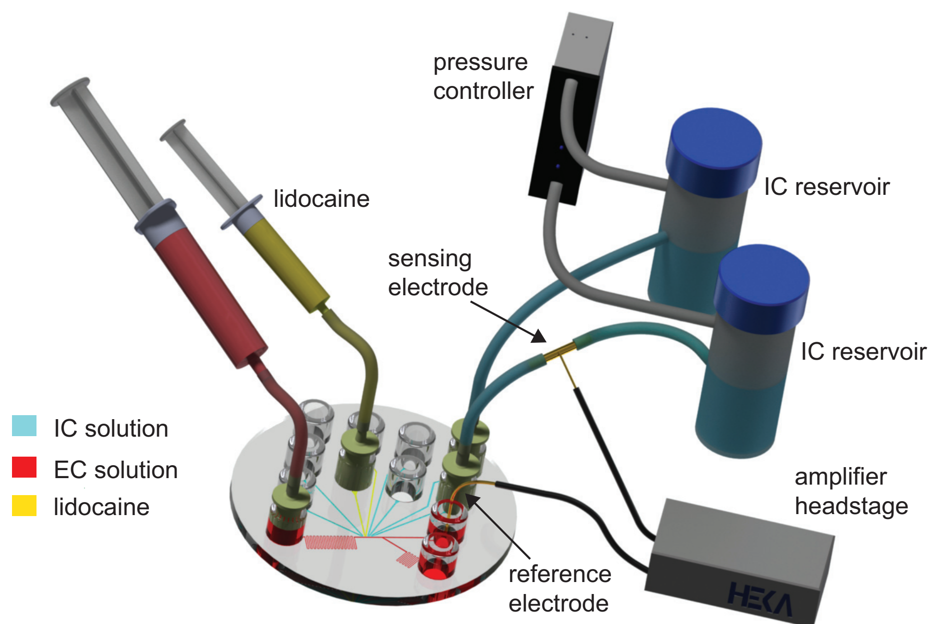

Figure 3.5: Illustration of the set-up used for the recordings. The polymer device is connected to two intracellular solution reservoirs and then to the pressure controller. Ag/AgCl electrodes are connected to the headstage of the amplifier. Syringes are used respectively to tranport cells from the inlet to the patch zone and to perfuse lidocaine through one of the lateral apertures.

whole-cell configuration and the resistance gradually increased over the following minutes during the experiments.

3.1.5 Voltage protocols

For IV relationships experiments, a protocol with incremental steps of +10 mV from -90 mV to +70 mV of 1000 ms duration was used. Steady-state inactivation was investigated at +10 mV for 100 ms after the 1000 ms pre-pulse. Each incremental sweep took place with 5 second intervals. For concentration-response experiments, two consecutive depolarizations to 0 mV respectively of 100 ms and 20 ms duration from a holding potential of -100 mV were used. The two depolarizations were spaced out by 15 ms at holding potential. Similar voltage protocols were used for the experiment with the QPatch^{TM} system.

3.1.6 QPatch^{TM} settings

The experiments on the QPatch^{TM} were set up using standard assay settings. In brief, cells were positioned with a negative pressure of -100 mbar until a gigaseal was formed. The cell membrane was then ruptured with a negative pressure pulse of -250 mbar in order to get electrical access to the cell membrane. During this process the offset potential, the chip capacitance and the cell capacitance were canceled out. The actual experiment protocol with the relevant voltage protocols and compound additions was programmed in

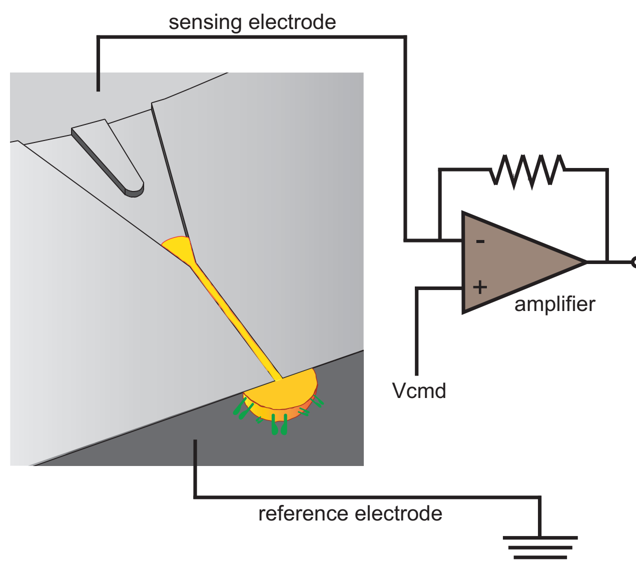

Figure 3.6: Schematic of the patch clamping recording: a cell captured to a patching capillary. Electrodes are located across the orifice.

the Sophion Assay Software and it was executed after whole cell formation was established. QPatch^{TM} data were sampled at 10 kHz and filtered with an 8 pole Bessel filter at 3 kHz.

3.2 Chip resistance and chip capacitance

Chip resistance. As shown in Chapter 2 and reported in Tanzi *et al* [34], injection molding enables high replication accuracy of micro and nano features. The uniformity of the patching channels was confirmed for several devices by the narrow range of chip resistances, the resistances were measured across the 45 µm long patching capillaries with the presence of only the electrolyte solutions. This was 9.4 ± 0.2 MΩ (mean ± Standard Error of the Mean, n = 33) for type A devices and 10.5 ± 0.2 MΩ (n = 14) for type B devices. The devices with semicircular profile (type B) had a slightly larger chip resistance as expected from their smaller cross-sectional area. Both devices showed exactly the same resistance variation. Since the chip resistance is mainly a function of the capillary geometry, its variation is a good indication of variations in channel geometry [83]. The chip resistances are comparable to those reported by Zanetti [22] and Chen [84], however the variation is significantly smaller, indicating a better reproducibility of the present method. However, the chip resistance is significantly higher than the typical 2-4 MΩ access resistance reported for planar patch clamping devices where the holes are tapered on the back side [23]. The Y shaped channel contributes most significantly to the chip resistance while only 10 % is contributed by the rest of the hydraulic paths to the electrodes. The main reason for keeping the capillaries short in the first attempt was indeed to avoid high chip resistances.

Chip capacitance. At the same time the chip capacitance was monitored. This was 11.4

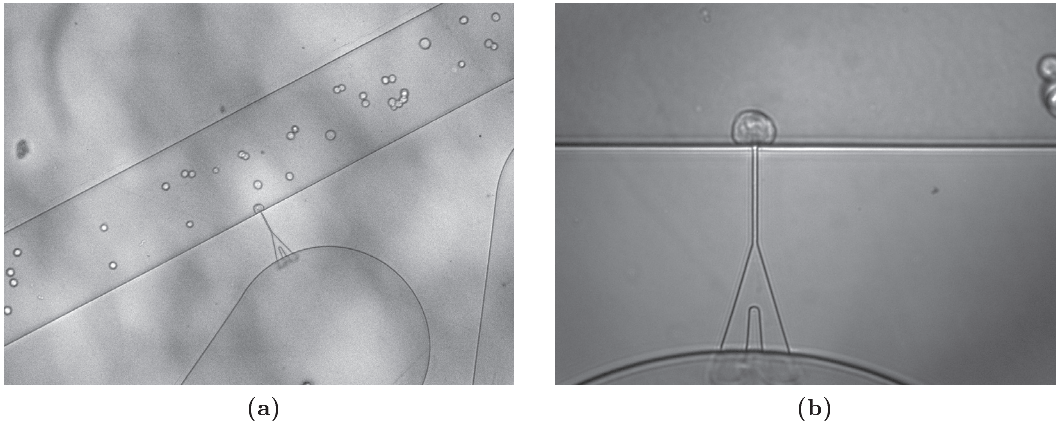

(a) (b)

Figure 3.7: Images of a HEK cell captured at one of the lateral patching channel. (a) Typical cells concentration when the cells were flowing in the carrier channel before being captured. (b) Close-up on the Y shaped patching channel with a captured cell.

± 0.3 pF (mean ± Standard Error of the Mean, n = 33) for type A devices and 11.6 ± 0.5 pF (n = 14) for type B devices. The two devices showed very similar capacitances. For the present device, the chip capacitance can be estimated by using the model of a pair of parallel wires, where, in the proximity of the patching channel, the two deep channels for intra and extra cellular solution are assumed as wires separated by a gap of 100 µm (the Y shape patching channel). Our calculations, using this basic geometrical approximations and the dielectric constant of TOPAS (ε_r= 2.35) [85] yielded a predicted device capacitance of C_{chip}= 10 fF, being much lower than the measured capacitance. From the different order of magnitude, we can then conclude that the capacitance measured during the experiments was due to the connections between the device and the patch-clamp amplifier, while the contribution from the device was negligible. The same observation was reported in one of the first work about lateral patch clamping in PDMS [31]. For comparison chip capacitances for glass or silicon based devices were reported in the order of pF [86, 18].

3.3 Sealing properties

During the experiments, we could observe that the cell membrane tended to protrude a long distance into the patching capillaries right after it was captured. The Figure 3.8 shows a sequence of images taken just before the cell was captured at one of the orifices (Figure 3.8a), immediately after the capturing (Figure 3.8b) and after 20 seconds (Figure 3.8c). The same behavior was previously reported for PDMS devices employing lateral apertures [22, 84], but the authors did not mention the protrusion length.

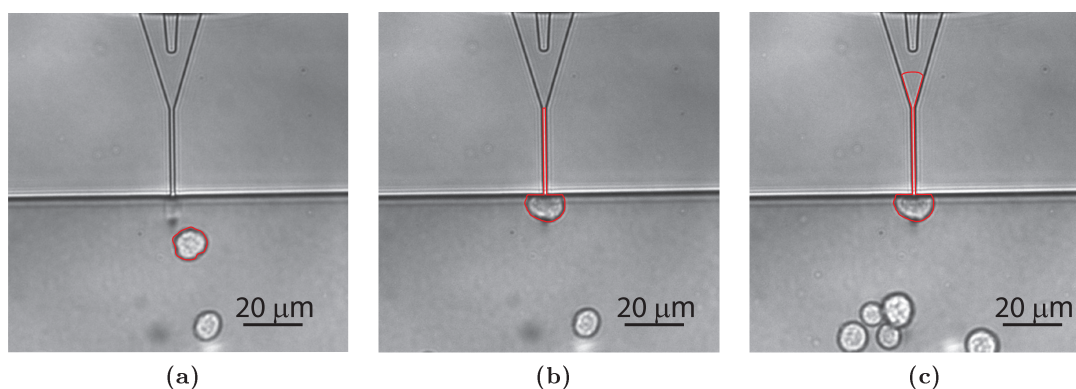

Figure 3.8: Sequence of optical microscope images of a HEK cell captured at one of the patching orifices. The cell membrane is highlighted in red colour. (a) Image taken just before the cell was captured. (b) Image taken immediately after the capturing. (c) Image taken after 20 seconds that the cell was captured. It can be seen that cell membrane tends to protrude a distance of about 50 μm into the patching capillary shortly after being captured.

3.3.1 Lenght of the patching capillaries

In order to find the optimal length of the patching channels, we made the four patching channels with different lengths of the straight part, ranging from 15 μm to 45 μm, as shown in Chapter 2 on page 9. A first series of cell tests showed that a patching channel approximately 10 μm long was somehow too short for establishing a good seals. Sometimes the cell passed through the shallow channel and disappeared into the intracellular solution at the other side. Therefore, channels longer than 10 μm were adopted here. The optimal length of the straight capillary fraction appeared to be the largest we had on the chip (45 μm), while shorter capillaries did not show good sealing properties. We need to mention that from the moment when the longest channel was found to work successfully, this channel was used in the rest of the experiments. Therefore, we cannot provide any statistical evaluations for the shorter capillaries, beside report the evidence that longer channels worked better and thus they are preferable. This indicates that formation of high seals must occur due to the interactions between the cell membrane and the polymer surface along the whole length of the patching capillary and not only in the proximity of the orifice. The length of the patching capillary was therefore indicated as one of the factors which influence the quality of the seal in these devices.

3.4 Gigaseal

For any type of patch clamping experiments there are two key factors in order to achieve successful results: formation of a good and stable seal, preferably gigaseal, and achievement of whole-cell configuration. Both are fundamental and the combination of the two allows for high quality ion channels recordings. Obtaining high seal without perforation of the cell membrane in whole-cell mode would not reveal the presence of ionic currents. On

the other hand, achievement of the whole-cell configuration but with a loose seal would introduce a large leak current making the recording useless.

3.4.1 Gigaseal frequency

In our experiments, of 47 HEK cells captured, 19 cells (40 % of the total) allowed for whole-cell access with seal resistance of at least 100 MΩ and of those 7 (15 %) were gigaseals. A success rate of 15% is thus attributed to our experiments. The rest of the cells showed either no whole-cell achievement or seal resistance below 100 MΩ. More precisely, tests were carried out on devices both having patching capillaries with rectangular (type A, n=33) and semicircular (type B, n=14) profiles. As shown in Table 3.1, both device types showed very similar sealing capability and ability to achieve the whole-cell configuration in a range of seal resistances. Both profiles also have similar gigaseal frequency. The exact confidence interval for gigaseal frequency was calculated with the Clopper-Pearson method [87] and is given at a confidence level of 90 %. The confidence intervals for gigaseal frequency were also comparable for the two profiles. During cell experiments it was noted that high resistance seals could only be achieved on longer channels, shorter channels were also tested with cells, but they all failed to deliver quality seals. Importantly, for the 45 µm long channels each cell showing a seal resistance above 250 MΩ also allowed for whole-cell recordings. It was observed that tight seals appeared gradually after the whole-cell configuration was established, eventually reaching gigaseal during a period of 10-20 minutes. This is in contrast with traditional patch clamping where first a gigaseal is obtained and then the cell in perforated in whole-cell mode. The passage from cell-attached to whole-cell is often responsible for a significant drop in the seal resistance.

Table 3.1: The table shows the number of cells that were successfully sealed and perforated into whole-cell configuration. The numbers include the cells with higher seals. In parenthesis, the number of cells that were successfully perforated into whole-cell configuration. The exact confidence interval for the gigaseal frequency was calculated at a confidence level of 90 % .

Device	Total of cells tested	R < 100 MΩ	R > 100 MΩ	R > 250 MΩ	R > 1000 MΩ	Gigaseal frequency	Confidence interval for gigaseal
Rectangular profile (A)	33	14 (9)	20 (13)	8 (8)	5 (5)	15%	6% - 29%
Semicircular profile (B)	14	6 (4)	8 (6)	3 (3)	2 (2)	14%	3% - 38%

Achievement of the whole-cell configuration was verified by activation of sodium currents through a depolarization of the cell membrane. The seals had an average lifetime of 30 minutes. Furthermore, it was also observed that the whole-cell configuration with rupture of the patched cell membrane was obtained spontaneously upon cell capture without an intermediate cell-attached state, where electrical access to the interior of the cell goes

through the patched piece of cell membrane inside the pipette in traditional patch clamping experiments. This seems to differ from other systems, both those using traditional pipettes and planar chips, where a drop in resistance when breaking the cell membrane is normally observed.

3.5 Factors for high seal formation

In the literature numerous discussions regarding the importance of various device parameters for high quality seal formation exist, such as the aperture diameter [27], length of membrane protrusion into the microhole [88], smooth edges of the microholes [89], and hydrophilicity of the substrate [27]. These evaluations were done with different substrate materials and capturing geometries and none with thermoplastic polymers. The experiments indicate that long and smooth patching channels and apertures of approximately 4 μm^2 with clean and smooth orifice edges allow for good seal quality. Furthermore, these parameters contribute to an increase in the total contact area between the cell membrane and the polymer surface and therefore the effective contact area seems to be the most critical prerequisite to look at. To support this hypothesis, the topography of the orifices and the inside of the patching capillaries were characterized by atomic force microscopy (AFM), see Figure 2.21 on page 30. The profiles taken across the patching channels revealed the presence of scallops with an average periodicity of approximately 180 nm for type A profile chips as was expected from Bosch type reactive ion etching process employed for origination of the patching channels in the silicon master. The formation of the scallops at the sidewall during the etching process has been described in Chapter 2. As discussed, after filtering the surface roughness of the sidewalls for both the rectangular and semicircular channels was in the range of 1 to 2 nm. The surface roughness R_q of the sidewalls seems to be determined primarily by the smoothing steps that were the same for both. In general, the inside of the patching channel, including the bottom of the channel and the foil, exhibits very low surface roughness R_q of 1 to 2 nm, and it is also here, between the cell membrane and the polymer, the seal is assumed to form.

These findings suggest that the surface roughness inside the patching channel is a second prerequisite for good seal formation. On the contrary, the waviness originating from the scallops does not seem to influence the seal quality. Our understanding is that the cell membrane, which has a thickness of only 5-10 nm, is likely to conform to the shape of the surface waviness, which has a periodicity much larger than the thickness of the cell membrane, but not to the shape of the surface roughness, which has a length scale of few nanometers, leaving a path for the leakage currents. Figure 3.9 shows an illustration of this hypothesis. This effect has been also studied before for pipette tip roughness [90]. Hence, one can hypothesize that low surface roughness in addition to the patch channel length increases the effective contact area between the cell membrane and the polymer surface and thus facilitates the formation of tight seals. Most likely, the large sealing area

required for the polymer patching channels is necessary to assist sealing due to slow van der Waals type interactions between the relatively low energy polymer surface and the cell membrane. The shape of the cross section, either rectangular or semicircular, instead did not influence the capability of seal formation and therefore do not appear to be a critical parameter.

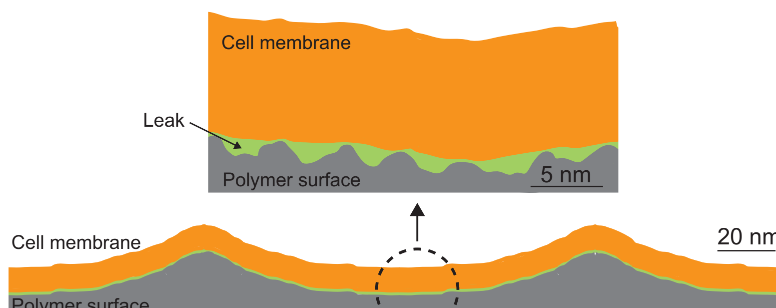

Figure 3.9: Illustration for the hypothesized behaviour of the cell membrane at the interface with the polymer substrate.

3.6 Patch clamp recordings

Electrophysiological cell experiments were designed to record activation and inactivation currents in whole-cell voltage clamp mode from voltage-gated sodium ion channels $Na_v1.7$.

3.6.1 Voltage-gated sodium channels

Sodium channels are proteins that can selectively conduct sodium ions. They play an essential role in the generation of action potentials in excitable cells and they have a key role in pain perception [91]. They can exhibit three different states: one open state and two closed states. At the resting potential, their open probability is extremely low (only very few channels open randomly) [7]. Therefore when they are clamped at negative potentials (-100 mV) no inward sodium current can be recorded. A change in the voltage (upon depolarization of the membrane) causes activation of the channels by a significant increase of the open probability. If the depolarization is prolonged, the open probability, that is time-dependent and not voltage-dependent, is gradually reduced by channel inactivation. The channels are in a closed "inactivated" state, in which they are refractory to further opening until the stimulus has been removed. Once they have been inactivated, sodium channels require repolarization (to -100 mV) and a certain time for recovery before being active again [7]. Activation and inactivation of sodium channels are studied by applying consecutive depolarization steps from a negative potential where the channels are known to be closed. Between each depolarization, the potential is stepped back to the negative holding potential (-100 mV). A typical recording obtained from such a depolarization protocol is shown in Figure 3.10. Peak inward currents are extracted from these recordings

and they are shown as a function of the step voltage in a current-voltage (I-V) relationship, Figure 3.10b.

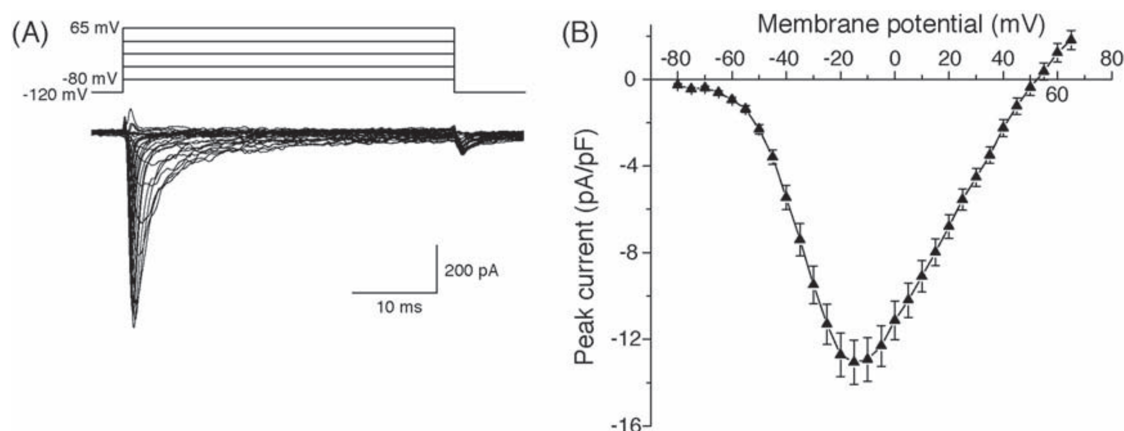

Figure 3.10: Properties of transient inward currents in HEK293 cells. (a) Representative current traces recorded during a 40-ms step depolarization from −120mVto test potentials from −85mV to 65mV in 5-mV increments. (b) Current–voltage plot of multiple datasets such as those in panel A. Values are means±SE of 67 separate determinations with different cells and are normalized to the capacitance (in pF) measured for each cell. Adapted from [92].

3.6.2 Whole-cell recordings

Experiments were designed to record activation and inactivation currents in whole-cell voltage clamp mode for voltage-gated sodium channels. In order to benchmark the performance of our polymer device, the same experiments were repeated on the QPatch™ system. Data taken from both systems are compared in this section. The cells, the electrolyte solutions and the compounds used on the QPatch™, and the polymer chip setup were exactly the same. The QPatch™ was operated by QPatch™ product manager Søren Friis. For the polymer device, raw data were collected with Pulse software from HEKA and exported and elaborated in Origin. Data were leak subtracted in order to compensate for the linear component of the total current recorded and thus leaving only the ionic currents which are assumed to have passed through the ion channels. A +10 mV square pulse of 10 ms from -90 mV prior to depolarization was used to calculate the leak current that was subtracted from the recorded data [93]. A description of leak subtraction is provided later in this chapter.

3.6.3 Current-voltage relations

An example of a family of sodium activation and inactivation currents recorded with our polymer device are shown at the bottom of Figure 3.11 and Figure 3.12. Activation currents were obtained after the start of depolarization pulses from -90 mV to 70 mV while the holding potential was kept at -90 mV for all the experiments. These voltage steps applied

for studying the activation, worked as conditioning pulses for studying the steady-state inactivation. The pulses of 1000 ms were long enough to allow the inactivation process to reach its steady-state level. Next, a 100 ms test pulse was applied to +10 mV. The resulting sodium peak currents represent the portion of sodium channels in the activated and inactivated state, respectively.

Activation currents. We detected inward sodium currents with peak amplitudes of 1-3 nA in all the perforated cells tested in the experiments. Both activation and inactivation currents were detected within few milliseconds after the step was applied. Peaks were typically observed upon depolarization to a potential between -30 and -20 mV. The activation threshold, corresponding to the voltage at which the sodium inward currents started to activate, was found between -50 and -40 mV. At more positive potentials the current amplitude gradually decreased as the electrochemical driving force disappeared. Figure [fig:Inward-currents-from] shows current traces recorded during step depolarization from -90 mV to test potentials from -50 mV to +40 mV, corresponding to the potential interval where the sodium currents were activated. Figure 3.11a shows a representative current trace recorded during the 1000 ms step depolarization from -90 mV to the test potential of -20 mV. In the enlargement, the peak inward currents are shown. At the bottom of the same figure, all traces are grouped together and shown before and after the leak subtraction was applied. From these recordings, the peak current-voltage (I-V) relationship is obtained and it is illustrated in Figure3.13a . The curve shows good agreement with those obtained with the QPatch^{TM} system. However, IV curves from the polymer device had a tendency to shift towards more negative potentials.

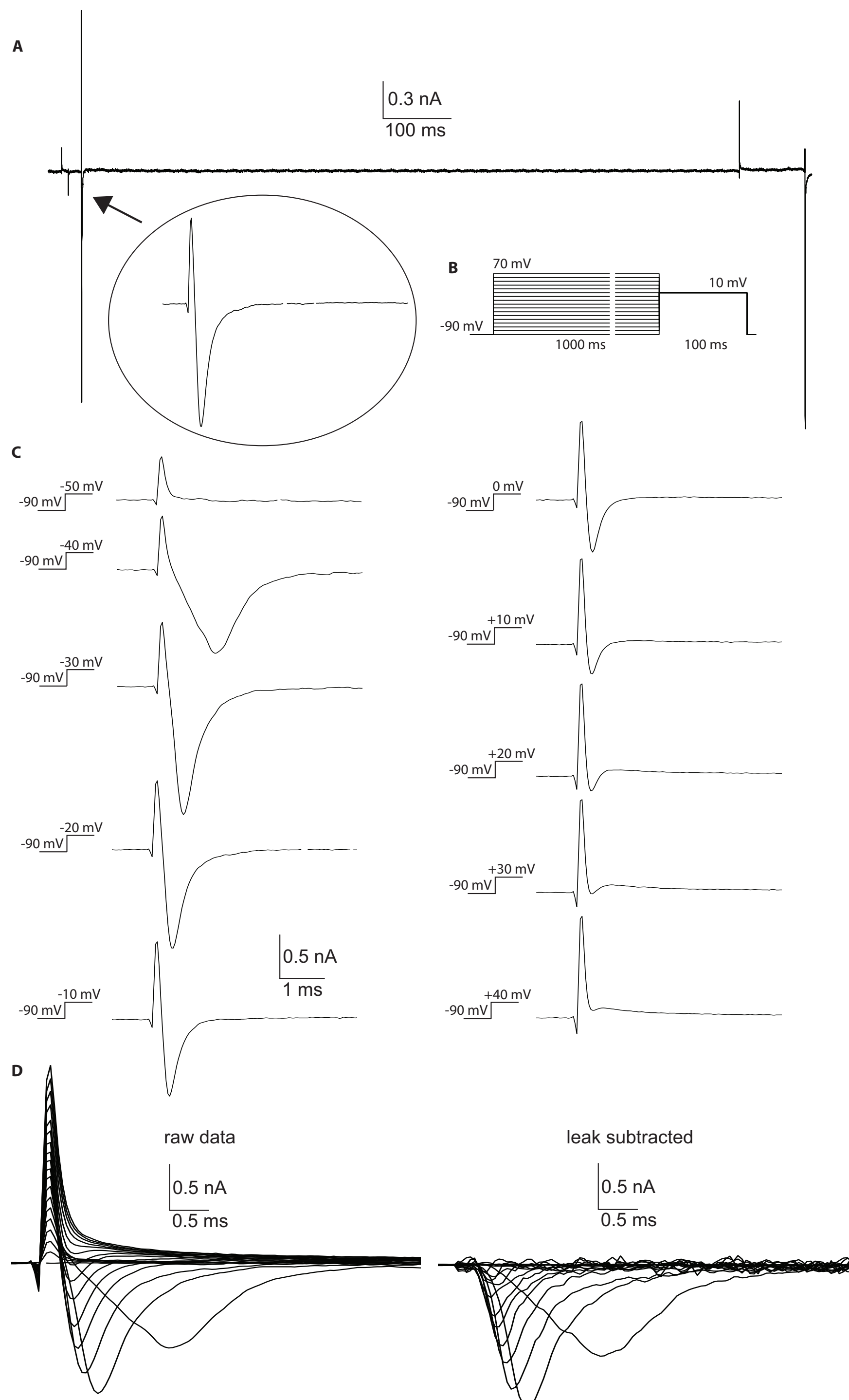

Figure 3.11: Example of inward currents from voltage gated sodium channel $Na_v1.7$ expressed in HEK cells, measured on the polymer device. (a) Representative current trace recorded during a 1000 ms step depolarization from -90 mV to test potential at -20 mV. In the enlargement, inward currents from Na^+ channels. (b) The protocol used for determining activation and inactivation. The membrane potential was held at a holding potential of -90 mV, subsequently shifted to potentials ranging from -90 to 70 mV for 1000 ms, and finally to 10 mV. (c) Inward Na^+ currents (d) A family of Na^+ activation currents in response to depolarization pulses from -90 mV to 70 mV. To the left, the raw current responses are shown, and to the right the data after leak subtraction.

Inactivation currents. From the same voltage protocol we could study the inactivation of the sodium channels. Figure 3.12a shows a representative current trace recorded during the 100 ms step from the conditioning potential of -90 mV to the test potential of 10 mV. In the enlargement, the peak inward current is shown. Figure 3.12b shows currents traces recorded at 10 mV with depolarizing steps from -90 mV to -50 mV, corresponding to the potential interval where the inactivation current could be recorded. At the bottom of the same figure, all traces are grouped together and shown before and after the leak subtraction was applied. From these recordings, a peak current-voltage (I-V) relationship for steady state inactivation was obtained and it is illustrated in Figure 3.13b. The peak current is shown as a function of the conditioning potential. The graph shows the gradual transition from a state where the sodium channels were predominantly closed to a state where they were predominantly inactivated; above -50 mV for the polymer devices. The cut off at -90 mV does not show at which potential the transition starts, but is presumed to be at about -100 mV. As mentioned for the activation currents, the IV relationships obtained for the polymer devices, when compared to IV curves from the QPatch^{TM} system, had the tendency to shift towards more negative potentials. The reason of this shift was not completely understood. It could be attributed either to voltage drops across the higher chip resistance of the polymer device, which was not compensated for, or to differences in offset voltage between the two recording systems or a combination of the two effects. As we shall see in the following, this difference did not influence the pharmacology studies.

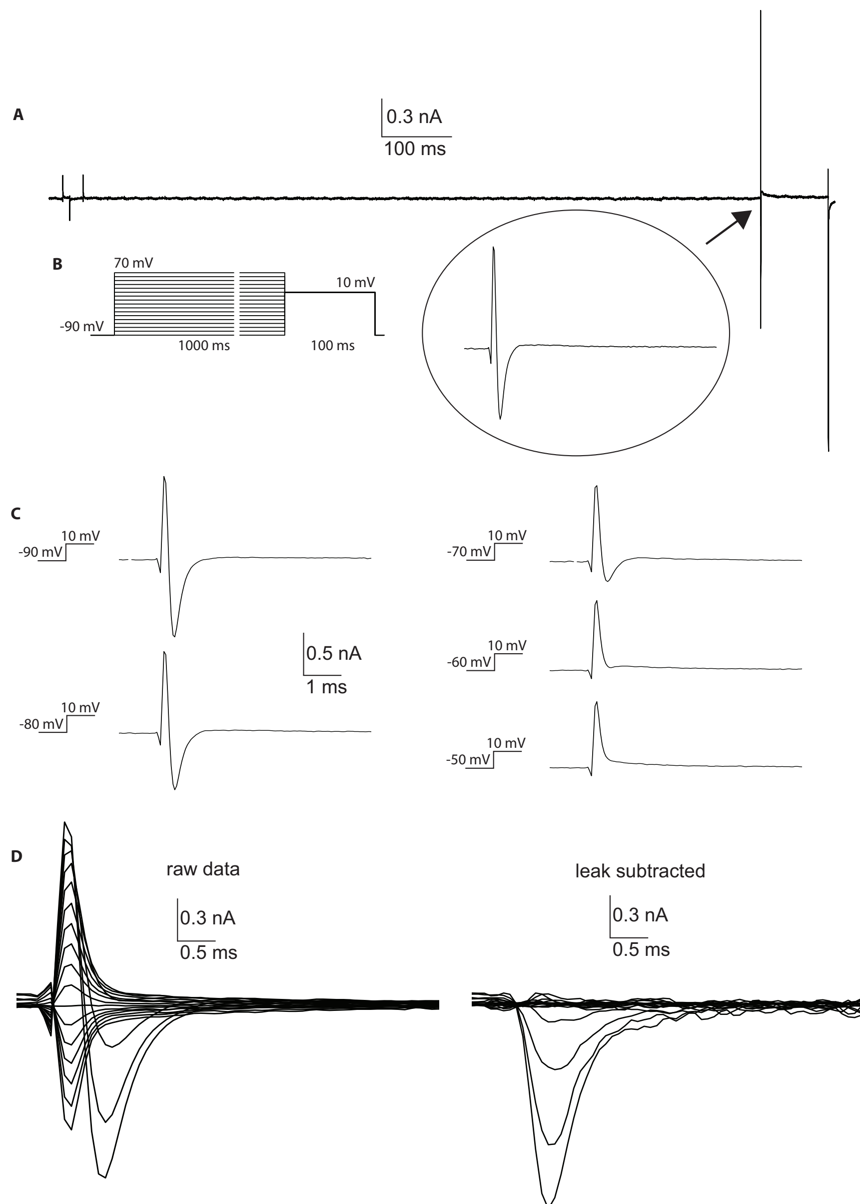

Figure 3.12: Example of inward currents for steady state inactivation from voltage gated sodium channel $Na_v1.7$ expressed in HEK cells, measured on the polymer device. (a) Representative current trace recorded during a 100 ms step at +10 mV from conditioning step at -90 mV. In the enlargement, inward currents from Na^+ channels. (b) The protocol used for determining activation and inactivation. The membrane potential was held at a holding potential of -90 mV, subsequently shifted to potentials ranging from -90 to 70 mV for 1000 ms, and finally to 10 mV. (c) Current traces recorded at 10mV with depolarizing steps from -90 mV to -50. (d) A family of Na^+ inactivation currents in response to polarization pulses from conditioning potenatial to +10 mV. To the left, the raw current responses are shown, and to the right the data after leak subtraction.

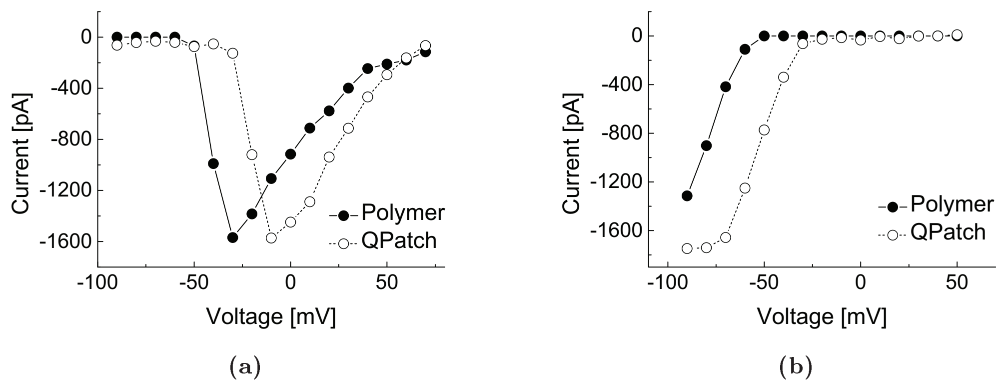

Figure 3.13: Current-voltage (IV) relationships for peak Na^+ channel currents. (a) The activation threshold was -50 mV, and the maximal current amplitude was obtained at -30 mV for the polymer device. The threshold was -30 mV with a maximum at -10 mV for the QPatch^{TM}. (b) The inactivation graph for the Na^+ channel. At potentials more negative than -80mV the channels were predominantly closed, whereas at potentials above -30 mV they were predominantly inactivated for the QPatch^{TM}. For the polymer device, the channels were predominantly inactivated at potentials above -50 mV.

3.6.4 Leak subtraction

The total current response to a voltage step recorded from a cell in voltage clamp mode comprises two current components: a component with amplitude that has a non-linear dependence on the voltage step and a component with amplitude that has a linear dependence on the voltage step,

$$I_{tot}(t) = I_l(t) + I_i(t) \tag{3.1}$$

where $I_{tot}(t)$ is the total current signal evoked by the depolarizing voltage step V_t , $I_l(t)$ is the linear current amplitude response and $I_i(t)$ is the ionic non-linear current response which is assumed to have passed through the voltage-gated ion channels [93, 94]. The linear current response consists of capacitive currents, associated with the rapid change in voltage, plus a DC leakage current. The leakage current and the amplitude of the capacitive current response are both linearly related to the size of the voltage step. The linear component can be subtracted from the total current by means of a method called leak subtraction, leaving only the ionic current. It is possible to calculate the leak subtraction current $I_{sub}(t)$ produced by a small 10 mV step, in a voltage range where voltage-gated channels are closed (and hence where $I_i(t)$ is zero), and to scale it up with the ratio of the amplitudes of the two stimuli,

$$I_{sub}(t) = I_c(t)\frac{V_t}{V_c} \tag{3.2}$$

where $I_c(t)$ is the current evoked by the 10 mV test pulse amplitude V_c. The subtraction

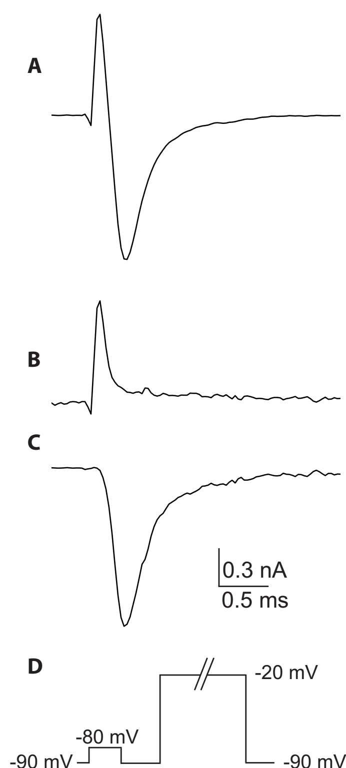

Figure 3.14: Leakage current subtraction using leak subtraction method. (a) Whole-cell current recorded in response to voltage step from -90 mV (holding potential) to -20 mV. (b) Leak current record produced by 10 mV test pulse multiplied by ratio between the two stimuli (70 mV/ 10 mV). (c) Subtracted response of B from A in order to eliminate capacitive current. (d) Voltage protocol.

current $I_{sub}(t)$ can then be subtracted from the recorded signal, leaving the ionic current,

$$I_i(t) = I_{tot}(t) + I_{sub}(t) \tag{3.3}$$

Subtraction of capacitive currents may reveal small current contributions that would otherwise be hard to identify especially the one happening very rapidly after the start of the pulse. Figure 3.14 shows an example of a record of sodium current that has been leak subtracted. The QPatch^{TM} system employed an automated P/N leak subtraction [95] directly implemented in the software. In this method, each depolarization is preceded by a series of N (typically 4) voltage steps of 1/N amplitude of the depolarizing pulse. The voltage steps are activated from a potential at which no voltage-dependent currents are activated [94]. These N traces are the summed together and they are subtracted from the recorded current trace and this will isolate the ionic currents.

3.6.5 Inhibition

Dose–response experiments were carried out to further benchmark the polymer device with a pharmacological application. Lidocaine inhibition of whole-cell sodium currents was

explored in voltage-clamped mode by application of lidocaine concentrations ranging from 30 µM to 1 mM (5 different concentrations). Each concentration was added to separate cells. The ability of lidocaine to bind to sodium channels is state dependent, as lidocaine binds to the sodium channel in the inactivated state only [96]. To explore state-dependency, the cell was depolarized twice at 0 mV for 100 ms and 20 ms respectively, from a holding potential of −100 mV with a temporal separation of 15 ms, see Figure 3.15a. Depolarization was repeated every 5 seconds. Lidocaine response was studied at the start of the second pulse after the resting interval, during which only a portion of the sodium channels were able to recover from inactivation. Figure 3.15b shows a typical recording in the absence of compound where the activation peak 2 was about 80 % of the size of the activation peak 1, used as a reference. When lidocaine was applied, reference peak 1 exhibited a current that was almost unchanged, while peak 2 was substantially reduced. Figure 3.15c shows activation currents from the same cell before and after 100 µM lidocaine was delivered to the cell. The current-time relationship for the peak sodium currents recorded in response to the first (empty circle) and the second (full circle) depolarization is shown in Figure 3.16a. Inhibition is plotted against lidocaine concentration in Figure 3.16b. The amplitudes of sodium currents immediately prior to lidocaine application were set to 100 %. Complete inhibition was observed at 1mM lidocaine, while the inhibition was only 20 % at 30 µM lidocaine which was also the lowest concentration applied. From Figure 3.16a it can be observed that the inhibition produced by lidocaine was reversible within 60 seconds after its perfusion was stopped. For the polymer device, the half-blocking concentration IC_{50} was 119 ± 11 µM. This value is in excellent agreement with the IC_{50} of 152 ± 11 µM found with the QPatch^{TM}. The Hill coefficients were also very similar for the two systems. IC_{50} and Hill coefficient (n) were estimated from best fits to the experimental dose-response data by the Hill equation:

$$\% \, inibition = \frac{[X]^n}{(IC_{50})^n + [X]^n} \tag{3.4}$$

where [X] is the concentration of lidocaine, h is the Hill coefficient, and IC_{50} is the concentration that gave half maximal inhibition.

3.6.6 Perfusion of blocking compounds

Conveniently, one of the unused patching capillaries could be used for perfusion of lidocaine by using a syringe connected to the corresponding Luer port. In order to study the lidocaine dose response on sodium channels, we needed to know the exact concentration that was delivered to the cell during each perfusion. The diffusion coefficient for lidocaine (2.21×10^{-10} m^2/s) was calculated from the Stokes-Einstein equation with the assumptions that lidocaine molecules are comparable to small spherical molecules and that their radius can be derived from the molecular weight (234.4 g/mol). The viscosity of the extracellular electrolyte solution was assumed to be the same as water,

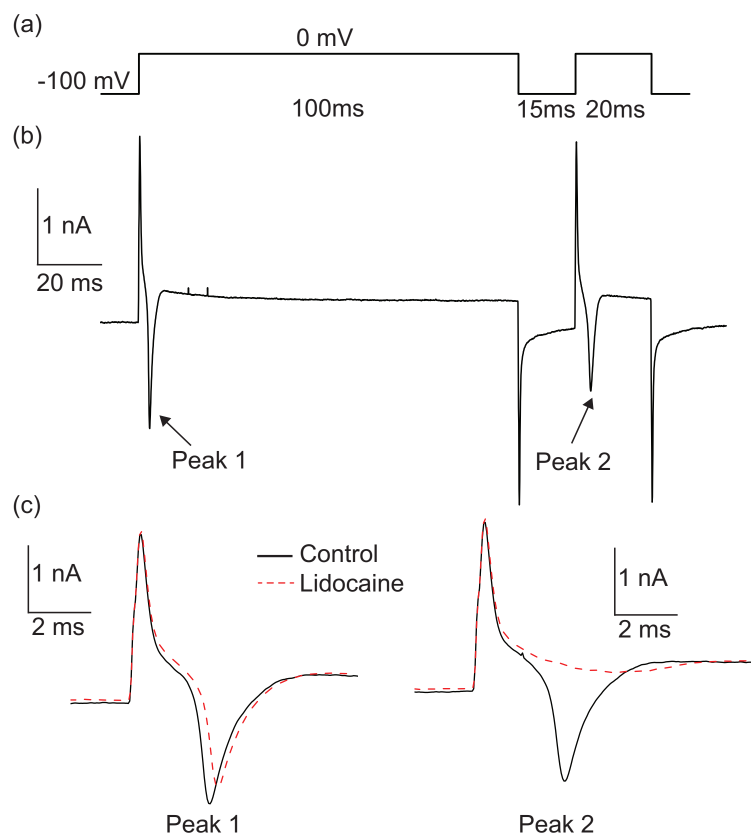

Figure 3.15: (a) Protocol used for determining the concentration–response relationship of lidocaine inhibition on $Na_v1.7$ channels consisting of two depolarizations to 0 mV from a holding potential of -100 mV with an interval of 15 ms. (b) Raw current response from a recording on the polymer device before lidocaine application. Amplitude of peak 2 is about 80 % of the amplitude of peak 1. (c) Raw current response for peak 1 and peak 2 before (black) and after (red) 100 µM lidocaine was applied to the cell.

$$D = \frac{kT}{6\pi r\eta} \tag{3.5}$$

where k is the Boltzman costant, η is the viscosity of water, T is the absolute temperature and r is the hydraulic radius of the lidocaine molecules. In order to evaluate the delivery of lidocaine to the cell, the entire channel geometry was set up as a model in COMSOL®. The flow rates in the main channel and the perfusion channel, respectively, were estimated from both the speed at which the syringes containing lidocaine were operated during the experiments and the observed flow velocity in the main channel. The latter was in the order of 1 mm/s, and from this the flow in the main channel was estimated to be 4 nL/s. The flow in the perfusion channel was estimated to be roughly 20 % higher than this, i.e. 4.8 nL/s. These values were used as boundary conditions in the model at the channel inlets, along with the assumption of steady state flow. The lateral flow was applied for less than 10 seconds. The result from the simulation, shown in Figure 3.17, supports the premise

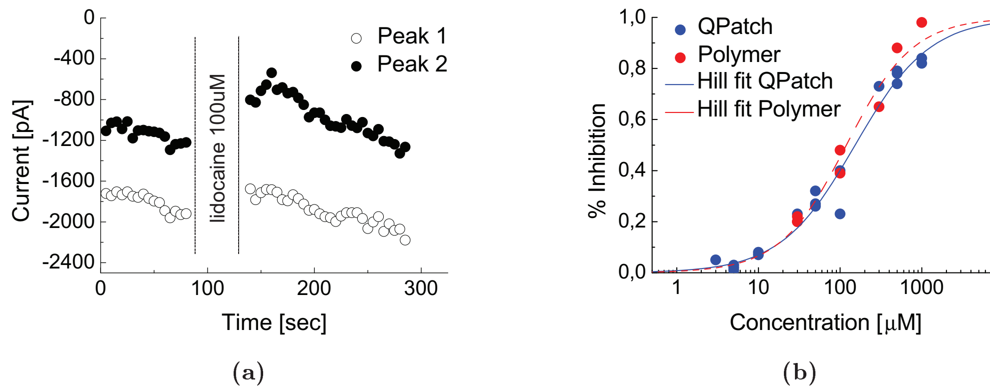

(a) (b)

Figure 3.16: (a) Activation currents for $Na_v1.7$ channels for determining the lidocaine inhibition on $Na_v1.7$ channels. The graph shows values of the current amplitudes of peak 1 and 2 before and after 100 µM lidocaine was applied to the cell. Peak 1 is not affected and peak 2 is reduced by 50 %. (b) Concentration–response relationships of lidocaine inhibition on $Na_v1.7$ channels. Data were fitted with a Hill type equation. IC_{50} was 119 ±11 µM (Hill coefficient n = 1) for the polymer device and 152 ±12 µM (Hill coefficient n = 0.9) for the QPatch^{TM}.

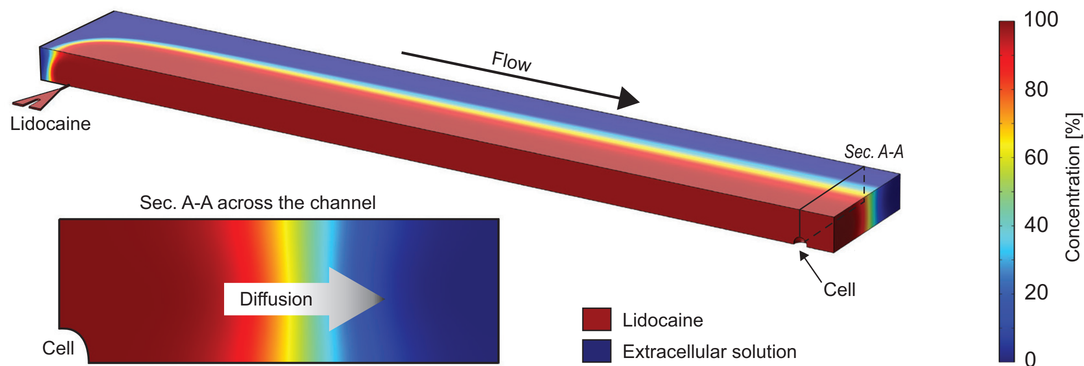

Figure 3.17: Lidocaine (1mM) delivery to the cell being patched simulated in COMSOL®. A lateral flow (in red) perfused into the flow in the carrier channel (in blue). The simulation took account of the diffusion of lidocaine into the extrallular solution. A sectional view across the channel shows how the concentration corresponds to 100 % in the proximity of the cell.

that 100 % of the lidocaine in solution was successfully delivered to the cell. Therefore, the lidocaine concentration delivered to the cell was the same contained in the syringe. The simulation considered a worst case scenario of lidocaine diffusion when a high lidocaine concentration of 1 mM was perfused.

3.7 Conclusions

The purpose of the experiments reported in the this chapter was to validate the injection polymer device by comparing the generated results with those obtained with state-of-the-art QPatch^{TM} system and to demonstrate the ability of the polymer device to generate dose-response data. We have demonstrated that high-quality electrophysiological recordings are possible on the presented polymer device. This was done for the first time on a thermoplastic platform and with no need for any surface modifications or treatments before the experiments. The results demonstrate that polymer devices can provide whole-cell current responses from voltage gated sodium channels and permit accurate analysis of drug potency for state-dependent inhibitors such as for the local anesthetic lidocaine. Moreover, the devices exhibit excellent data quality when benchmarked against the commercially available QPatch^{TM} system. Formation of gigaseals (15 % of the total cells) between the polymer surfaces and the cell membranes was achieved on patching capillaries that allowed for a large sealing area. The length of the patching channel together with the low surface roughness on the inside of the patching capillaries were identified as the most important parameters for good seal formation. We attribute this observation to indicate that a large effective sealing area between the cell membrane and the polymer surface is required to obtain tight seals. The polymer device had the ability to deliver precise concentrations of blocking compounds to the patched cell by perfusion through one of the lateral channels. A simulation in COMSOL® showed that the compound in solution reached the cell without significant loss in concentration.

Chapter 4

Functional characterization of scorpion toxin peptides #9 and #10

In this chapter, the results from the work carried out in collaboration with Dr. Julie Daziel at AgResearch, Palmerston North, New Zealand are presented. The aim of the stay was to acquire the basic knowledge of cell culturing and conventional patch clamping on a well established manual patch clamping set-up. Therefore, this work represents a short walk-away from the rest of this thesis. The inhibitory effects of two new "long chain" toxins (#9 and #10) were studied through whole-cell recordings of BK large conductance potassium channels expressed in human embryonic kidney (HEK) cells. Only one of the two peptides, the #9, showed an inhibitory effect comparable whit that previously reported for other "long chain" toxins. This work, together with the description of the biochemical purification and gene cloning, will be submitted for publication together with Dr. Shunyi Zhu, Chinese Academy of Science, Beijing, China.

4.1 Peptide toxins

Two "long chain" peptides toxin genes were first isolated and purified from the venom of scorpion Mesobuthus Eupeus according to the method described in Gao et al [97]. The peptides are related to the peptide toxin BmP09 [98]. The two toxins were shiped to AgResearch, NZ by Dr. Shunyi Zhu in order to determine whether they inhibit BK large conductance potassium channels. They are name by the supplier peptide #9 and peptide #10. The main reason to believe that the two new toxins could effect the functionality of BK channels was their similarity with the already studied inhibitors of BK channels, BmP09 (BmKAs1) [98]. As shown in 4.1, the two peptides share sequence homology with the toxin BmP09 (BmKAs1). To be more precise, peptide #9 shares 61/66 residues in common with BmP09 and peptide #10 shares 52/66 residues in common with BmP09 (including two deletions).

```
#9              DNGYLLDKYTGCKVWCVINNESCNSEC-KIRRGNYGYCYFWKLACYCEGAPKSELWHYETNKCNGRM
#10             DNGYLLDKYTGCKIWCVINNDSCNSHC-IGSGGYYGYCYFWKLACYCQGAPRSELWHYETNRCRA--
BmKAS           DNGYLLDKYTGCKVWCVINNESCNSEC-KIRGGYYGYCYFWKLACFCQGARKSELWNYNTNKCNGKL
AaHIT4          EHGYLLNKYTGCKVWCVINNEECGYLCNKRRGGYYGYCYFWKLACYCQGARKSELWNYKTNKCDL--
BmP09(BmKAs1)   DNGYLLNKYTGCKIWCVINNESCNSEC-KLRRGNYGYCYFWKLACYCEGAPKSELWAYETNKCNGKM
Lqhβ1           DNGYLLNKATGCKVWCVINNASCNSEC-KLRRGNYGYCYFWKLACYCEGAPKSELWAYATNKCNGKL
```

Figure 4.1: Multiple sequence alignment of #9 and #10 and related toxins from scorpion venoms.

4.2 BK potassium channel

We tested the BK potassium channel expressed in HEK cells. BK potassium channels (aka MaxiK, Slo1 and BKCa) are large conductance ion channels that can be calcium- and voltage- activated. They are expressed in a many tissues throughout the human body and are activated by both membrane depolarization and increase in intracellular Ca^{2+}[99]. BK channels regulate several physiological processes from electrical excitability in neurons and regulation of smooth muscle tone to tuning of auditory hair cells [99].

4.3 Cells and solutions

hSlo α subunit (GenBank accession number U11058) BK channels were stably expressed in HEK cells and grown in Dulbecco's modified Eagle's medium and 2.5 mM HEPES, supplemented with minimal essential amino acids and 10% fetal bovine serum at 37 °C. Cells were plated onto glass coverslips. All the cells used for the experiments shown in this chapter were cultured under the supervision of Dr. Julie Daziel in the cell-culture laboratory at AgResearch, NZ.

The bath solution contained (in mM): 135 NaCl, 5 KCl, 2 $MgCl_2$, 2 $CaCl_2$ and 5 HEPES. The pH was adjusted to 7.4 with NaOH. The pipette solution contained (in mM): 140 KCl, 1 EGTA, 10 HEPES and 1 $CaCl_2$. The pH was adjusted to 7.2 with KOH, giving 1.5 µM free calcium. Both solutions were stored in the fridge at 4 °C. The two peptide toxins were stored in the freezer at -20 °C.

4.4 Electrophysiological recordings of BK channels

Currents were recorded using whole-cell voltage-clamp at room temperature (18-22°C). Pipettes were pulled from borosilicate glass using a 2-stage microelectrode puller from List-Medical and gave resistances of 2-5 MΩ when filled with pipette solution. Data were recorded using an Axopatch 200B and Axon Digidata 1440A digital interface using pClamp 10.2 software from Molecular Devices. Capacitance and series resistance compensation were used. Leak subtraction was applied using a P/5 protocol. Data were filtered at 5 kHz and sampled at 100 µs intervals. The peptides in dried form were diluted in bath solution

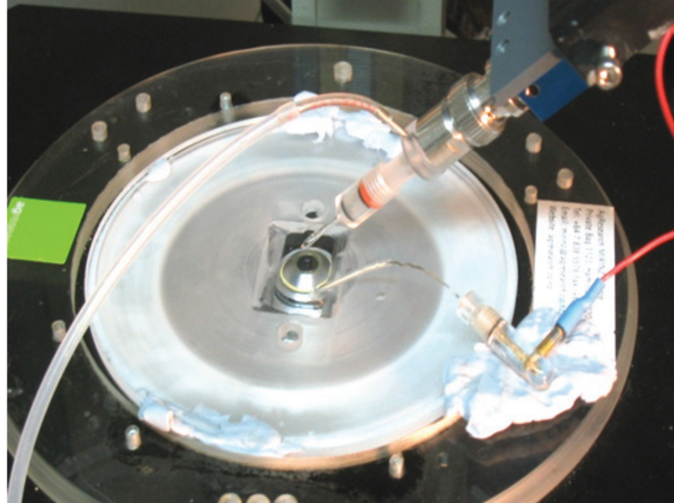

Figure 4.2: Manual patch clamping set-up used for the experiments.

and then applied directly to the bath (2.5 ml volume) as a 1/5 dilution. The known potent BK inhibitor lolitrem B was used in some experiments to check that BK currents could be inhibited under these experimental conditions [100]. A stock of 100 µM lolitrem B was prepared in dimethyl sulfoxide (DMSO) and then was diluted to the appropriate concentration with bath solution. All data are shown as mean ± S.E.M.

4.5 Functional characterization of peptides #9 and #10 on BK channels

Macroscopic currents were recorded from voltage-clamped cells held at −60 mV between pulses. Cells expressing hSlo channels produced robust outward currents in response to activation by depolarising voltages in the presence of 2,5 M free calcium. Upon depolarisation to +100 mV for 50 ms from 20 ms at −80 mV, outward potassium currents of 1–3 nA were routinely observed. Control current responses were recorded every minute for 5 minutes. Only cells that remained stable or did not change by more than 10% over this time were used in experiments. Peptides were carefully applied to the perfusion with a micropette and allowed to diffuse for 1 minute. To monitor the time course of the inhibition, depolarising voltages were applied every minute. When 2 µM of peptide #9 was applied to the bath, the current response to a 100 mV voltage pulse decreased over 10 minutes (Figure 4.3a), or over a range of voltages tested (Figure 4.3c). The mean decrease in response to peptide #9 was a 41 ± 9 % compared to the control current (n = 6). Outward currents first emerged at 0 mV, and they increased gradually at positive potentials, as expected for BK channels. To ensure that the cell was accessible to the peptide, the BK inhibitor lolitrem B was added at the end of the experiment which inhibited the current response by 86 ± 4 % (n = 5). When 2 µM peptide #10 was applied to cells expressing hSlo for 10 minutes, no change in current amplitude was observed in response to a 100 mV voltage

pulse (Figure 4.3b), or at a range of voltages tested (Figure 4.3d). The mean decrease in response to peptide #10 was 5 ± 8 % compared to the control current (n = 6). Lolitrem B inhibited the current response by 91 ± 2 % (n=6). This also confirmed that most of the potassium current response recorded was from BK channels.

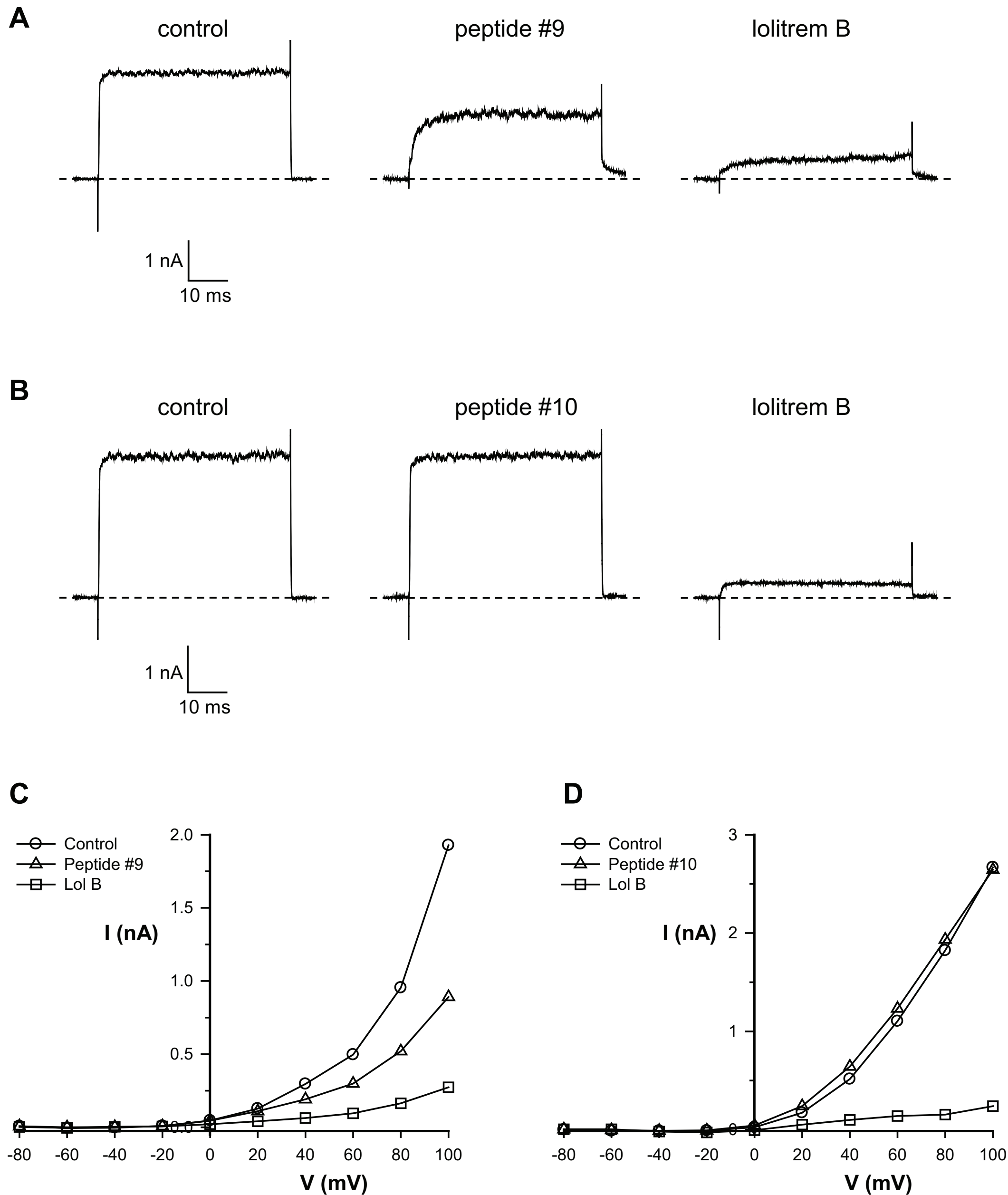

Figure 4.3: Effect of peptides on BK channels. Representative whole-cell recordings from HEK cells expressing hSlo. Currents in response to a +100 mV voltage pulse for 50 ms 10 minutes after addition of 2 µM peptide #9 (a) and peptide #10 (b), followed by 400 nM lolitrem B (Lol B). The effect of peptide #9 (c) and peptide #10 (d) on the current–voltage relationship is shown at voltage steps between -80 and +100 mV for 50 ms. The holding potential was -60 mV. The current is the mean of the last 25 ms of the voltage pulse. The dotted line indicates the zero-current level.

4.6 Conclusions

Only the peptide #9 showed a significant inhibitory effect comparable whit that previously reported for other “long chain” toxins. The peptide #10 did not show any inhibitory effect on BK channels. Since 12 residues (includes two deletions) differ between peptide #10 and BmP09, that also differ from peptide #9, these residues appear to be responsible for the inhibitory effect of the BK large conductance potassium channel reported for BmP09.

Chapter 5

Manufacturing cost

In this chapter, the economy of the manufacturing method and an illustrative study of costs for production of polymer devices are presented. The cost analysis is based on work carried out at the facilities at DTU Danchip. In case of commercialization, the manufacturing framework will change and with it also the production cost per device. There are many reasons to prefer the presented fabrication method over the ones employed currently and we will explain some of those. The technological readiness level of this method is high, while the design presented in this thesis was only aimed for prototyping. Thus, the device could be designed differently for a much smaller unit footprint and higher throughput. Since we have not a thorough knowledge of production theory in industry, a manufacturing expert might find this analysis somehow inadequate. The purpose of this section is not to give a detailed manufacturing cost estimate, but to illustrate the potential low cost of the device.

5.1 Background

Three materials are currently employed for the fabrication of patching apertures capable of gigaseal recordings in APC systems, namely silicon [23], glass [18] and PDMS [22]. All these materials have drawbacks that have encouraged researches to continuously look for innovative substrate materials. Silicon and glass have the main drawbacks in their high cost both to purchase and to machine and their requirement for clean room facilities. On the other hand, PDMS is cheap and versatile. However, PDMS is far from being suitable for mass production and it has issues when used for biological applications such as high permeability for small molecules, non-crosslinked oligomers, and surface diffusion of low molecular weight chains [101].

Advantages of the presented fabrication method derive from both the use of cornered apertures and the employment of injection molding. As shown in Chapter 2, using the lateral approach simplifies the microfluidic integration as only one side of the substrates needs to be shaped. Any other approach requires the creation of at least two compartments

across the patching channel in separate substrates. Thus, the simplest patch clamping device based on a vertical approach is at least composed of three layers, where the middle one includes the micro sized hole and is typically silicon or glass made. On the other hand, injection molding is a fabrication method already widely employed for mass production of polymer components in many engineering fields. Therefore, polymer injection molding will allow the device to be mass fabricated with much simpler transfer of technology from prototyping to production.

5.2 Manufacturing cost: three important factors

Despite their enormous potential, only few Lab-on-Chip based devices have been successfully introduced into the market since this technology was introduced in the nineties [102]. The possible factors responsible for this have been discussed by Dr. H. Becker, Co-founder and CSO microfluidic ChipShop GmbH, in a series of Focus articles published in Lab on a Chip [103, 104]. From his analysis, it seems that the most significant obstacle on the road to commercialize microfluidic devices has been and still is the cost of manufacturing when the device is brought from the prototyping phase, typically carried out at university, to production. Becker has identified three main requirements for inexpensive and successful manufacturing of polymer microfluidic devices on a large scale: Design-to-manufacturability, economy of scale and production yield [103]. Each of these factors will be discussed here in reference to our method.

Design-to-manufacture. Design-to-manufacture can be seen as the number of steps required to assemble a microfluidic device in its final form and it mainly depends on the number of back-end processes such as drilling of access holes, dicing, surface treatment or bonding. All these back-end processes massively influence the overall manufacturing cost. The strength of the presented method is based on a very limited number of back-end processes, being only the bonding with no requirement for alignment.

Economy-of-scale. If we think in terms of production volume, the way this influences the variation of the cost per device is known as economy-of-scale. In general, a good economy-of-scale in a production process is accomplished if the cost tends to decrease when the volume of production increases. In the case of microfluidic systems, the cost per device mainly depends on the cost of raw materials and the cost of the equipments, often referred to as initial cost. The initial cost is a fixed cost that does not depend on the number of parts produced. Figure 5.1 shows a qualitative comparison between economy-of-scale of the three most used polymer replication methods, hot embossing, injection molding, and PDMS casting [103]. Injection molding has the highest initial investment cost for shaping of the nickel insert and acquiring expensive equipments (polymer injection molder and molding tools). However, when the process is applied on a large scale, the cost per part rapidly decreases with the number of parts, becoming the cheapest technology over 10k units, that is also the range we are looking at for commercial APC systems. Therefore,

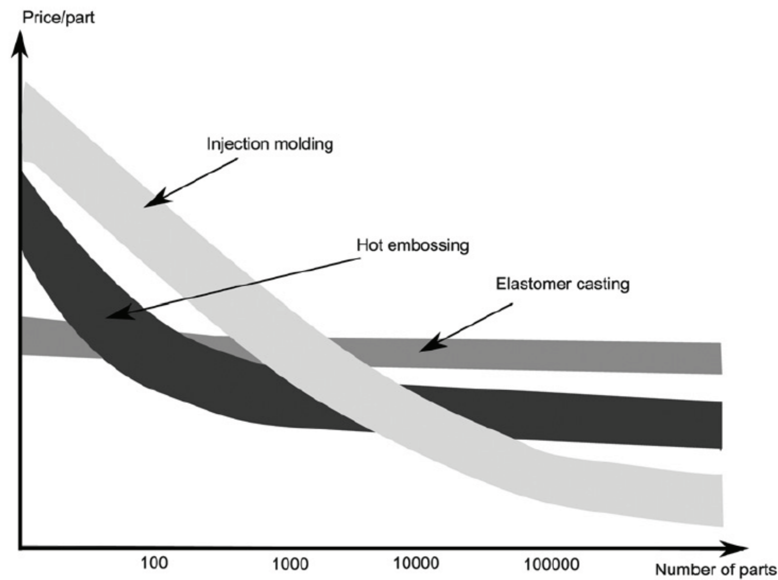

Figure 5.1: Qualitative economy-of-scale comparison for the most common polymer replication processes: Hot embossing, injection molding, and PDMS casting. Adapted from [103].

injection molding can be considered a production technology with very good economy-of-scale. Opposite to this, PDMS casting has very little initial investments (only the master that could also be shaped in silicon with no need for the electroforming step), but the lengthy process time keeps the cost per device constant. PDMS casting thus seems a favorite choice only in the prototyping phase.

Process Yield. The third factor to be considered is the overall production yield of the fabrication process. It consists of the product of the yield of all the individual steps in the process. Three factors have been indicated to influence the yield: the number of process steps, the individual yield for each process step and the number of parts which composes the device [103]. All these factors interplay in defining the overall production yield of the process. Therefore, it is presumable that the simpler the device fabrication and the smaller the number of parts employed, the higher the overall yield will be. The presented fabrication method, with only two steps, seems to have a privileged position here. The shaping of the nickel inserts is part of the initial costs. The only two steps that influence the overall yield are the injection molding and the thermal bonding.

5.3 Production cost estimate

In this section, an assessment of the cost of production for the polymer device using injection molding is presented. With this, we would like to set a range of costs of manufacturing for the polymer device as it has been presented in this work. One has to take into account that if the device will be commercialized, the design and the manufacturing framework will change and with them also the price per device. The price per device is expected to

benefit from a mass production environment. However, those changes would involve in particular the injection molding and the thermal sealing of the chips, while the production of the nickel inserts will remain substantially unchanged. As discussed in Chapter 2, injection molding of micron sized structures is achieved using a molding process known as variotherm [74]. This process requires a cycle time substantially longer than what one can expect from a standard injection molding process (3 minutes with the actual set-up instead of 5-20 seconds). However, we believe that the cycle time could be significantly reduced in an industrial environment by redesigning the mold for smaller thermal mass, and a more localized cooling and heating system. In addition, semi or full automation of the bonding process would significantly increase the productivity.

In the following, we present an illustrative study for the fabrication of nickel inserts, for the injection molding of the polymer parts and for the sealing of the final devices. Costs are based on work that a process engineer with expertise in micro fabrication could carry out at the facilities at Danchip DTU [105]. For the engineer, a standard cost of 600 DKK/hour (including overhead costs) is estimated and is included in the analysis.

Nickel insert. The fabrication of the nickel insert is entirely carried out inside the cleanroom, while the molding and the sealing is done outside. A cleanroom access of 750 DKK/hour with a maximum cap of 20 hours per month needs to be paid. The usage above the cap is charged as 0 DKK/hour. Each machine has a price per hour where indicated. The cost of materials and chemicals (photoresist, chemical etchants, polymer, etc) is already included in the machinery costs. Cost of the silicon wafers is also considered. This analysis is based on batch production. We expect that the production of one batch will not take more than one month and therefore we include one month of salary for the engineer (37 hours/week for 4 weeks) at the end of the analysis.

The process has been divided into three phases and each phase ends with inspection by means of scanning electron microscope. A yield has been assigned to each phase and therefore the number of wafers transferred to the next phase is somehow reduced (e.g., phase one starts with a batch of 20 wafers and finishes with only 12 that will go through

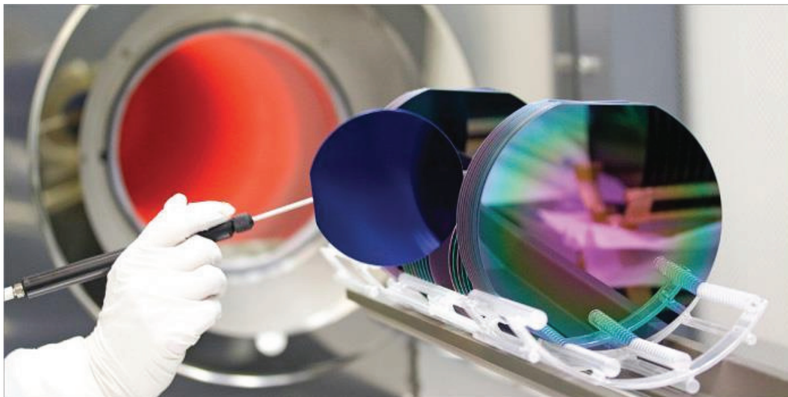

Figure 5.2: DTU Danchip is the national center for micro- and nanofabrication in Denmark. Figures borrowed from http://www.danchip.dtu.dk/.

Table 5.1: Phase one: shaping of the silicon wafers consisting of photolithography, ecthing, cleaning, and oxidations. The estimated overall yield for this phase was 60%.(*) All prices are from "Pricebook for DTU Danchip 2013. Effective: January 1st - 2013" [105]. All prices are in Danish kroner without VAT and they are intended for commercial activities.

Process	**Machine**	**Time [h] or Number of parts**	**Price per hour [DKK/h]* or Price per unit**	**Total costs [DKK]***
Cleanroom access	-	20	750	15000
Silcon wafer	-	20	160	3200
Photolitography 1/2	SSE Spinner	1	350	350
Photolitography 2/2	KS Aligner	1	350	350
Silcon etching	DRIE-Pegasus	5	600	3000
Cleaning	Plasma asher	0,4	0	0
Cleaning	RCA (4",6")	3,3	0	0
Oxidation	Furnace: Phosphorus Drive-in	4	350	1400
Preparation	HMDS oven	0,5	0	0
Photolitography 1/2	SSE Spinner	1	350	350
Photolitography 2/2	KS Aligner	1	350	350
Oxide etching	AOE	2	600	1200
Silicon etching	DRIE-Pegasus	8	600	4800
Cleaning	Plasma asher	0,4	0	0
Wet etching	Polysilicon etch	0,5	0	0
Cleaning	RCA (4",6")	3,3	0	0
Oxidation	Furnace: Phosphorus Drive-in	5,3	350	1855
Oxidation	Furnace: LPCVD TEOS	2	600	1200
Inspection	SEM Zeiss	6	600	3600
Total cost per batch				36655
Cost per wafer (to be used)		12		3055

phase two). The yields were assigned based on the experience of working in an environment exclusively devoted to research and development and they also represent a worst case scenario. An average number of 100+ users work every day at DTU Danchip and one can expect that some of the failures may be due to that. From an initial batch of 20 silicon wafers, 9 nickel inserts ready to be used in the injection molding tool are obtained. The salary cost for the operator is added to these 9 inserts in order to find the final cost estimate per insert. The inspections are intended to check the quality of the wafers during the process and to avoid that faulty wafers would be processed further. One can also expect that wafers with microscopic defects would be discarded by the engineer.

More specifically, phase one employs machines that allow for processing of the entire batch

Table 5.2: Phase two: sputtering of metal seed layer. The estimated yield for this phase was 90%.(*) All prices are from “Pricebook for DTU Danchip 2013. Effective: January 1st - 2013” [105]. All prices are in Danish kroner without VAT and they are intended for commercial activities.

Process	**Machine**	**Time [h] or Number of parts**	**Price per hour [DKK/h]* or Price per unit**	**Total costs [DKK]***
Shaped wafer	-	12	3055	36655
Metalization	Sputter System (Lesker)	9	600	5400
Inspection	SEM Zeiss	6	600	3600
Total cost per batch				45655
Cost per wafer (to be used)		10		4565

Table 5.3: Phase three: electroforming of the nickel insert.The estimated yield for this phase was 90%.(*) All prices are from “Pricebook for DTU Danchip 2013. Effective: January 1st - 2013” [105]. All prices are in Danish kroner without VAT and they are intended for commercial activities.The salary cost includes taxes.

Process	**Machine**	**Time [h] or Number of parts**	**Price per hour [DKK/h]* or Price per unit**	**Total costs [DKK]***
Metalized wafer	-	10	4565	45655
Nickel Electroplating	Technotrans	115	350	40250
Wet etching	KOH bath	80	0	0
Inspection	SEM Zeiss	6	600	3600
Total cost per batch				89505
Salary cost (1 month)				88000
Final cost				177505
Cost per wafer (to be used)		9		19720

of wafers. In phase two and three instead, the wafers are processed individually. The estimated overall yield for phase one was 60% and so the outcome number of wafers from this phase was 12, Table 5.1. A yield of 90% was assigned to phase two and phase three, Table 5.2 and Table 5.3. Taking in account the yields and salary cost, each nickel insert has a final cost of production of approximately 20000 DKK, Table 5.3. In the end of each table, both the total cost for the batch and the cost per wafer is shown. The cost per wafer is found dividing the total cost per batch by the number of wafers that are transferred to the next phase. When the yield gave a fractional number, the number of wafers was under estimated to the closest unit.

In order to be used in an injection molding tool, the nickel plates need to be shaped into a smaller diameter. This was done both to ensure rotational direction definition when

mounted in the injection molding tool and to eliminate the rough edge from the nickel plates. The electroforming process tends to form nickel plates with a rough edge around that needs to be removed. In this thesis, this was done by mechanical punching using a hydraulic press. Alternatively laser cutting could also be employed. However, this operation should not substantially change the cost of 20000 DKK.

Now, the influence of the cost of the nickel insert will strongly depend on the number of parts that can be molded from each insert. A good estimation for this can be borrowed from the CDs and DVDs industry. CDs and DVDs are the by far most widely used products with microscale features produced via injection molding [106]. Typically CDs have pits 1-3 μm long and about 0.6 μm wide with a depth of 0.1 μm. For DVDs these dimensions are roughly half [106]. Like CDs and DVDs, our microfluidic device contains micron-sized features and therefore they can be compared. Usually a nickel insert can be used to produce tens of thousands of CDs before it wears out [106]. To play on the safe side, we estimate here that 10000 can be produced from a nickel plate. The contribution of the nickel insert to the cost of each device will then be 2 DKK. As we can see below, the major contributions to the cost per device are assigned to the injection molding process and to the bonding process.

Molding and bonding. With the present set-up, the cycle time for injection molding was three minutes, and this gives 20 polymers chips per hour. The price per hour for using the polymer injection molder is 350 DKK and it includes the costs for the raw material [105]. The cost per hour for the operator is more difficult to estimate here, since the injection molding is an automated process and the operator is not expected to interact with the machine the all time. The salary cost per hour is then multiplied by an arbitrary factor of 0.3, leading to a contribution of 200 DKK/hour from the operator. Therefore, the overall cost of the molding machine and the operator is 550 DKK/hour. The injection molding step contributes with 27.5 DKK to the cost of each chip.

The sealing of the chips was performed with a UV lamp and a thermal press available free of charge in the laboratory at DTU Nanotech. However, we can estimate a price of 100 DKK/hour for this process. In this case, the presence of the operator is required for the full process and therefore 600 DKK/hour are added to the machinery cost. By using a customized aluminum holder, 7 chips could be bonded at the same time for a total of 21 chips per hour.

The price of the polymer foil used as a cover lid needs to be considered. With a price of 50 DKK per sheet (order of 50 sheets at the same time) and 20 lids obtained from each sheet, the cost per device is approximately 2.5 DKK. Finally, the bonding step, counting machinery, operator and materials contributes with 35.5 DKK per each device.

The total estimated cost per device is 65 DKK, with the assumption that 10000 parts could be molded from a single nickel insert before this wears out, Table 5.4. The throughput for both the injection molding and bonding was set at about 20 parts per hour. One should

Table 5.4: Total cost of the finished device. The price of the injection molding is from "Pricebook for DTU Danchip 2013. Effective: January 1st - 2013" [105]. Prices are in Danish kroner without VAT and they are intended for commercial activities.

Process	**Total cost [dkk]***
Mold insert	2
Injection molding	27.5
Bonding	35.5
Finished device	65

be aware that these processes also have a yield somehow smaller than 100% and therefore some devices will be discarded. This will cause an increase of the production cost that is difficult to estimate within this analysis. However, we can indicate that some of the chips (estimated 30%) were discarded after injection molding in this work. The decision was arbitrarily taken based on investigation of the patching capillaries aspect by means of optical microscopy. A wider line at the edge of the patching channels was seen as a defect and was usually the reason to discard the chips. On the other hand, very few devices ($<$ 5%) were discarded after bonding. We do not have the countercheck that the discarded chips could not work during the experiments. The evaluation of the process yield was beyond the scope of this thesis at the time that the molding was performed. Therefore, this should only be considered as an indication.

However, from this analysis, one can conclude that the influence of the nickel insert cost on the final production cost fluctuates a lot with the number of parts that can be replicated from each insert. At the range of cost estimated here, the influence of the cost of the insert will dramatically change if 1000 or 10000 parts will be produced. The change is insignificant if this number exceeds 10000 units. Once again, we would like to remark that the facilities available at DTU Danchip are not intended for production, especially the polymer injection molding and the bonding. If the payment of a price per hour is a possible scenario for the processes in the cleanroom, this is not realistic for injection molding and bonding where companies usually own the machineries or commit the work to a supplier. Therefore, a more realistic production scheme would involve commercial partners for the molding and bonding and some time/costs for transfer of the know-how should be considered.

5.4 Standard format

If an APC system will be commercialized, the device will be designed differently for a much smaller unit footprint and higher throughput. A standard format will be chosen, most likely the 384 or 1536 microtiter plates [107]. This will require the use of larger nickel insert and therefore the use of larger master silicon wafers to start with. six inches

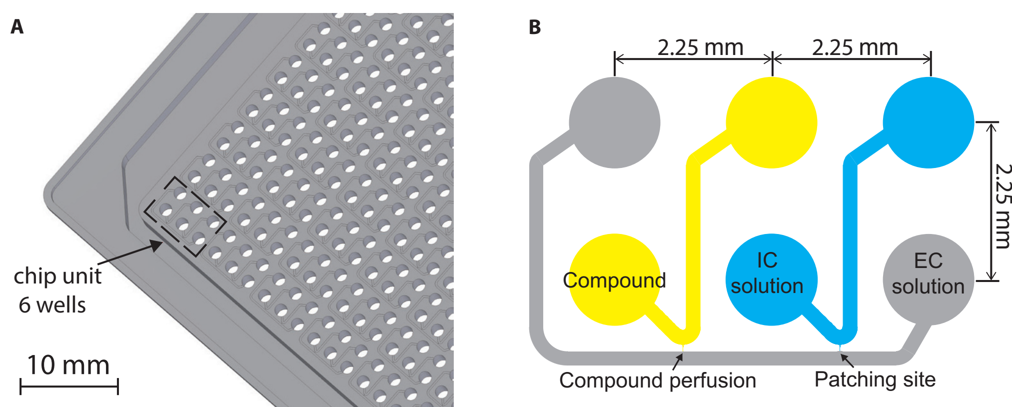

Figure 5.3: (a) Illustration of the back side of a standard 1536 microtiter plate. (b) A single unit of a 1536 microtiter plate comprising a channel for extracellular solution, one for intracellular solution and one for compound perfusion. According to standards, the distance between two consecutive wells is 2,25 mm [107].

wafers (approximately 152 mm in diameter) could be employed for fabrication of half a microtiter plate, one entire microtiter plate will require eight inches wafers. All the cleanroom processes employed for the fabrication, beside the TEOS furnace, are already available for the six inches wafers at DTU Danchip and they are becoming more standard.

For maintaining the same functionality of the presented device, six inlet/outlet wells are required. As shown in Figure 5.3, the design could be miniaturized into a 6.75 mm x 6.75 mm basic unit of a 1536 microtiter plate, where the well-well pitch distance is 2.25 mm. A basic unit comprises a Y shaped channel for recordings and one for compound perfusion. With six wells per chip unit, the 1536 plate format would allow for 256 units and therefore 256 cells would be patch clamped at the same time. For shared cell and drug inlets, one chip unit would only require four ports, and 384 units could be layed out on the 1536 plate. The larger area per device will require a higher uniformity and reproducibility for molding and bonding among several devices and among several patching channels on the same device.

5.5 Conclusions

We have estimated the manufacturing cost of polymer devices using the DEEMO method presented in Chapter 2. A total cost of 65 DKK per device was found based on the production of 10000 parts from each nickel insert. For production volumes larger than 10000 units produced per insert, the manufacturing cost of the nickel insert contributes with only 3 % to the total cost per device. Therefore, this is considered negligible.

However, the injection molding and the bonding share the major contributions to the final cost per device almost equally. We can predict that both steps would benefit from an industrial environment. Volume of production will require a semi or fully automated

bonding process perhaps by using much larger presses. It can also be seen that the cycle time of the molding process has a high impact on the manufacturing cost. It is unclear how a shorter cycle time would affect the device quality, since this has not been investigated in depth. In a further commercialization of this technology, a reduction of the molding time while maintaining the quality, would naturally have a high priority.

We have also sketched how the device could be redesigned into a standard 1536 microtiter plate for a much smaller unit footprint and higher throughput. This was only aimed to remark that the key features in the presented device can be contained in a small area of 1-2 mm^2 compatible with the well-well pitch distance in the 1536 microtiter plate. The overall shape of the device as presented in this work should not be misleading about this point.

Chapter 6

Conclusions

The main outcome of this work was the demonstration that high quality ion channels recordings are possible on a thermoplastic polymer platform. It was shown that gigaseals can be formed between the cell membrane and a COC substrate, making COC a promising substrate material for patch clamping. This was done on an all polymer microfluidic device fabricated by injection molding.

The development of such an inexpensive polymer device for automated patch clamp was described in this thesis. The fabrication has been particularly challenging, mainly due to the required optimization of the etching process employed for the multi-levels patterning in the silicon wafers, and to the demolding. Once a reliable fabrication scheme was optimized, hundreds of identical chips presenting smooth (Rq of 2 nm) micro sized patching apertures were fabricated by means of injection molding. The packaging of these chips was successfully done via thermal bonding with a thin polymer foil of the same material. Chips were then tested with cells and revealed good capture ability of single cells in suspension. High quality electrophysiological recordings of the ion current across the cell membrane in whole-cell mode were demonstrated. About two years were dedicated to the fabrication and optimization of the polymer chip in its final form, while the last year was entirely devoted to patch clamping.

We have developed a fabrication scheme which can be employed to produce polymer microfluidic chips for a large variety of biological applications. Specifically, we have demonstrated that multilevel all-polymer devices for capturing of single cells can be used for electrophysiological recordings. We employed a method termed DEEMO, which enables the direct etching of the silicon substrate, and exploits the large MEMS tool box for silicon micromachining. Using dry etching techniques, such as deep reactive ion etching, a positive master of the desired microfluidic device was structured in a silicon wafer, then inverted in a nickel plate by electroforming, and finally replicated in thermoplastic polymers by injection molding. A modified DRIE etching process combined with an isotropic polysilicon etch was found to result in slightly tapered sidewalls and ensured the ease of demolding. In addition, a sacrificial layer of silicon oxide and a layer of TEOS oxide were employed to

reduce the roughness of the silicon and consequentially of the final polymer device. The device was produced in two variants regarding the cross-sectional profile of the patching capillaries: a semicircular profile and a rectangular profile. A thorough characterization of the patching orifices was carried out by means of SEM and AFM and showed high replication accuracy through the process for both profiles. The uniformity of the patching channels was also confirmed for several devices by the narrow range of chip resistances. UV-assisted thermal bonding was employed as a powerful method to attach a lid to the microfluidic channels on the molded parts.

We believe that the replication method demonstrated here is suitable for prototyping, but also directly applicable to mass production in industry with minimal needs for technology transfer. The strongest argument in favor of this statement is the use of a standard injection-molding machine for molding of the devices.

We have demonstrated that high-quality electrophysiological recordings are possible on such injection molded polymer devices. This was done for the first time on a thermoplastic platform and with no need for any additional surface modifications or treatments before the experiments. The results reported in chapter 5 demonstrate that polymer devices can provide whole-cell current responses from voltage gated sodium channels, one of the most commonly investigated ion channels in electrophysiology. Moreover these devices permit accurate analysis of drug potency for state-dependent inhibitors such as the local anesthetic lidocaine. The devices exhibit excellent data quality when benchmarked against the commercially available QPatch^{TM} system.

Formation of gigaseals (with a 15% success rate, n=47) between the polymer surfaces and the cell membranes was achieved on patching capillaries (45 um long) that allowed for a large sealing area. Moreover, the gigaseals coupled with whole-cell configuration were stable and had an average duration of 30 minutes, leaving sufficient time for application of the screening protocol. Delivering of accurate concentrations of lidocaine was demonstrated and dose response experiments were performed.

As the case for all the other patch clamping devices, it is difficult to determine which are the most relevant parameters for forming gigaseals. The mechanism of gigaseal formation is not yet fully understood in the patch clamping community. For the presented polymer device, our findings indicate that the length of the patching channel together with the very low surface roughness, most probably are the most important parameters for good seal formation. Both factors contributed to increase the effective sealing area between the cell membrane and the low energy polymer surfaces apparently required to obtain tight seals. In the end, this can be considered the major discovery of this work. The cross-sectional shape of the orifice was found to be less critical, as both rectangular and semicircular profiles within experimental accuracy seemed to have almost the same ability to form tight seals with cells.

Finally, we have successfully combined the simplicity of lateral cornered apertures with

the use of injection molding to demonstrate the most cost effective production and materials platform for APC systems to date. The technological readiness level of the reported material and production platform is high, while the specific design presented in this work was only aimed for prototyping. Thus the Y shaped patching channel constitutes the only essential feature of the design and microfluidic channels could be redesigned differently for a much smaller unit footprint. For maintaining exactly the same functionality per functional chip unit, six inlet/outlet wells would still be required. However, if shared cell and compound inlets are employed, one chip unit will require only four ports.

Through an estimation of the manufacturing costs, we have also demonstrated the cost-efficency of the presented polymer device when produced in high-volume. The estimated cost for the final chip was found to be 65 DKK based on production carried out at DTU Danchip. Additionally, it was shown that for production volumes higher than 10000 parts per insert, the cost for production of the nickel insert is negligible.

We anticipate that the findings in this work will have a positive impact on the development of the next generation of chips for automated patch clamping. We hope that a new *era* for extremely cheap disposable devices is not far to come. Ultimately, we hope this will have an impact on the discovery of new pharmaceutical compounds with the possibility that APC can be employed for primary screening.

Bibliography

[1] B. Alberts, A. Johnson, J. Lewis, M. Raff, K. Roberts, and P. Walter, *Molecular Biology of the Cell.* New York: Garland Science, 4th edition. ed., 2002.

[2] B. Hille, *Ion Channel of Exitable Membranes.* Sunderland, MA U.S.A: Sinauer Associates, Inc., third ed., 2001.

[3] A. Molleman, *Patch Clamping An Introductory Guide to Patch Clamp Electrophysiology.* Chichester: Wiley, 2003.

[4] M. Ackerman and D. Clapham, "Mechanisms of disease - ion channels - basic science and clinical disease," *New England Journal of Medicine*, vol. 336, pp. 1575–1586, MAY 29 1997. PT: J; NR: 68; TC: 204; J9: NEW ENGL J MED; PG: 12; GA: XB087; UT: WOS:A1997XB08700007.

[5] D. Johnson and S. M.-S. Wu, *Foundations of Cellular Neurophysiology.* Cambridge: A Bradford Book, 1995.

[6] F. Ashcroft, "From molecule to malady," *Nature*, vol. 440, pp. 440–447, MAR 23 2006. PT: J; NR: 51; TC: 142; J9: NATURE; PG: 8; GA: 024DV; UT: WOS:000236176100040.

[7] F. Lehmann-Horn and K. Jurkat-Rott, "Voltage-gated ion channels and hereditary disease," *Physiological Reviews*, vol. 79, pp. 1317–1372, OCT 1999. PT: J; NR: 604; TC: 279; J9: PHYSIOL REV; PG: 56; GA: 244GM; UT: WOS:000083043500007.

[8] J. P. Overington, B. Al-Lazikani, and A. L. Hopkins, "Opinion - how many drug targets are there?," *Nature Reviews Drug Discovery*, vol. 5, pp. 993–996, DEC 2006. PT: J; NR: 26; TC: 656; J9: NAT REV DRUG DISCOV; PG: 4; GA: 111TS; UT: WOS:000242478300012.

[9] A. Wickenden, B. Priest, and G. Erdemli, "Ion channel drug discovery: challenges and future directions," *Future Medicinal Chemistry*, vol. 4, pp. 661–679, APR 2012. PT: J; NR: 125; TC: 1; J9: FUTURE MED CHEM; PG: 19; GA: 929AH; UT: WOS:000303033100012.

[10] J. Xu, X. Wang, B. Ensign, M. Li, L. Wu, A. Guia, and J. Xu, "Ion-channel assay technologies: quo vadis?," *Drug discovery today*, vol. 6, pp. 1278–1287, DEC 15 2001. PT: J; NR: 41; TC: 118; J9: DRUG DISCOV TODAY; PG: 10; GA: 504BN; UT: WOS:000172837400010.

[11] J. P. Hughes, S. Rees, S. B. Kalindjian, and K. L. Philpott, "Principles of early drug discovery," *British journal of pharmacology*, vol. 162, pp. 1239–1249, MAR 2011. PT: J; NR: 25; TC: 6; J9: BRIT J PHARMACOL; PG: 11; GA: 724NL; UT: WOS:000287583200002.

[12] W. Zheng, R. Spencer, and L. Kiss, "High throughput assay technologies for ion channel drug discovery," *Assay and Drug Development Technologies*, vol. 2, pp. 543–552, OCT 2004. PT: J; NR: 38; TC: 63; J9: ASSAY DRUG DEV TECHN; PG: 10; GA: 875NM; UT: WOS:000225427300010.

[13] W. Zheng, R. Spencer, and L. Kiss, "High throughput assay technologies for ion channel drug discovery," *Assay and Drug Development Technologies*, vol. 2, pp. 543–552, OCT 2004. PT: J; NR: 38; TC: 61; J9: ASSAY DRUG DEV TECHN; PG: 10; GA: 875NM; UT: WOS:000225427300010.

[14] C. Farre, M. George, A. Bruggemann, and N. Fertig, "Ion channel screening automated patch clamp on the rise," *Drug Discovery Today: Technologies*, vol. 5, pp. e23–e28, 0 2008.

[15] E. NEHER and B. SAKMANN, "Single-channel currents recorded from membrane of denervated frog muscle-fibers," *Nature*, vol. 260, no. 5554, pp. 799–802, 1976. PT: J; NR: 15; TC: 977; J9: NATURE; PG: 4; GA: BP359; UT: WOS:A1976BP35900042.

[16] O. HAMILL, A. MARTY, E. NEHER, B. SAKMANN, and F. SIGWORTH, "Improved patch-clamp techniques for high-resolution current recording from cells and cell-free membrane patches," *Pflugers Archiv-European Journal of Physiology*, vol. 391, no. 2, pp. 85–100, 1981. PT: J; NR: 23; TC: 16789; J9: PFLUG ARCH EUR J PHY; PG: 16; GA: ME311; UT: WOS:A1981ME31100001.

[17] C. Wood, C. Williams, and G. Waldron, "Patch clamping by numbers," *Drug discovery today*, vol. 9, pp. 434–441, MAY 15 2004. PT: J; NR: 31; TC: 64; J9: DRUG DISCOV TODAY; PG: 8; GA: 820MR; UT: WOS:000221394000008.

[18] N. Fertig, R. Blick, and J. Behrends, "Whole cell patch clamp recording performed on a planar glass chip," *Biophysical journal*, vol. 82, pp. 3056–3062, JUN 2002. PT: J; NR: 40; TC: 175; J9: BIOPHYS J; PG: 7; GA: 555PP; UT: WOS:000175802700022.

[19] J. Xu, A. Guia, D. Rothwarf, M. Huang, K. Sithiphong, J. Ouang, G. Tao, X. Wang, and L. Wu, "A benchmark study with sealchip (tm) planar patch-clamp technology," *Assay and Drug Development Technologies*, vol. 1, pp. 675–684, OCT 2003. PT:

J; NR: 15; TC: 35; J9: ASSAY DRUG DEV TECHN; PG: 10; GA: 738WV; UT: WOS:000186311600009.

[20] J. Dunlop, M. Bowlby, R. Peri, D. Vasilyev, and R. Arias, "High-throughput electrophysiology: an emerging paradigm for ion-channel screening and physiology," *Nature Reviews Drug Discovery*, vol. 7, pp. 358–368, APR 2008. PT: J; NR: 87; TC: 108; J9: NAT REV DRUG DISCOV; PG: 11; GA: 282IQ; UT: WOS:000254561500017.

[21] M. Asmild, N. Oswald, K. Krzywkowski, S. Friis, R. Jacobsen, D. Reuter, R. Taboryski, J. Kutchinsky, R. Vestergaard, R. Schroder, C. Sorensen, M. Bech, M. Korsgaard, and N. Willumsen, "Upscaling and automation of electrophysiology: Toward high throughput screening in ion channel drug discovery," *Receptors and channels*, vol. 9, pp. 49–58, JAN-FEB 2003. PT: J; NR: 10; TC: 37; J9: RECEPTOR CHANNEL; PG: 10; GA: 739KQ; UT: WOS:000186344000007.

[22] C. Ionescu-Zanetti, R. Shaw, J. Seo, Y. Jan, L. Jan, and L. Lee, "Mammalian electrophysiology on a microfluidic platform," *Proceedings of the National Academy of Sciences of the United States of America*, vol. 102, pp. 9112–9117, JUN 28 2005. PT: J; NR: 25; TC: 91; J9: P NATL ACAD SCI USA; PG: 6; GA: 941CD; UT: WOS:000230191400006.

[23] J. Kutchinsky, S. Friis, M. Asmild, R. Taboryski, S. Pedersen, R. Vestergaard, R. Jacobsen, K. Krzywkowski, R. Schroder, T. Ljungstrom, N. Helix, C. Sorensen, M. Bech, and N. Willumsen, "Characterization of potassium channel modulators with qpatch (tm) automated patch-clamp technology: System characteristics and performance," *Assay and Drug Development Technologies*, vol. 1, pp. 685–693, OCT 2003. PT: J; TC: 34; UT: WOS:000186311600010.

[24] A. Y. Lau, P. J. Hung, A. R. Wu, and L. P. Lee, "Open-access microfluidic patch-clamp array with raised lateral cell trapping sites," *Lab on a Chip*, vol. 6, pp. 1510–1515, DEC 2006. PT: J; NR: 16; TC: 48; J9: LAB CHIP; PG: 6; GA: 122GB; UT: WOS:000243212600012.

[25] D. Martinez, C. Py, M. W. Denhoff, M. Martina, R. Monette, T. Comas, C. Luk, N. Syed, and G. Mealing, "High-fidelity patch-clamp recordings from neurons cultured on a polymer microchip," *Biomedical Microdevices*, vol. 12, pp. 977–985, DEC 2010. PT: J; NR: 43; TC: 4; J9: BIOMED MICRODEVICES; PG: 9; GA: 668CP; UT: WOS:000283246500003.

[26] A. Stett, V. Bucher, C. Burkhardt, U. Weber, and W. Nisch, "Patch-clamping of primary cardiac cells with micro-openings in polyimide films," *Medical and biological engineering and computing*, vol. 41, pp. 233–240, MAR 2003. PT: J; NR: 32; TC: 25; J9: MED BIOL ENG COMPUT; PG: 8; GA: 667QU; UT: WOS:000182244900018.

[27] K. Klemic, J. Klemic, M. Reed, and F. Sigworth, "Micromolded pdms planar electrode allows patch clamp electrical recordings from cells," *Biosensors and bioelectronics*, vol. 17, pp. 597–604, JUN 2002. PT: J; NR: 13; TC: 123; J9: BIOSENS BIOELECTRON; PG: 8; GA: 547JN; UT: WOS:000175329400020.

[28] K. Klemic, J. Klemic, and F. Sigworth, "An air-molding technique for fabricating pdms planar patch-clamp electrodes," *Pflugers Archiv-European Journal of Physiology*, vol. 449, pp. 564–572, MAR 2005. PT: J; NR: 21; TC: 40; J9: PFLUG ARCH EUR J PHY; PG: 9; GA: 903RV; UT: WOS:000227444200007.

[29] K. Klemic, J. Klemic, M. Reed, and F. Sigworth, "Micromolded pdms planar electrode allows patch clamp electrical recordings from cells," *Biosensors and bioelectronics*, vol. 17, pp. 597–604, JUN 2002. PT: J; NR: 13; TC: 123; J9: BIOSENS BIOELECTRON; PG: 8; GA: 547JN; UT: WOS:000175329400020.

[30] B. Xu, Z. Liu, Y.-K. Lee, A. Mak, and M. Yang, "A pdms microfluidic system with poly(ethylene glycol)/su-8 based apertures for planar whole cell-patch-clamp recordings," *Sensors and Actuators A-Physical*, vol. 166, pp. 219–225, APR 2011. PT: J; NR: 26; TC: 0; J9: SENSOR ACTUAT A-PHYS; SI: SI; PG: 7; GA: 753YD; UT: WOS:000289815700008.

[31] J. Seo, C. Ionescu-Zanetti, J. Diamond, R. Lal, and L. Lee, "Integrated multiple patch-clamp array chip via lateral cell trapping junctions," *Applied Physics Letters*, vol. 84, pp. 1973–1975, MAR 15 2004. PT: J; NR: 9; TC: 74; J9: APPL PHYS LETT; PG: 3; GA: 802SG; UT: WOS:000220182600053.

[32] A. P. Golden, N. Li, Q. Chen, T. Lee, T. Nevill, X. Cao, J. Johnson, G. Erdemli, C. Ionescu-Zanetti, L. Urban, and M. Holmqvist, "Ionflux: A microfluidic patch clamp system evaluated with human ether-a-go-go related gene channel physiology and pharmacology," *Assay and Drug Development Technologies*, vol. 9, pp. 608–619, DEC 2011. PT: J; NR: 50; TC: 2; J9: ASSAY DRUG DEV TECHN; PG: 12; GA: 863GT; UT: WOS:000298151500004.

[33] B. Fermini, "Recent advances in ion channel screening technologies," *Topics in Medicinal Chemistry*, vol. 3, pp. 1–25, 2008. PT: S; UT: BCI:BCI200900089948; NR: 63; TC: 1.

[34] S. Tanzi, P. F. Ostergaard, M. Matteucci, T. L. Christiansen, J. Cech, R. Marie, and R. Taboryski, "Fabrication of combined-scale nano- and microfluidic polymer systems using a multilevel dry etching, electroplating and molding process," *Journal of Micromechanics and Microengineering*, vol. 22, p. 115008, NOV 2012. PT: J; TC: 1; UT: WOS:000310534400009.

[35] T. L. Christiansen, "Design and development of a microfluidic chip for electrical measurements on biological cells," 2012.

[36] H. Becker and C. Gartner, "Polymer microfabrication methods for microfluidic analytical applications," *Electrophoresis*, vol. 21, pp. 12–26, JAN 2000. PT: J; NR: 62; TC: 423; J9: ELECTROPHORESIS; PG: 15; GA: 279VM; UT: WOS:000085065800003.

[37] A. de Mello, "Plastic fantastic?," *Lab on a Chip*, vol. 2, no. 2, pp. 31N–36N, 2002. PT: J; NR: 53; TC: 65; J9: LAB CHIP; PG: 6; GA: 594CG; UT: WOS:000178030700002.

[38] D. Figeys and D. Pinto, "Lab-on-a-chip: A revolution in biological and medical sciences.," *Analytical Chemistry*, vol. 72, pp. 330A–335A, MAY 1 2000. PT: J; NR: 31; TC: 220; J9: ANAL CHEM; PG: 6; GA: 312DE; UT: WOS:000086927300005.

[39] A. Curtis and C. Wilkinson, "Nantotechniques and approaches in biotechnology," *Trends in biotechnology*, vol. 19, pp. 97–101, MAR 2001. PT: J; NR: 17; TC: 237; J9: TRENDS BIOTECHNOL; PG: 5; GA: 432VN; UT: WOS:000168716600026.

[40] H. Andersson and A. van den Berg, "Microfluidic devices for cellomics: a review," *Sensors and Actuators B-Chemical*, vol. 92, pp. 315–325, JUL 15 2003. PT: J; NR: 94; TC: 313; J9: SENSOR ACTUAT B-CHEM; PG: 11; GA: 688TN; UT: WOS:000183452500009.

[41] D. HARRISON, K. FLURI, K. SEILER, Z. FAN, C. EFFENHAUSER, and A. MANZ, "Micromachining a miniaturized capillary electrophoresis-based chemical-analysis system on a chip," *Science*, vol. 261, pp. 895–897, AUG 13 1993. PT: J; NR: 23; TC: 1176; J9: SCIENCE; PG: 3; GA: LR897; UT: WOS:A1993LR89700032.

[42] H. Becker and L. Locascio, "Polymer microfluidic devices," *Talanta*, vol. 56, pp. 267–287, FEB 11 2002. PT: J; NR: 106; TC: 475; J9: TALANTA; PG: 21; GA: 524GT; UT: WOS:000174005400004.

[43] D. Duffy, J. McDonald, O. Schueller, and G. Whitesides, "Rapid prototyping of microfluidic systems in poly(dimethylsiloxane)," *Analytical Chemistry*, vol. 70, pp. 4974–4984, DEC 1 1998. PT: J; NR: 80; TC: 2048; J9: ANAL CHEM; PG: 11; GA: 143VW; UT: WOS:000077278700028.

[44] H. Klank, J. Kutter, and O. Geschke, "Co2-laser micromachining and back-end processing for rapid production of pmma-based microfluidic systems," *Lab on a Chip*, vol. 2, no. 4, pp. 242–246, 2002. PT: J; NR: 25; TC: 141; J9: LAB CHIP; PG: 5; GA: 617XG; UT: WOS:000179385800013.

[45] J. McDonald and G. Whitesides, "Poly(dimethylsiloxane) as a material for fabricating microfluidic devices," *Accounts of Chemical Research*, vol. 35, pp. 491–499, JUL 2002. PT: J; NR: 70; TC: 726; J9: ACCOUNTS CHEM RES; PG: 9; GA: 595GN; UT: WOS:000178100400001.

[46] M. Heckele, W. Bacher, and K. Muller, “Hot embossing - the molding technique for plastic microstructures,” *Microsystem Technologies*, vol. 4, pp. 122–124, MAY 1998. PT: J; CT: International Conference on High Aspect Ratio Microstructure Technology (HARMST 97); CY: JUN 20-21, 1997; CL: MADISON, WISCONSIN; NR: 9; TC: 159; J9: MICROSYST TECHNOL; PG: 3; GA: ZU220; UT: WOS:000074174300007.

[47] J. Giboz, T. Copponnex, and P. Mele, “Microinjection molding of thermoplastic polymers: a review,” *Journal of Micromechanics and Microengineering*, vol. 17, pp. R96–R109, JUN 2007. PT: J; NR: 108; TC: 57; J9: J MICROMECH MICROENG; PG: 14; GA: 173CP; UT: WOS:000246851400002.

[48] K. O. Andresen, M. Hansen, M. Matschuk, S. T. Jepsen, H. S. Sorensen, P. Utko, D. Selmeczi, T. S. Hansen, N. B. Larsen, N. Rozlosnik, and R. Taboryski, “Injection molded chips with integrated conducting polymer electrodes for electroporation of cells,” *Journal of Micromechanics and Microengineering*, vol. 20, p. 055010, MAY 2010. PT: J; NR: 53; TC: 4; J9: J MICROMECH MICROENG; PG: 9; GA: 591MN; UT: WOS:000277305000010.

[49] E. BECKER, W. EHRFELD, D. MUNCHMEYER, H. BETZ, A. HEUBERGER, S. PONGRATZ, W. GLASHAUSER, H. MICHEL, and R. VONSIEMENS, “Production of separation-nozzle systems for uranium enrichment by a combination of x-ray-lithography and galvanoplastics,” *Naturwissenschaften*, vol. 69, no. 11, pp. 520–523, 1982. PT: J; NR: 5; TC: 75; J9: NATURWISSENSCHAFTEN; PG: 4; GA: PT867; UT: WOS:A1982PT86700002.

[50] R. Kupka, F. Bouamrane, C. Cremers, and S. Megtert, “Microfabrication: Liga-x and applications,” *Applied Surface Science*, vol. 164, pp. 97–110, SEP 1 2000. PT: J; CT: 4th Porquerolles Workshop on Special Topics in Surface Science; CY: SEP 27-OCT 01, 1999; CL: ILE PORQUEROLLES, FRANCE; SP: CNRS, Commissariat Energie Atom, Dept Rech Etat Condense, Atomes Molec, Grp Francaise Croissance Cristalline, Club Nanotechnol; NR: 107; TC: 66; J9: APPL SURF SCI; PG: 14; GA: 345LT; UT: WOS:000088818000016.

[51] V. Piotter, T. Hanemann, R. Ruprecht, and J. Hausselt, “Injection molding and related techniques for fabrication of microstructures,” *Microsystem Technologies*, vol. 3, pp. 129–133, MAY 1997. PT: J; NR: 13; TC: 55; J9: MICROSYST TECHNOL; PG: 5; GA: YD297; UT: WOS:A1997YD29700008.

[52] C. Malek and V. Saile, “Applications of liga technology to precision manufacturing of high-aspect-ratio micro-components and -systems: a review,” *Microelectronics Journal*, vol. 35, pp. 131–143, FEB 2004. PT: J; NR: 212; TC: 66; J9: MICROELECTRON J; PG: 13; GA: 766PB; UT: WOS:000188383800005.

[53] R. McCormick, R. Nelson, M. AlonsoAmigo, J. Benvegnu, and H. Hooper, "Microchannel electrophoretic separations of dna in injection-molded plastic substrates," *Analytical Chemistry*, vol. 69, pp. 2626–2630, JUL 15 1997. PT: J; CT: HPCE 97; CY: JAN 26-30, 1997; CL: ANAHEIM, CA; NR: 39; TC: 383; J9: ANAL CHEM; PG: 5; GA: XK121; UT: WOS:A1997XK12100002.

[54] J. ELDERS, H. JANSEN, M. ELWENSPOEK, and W. EHRFELD, *DEEMO: A new technology for the fabrication of microstructures.* NEW YORK; 345 E 47TH ST, NEW YORK, NY 10017: I E E E, 1995. PT: B; CT: 8th IEEE International Workshop on Micro Electro Mechanical Systems (MEMS); CY: JAN 29-FEB 02, 1995; CL: AMSTERDAM, NETHERLANDS; SP: IEEE Robot and Automat Soc, ASME Dynam Syst and Control Div, MESA Res Inst, Daimler Benz AG, Municipal Amsterdam, Micro Montage BV, BRONKHORST High Tech BV, AQUAMARIJN MicroFiltration BV, Sinus Micro Engn, 3T BV, Philips Res, KNAW; NR: 0; TC: 0; PG: 2; GA: BD67E; UT: WOS:A1995BD67E00043.

[55] Y. Fintschenko and A. van den Berg, "Silicon microtechnology and microstructures in separation science," *Journal of Chromatography a*, vol. 819, pp. 3–12, SEP 11 1998. PT: J; CT: 5th International Symposium on Hyphenated Techniques in Chromatography and Hyphenated Chromatographic Analyzers; CY: FEB 11-13, 1998; CL: BRUGGE, BELGIUM; SP: Royal Flemish Chem Soc, Fonds voor Wetenschappelijk Onderzoek - Vlaanderen (FWO); NR: 39; TC: 47; J9: J CHROMATOGR A; PG: 10; GA: 122QE; UT: WOS:000076082300002.

[56] J. Judy, "Microelectromechanical systems (mems): fabrication, design and applications," *Smart Materials and Structures*, vol. 10, pp. 1115–1134, DEC 2001. PT: J; NR: 105; TC: 179; J9: SMART MATER STRUCT; PG: 20; GA: 516LZ; UT: WOS:000173555900002.

[57] B. Kastenmeier, P. Matsuo, J. Beulens, and G. Oehrlein, "Chemical dry etching of silicon nitride and silicon dioxide using cf4/o-2/n-2 gas mixtures," *Journal of Vacuum Science and Technology A-Vacuum Surfaces and Films*, vol. 14, pp. 2802–2813, SEP-OCT 1996. PT: J; NR: 33; TC: 61; J9: J VAC SCI TECHNOL A; PG: 12; GA: VJ242; UT: WOS:A1996VJ24200016.

[58] J. BONDUR, "Dry process technology (reactive ion etching)," *Journal of Vacuum Science and Technology*, vol. 13, no. 5, pp. 1023–1029, 1976. PT: J; NR: 13; TC: 99; J9: J VAC SCI TECHNOL; PG: 7; GA: CC605; UT: WOS:A1976CC60500004.

[59] P. Yih, V. Saxena, and A. Steckl, "A review of sic reactive ion etching in fluorinated plasmas," *Physica Status Solidi B-Basic Research*, vol. 202, pp. 605–642, JUL 1997. PT: J; NR: 119; TC: 66; J9: PHYS STATUS SOLIDI B; PG: 38; GA: XL897; UT: WOS:A1997XL89700030.

[60] R. Lamonte and D. McNally, "Uses and processing of cyclic olefin copolymers," *Plastics Engineering*, vol. 56, pp. 51–+, JUN 2000. PT: J; NR: 0; TC: 29; J9: PLAST ENG; PG: 6; GA: 322DN; UT: WOS:000087495100016.

[61] J. Shin, J. Park, C. Liu, J. He, and S. Kim, "Chemical structure and physical properties of cyclic olefin copolymers - (iupac technical report)," *Pure and Applied Chemistry*, vol. 77, pp. 801–814, MAY 2005. PT: J; NR: 20; TC: 41; J9: PURE APPL CHEM; PG: 14; GA: 929EN; UT: WOS:000229325000001.

[62] P. S. Nunes, P. D. Ohlsson, O. Ordeig, and J. P. Kutter, "Cyclic olefin polymers: emerging materials for lab-on-a-chip applications rid a-7838-2012 rid e-3256-2010," *Microfluidics and Nanofluidics*, vol. 9, pp. 145–161, AUG 2010. PT: J; NR: 109; TC: 14; J9: MICROFLUID NANOFLUID; PG: 17; GA: 612VJ; UT: WOS:000278932400001.

[63] M. Castano-Alvarez, M. Fernandez-Abedul, and A. Costa-Garcia, "Poly(methylmethacrylate) and topas capillary electrophoresis microchip performance with electrochemical detection," *Electrophoresis*, vol. 26, pp. 3160–3168, AUG 2005. PT: J; NR: 53; TC: 27; J9: ELECTROPHORESIS; PG: 9; GA: 962IA; UT: WOS:000231723500014.

[64] K. Faure, M. Albert, V. Dugas, G. Cretier, R. Ferrigno, P. Morin, and J.-L. Rocca, "Development of an acrylate monolith in a cyclo-olefin copolymer microfluidic device for chip electrochromatography separation," *Electrophoresis*, vol. 29, pp. 4948–4955, DEC 2008. PT: J; NR: 47; TC: 13; J9: ELECTROPHORESIS; PG: 8; GA: 396AX; UT: WOS:000262565700017.

[65] J. Liu, K.-W. Ro, R. Nayak, and D. R. Knapp, "Monolithic column plastic microfluidic device for peptide analysis using electrospray from a channel opening on the edge of the device," *International Journal of Mass Spectrometry*, vol. 259, pp. 65–72, JAN 1 2007. PT: J; NR: 34; TC: 26; J9: INT J MASS SPECTROM; PG: 8; GA: 121TQ; UT: WOS:000243180300010.

[66] I. S. ISO, *5941*. 1st ed., 1986.

[67] "Conical fittings with a 6other mediacl equipment - part 1: General requirements," 1994.

[68] W. Pfleging, A. Bruns, M. Przybylski, A. Welle, and S. Wilson, "Patterning of polystyrene by uv-laser raidiation for the fabrication of devices for patch clamping," *Laser-Based Micro- and Nanopackaging and Assembly Ii*, vol. 6880, p. 68800D, 2008. PT: S; CT: Conference on Laser-Based Micro- and Nano-Packaging and Assembly II; CY: JAN 22-24, 2008; CL: San Jose, CA; SP: SPIE; NR: 20; TC: 0; J9: PROC SPIE; PG: 11; GA: BHS38; UT: WOS:000255941700011.

[69] P. Dixit and J. Miao, "Effect of sf(6) flow rate on the etched surface profile and bottom grass formation in deep reactive ion etching process," *International Mems Conference 2006*, vol. 34, pp. 577–582, 2006. PT: S; CT: International MEMS Conference 2006; CY: MAY 09-12, 2006; CL: Singapore, SINGAPORE; SP: Inst Bioengineering and NanoTechnol; NR: 10; TC: 10; J9: J PHYS CONF SER; PG: 6; GA: BTE85; UT: WOS:000286667100095.

[70] D. S. Tezcan, K. D. Munck, N. Pham, O. Luhn, A. Aarts, P. D. Moor, K. Baert, and C. V. Hoof, *Development of vertical and tapered via etch for 3D through wafer interconnect technology.* NEW YORK; 345 E 47TH ST, NEW YORK, NY 10017 USA: IEEE, 2006. PT: B; CT: 8th Electronics Packaging Technology Conference; CY: DEC 06-08, 2006; CL: Singapore, SINGAPORE; SP: IEEE Reliabil Singapore Chapter, CPMT Singapore Chapter, EDSingapore Chapter; NR: 11; TC: 2; PG: 7; GA: BFX49; UT: WOS:000245279600005.

[71] G. Kovacs, N. Maluf, and K. Petersen, "Bulk micromachining of silicon," *Proceedings of the IEEE*, vol. 86, pp. 1536–1551, AUG 1998. PT: J; NR: 96; TC: 278; J9: P IEEE; PG: 16; GA: 100XG; UT: WOS:000074840200003.

[72] A. Yahata, S. Urano, T. Inoue, and T. Shinohe, "Smoothing of si trench sidewall surface by chemical dry etching and sacrificial oxidation," *Japanese Journal of Applied Physics Part 1-Regular Papers Short Notes and Review Papers*, vol. 37, pp. 3954–3955, JUL 1998. PT: J; NR: 6; TC: 9; J9: JPN J APPL PHYS 1; PG: 2; GA: 110CV; UT: WOS:000075363300017.

[73] K. R. Williams, K. Gupta, and M. Wasilik, "Etch rates for micromachining processing-part ii," *Microelectromechanical Systems, Journal of*, vol. 12, no. 6, pp. 761–778, 2003. ID: 1.

[74] G. Fu, N. Loh, S. Tor, B. Tay, Y. Murakoshi, and R. Maeda, "A variotherm mold for micro metal injection molding," *Microsystem Technologies-Micro-and Nanosystems-Information Storage and Processing Systems*, vol. 11, pp. 1267–1271, NOV 2005. PT: J; NR: 11; TC: 16; J9: MICROSYST TECHNOL; PG: 5; GA: 988CD; UT: WOS:000233568100004.

[75] T. Ussing, L. V. Petersen, C. B. Nielsen, B. Helbo, and L. Hojslet, "Micro laser welding of polymer microstructures using low power laser diodes," *International Journal of Advanced Manufacturing Technology*, vol. 33, no. 1-2, pp. 198–205, 2007. PT: J; NR: 5; TC: 9; J9: INT J ADV MANUF TECH; PG: 8; GA: 179CC; UT: WOS:000247265900026.

[76] A. Yussuf, I. Sbarski, J. Hayes, M. Solomon, and N. Tran, "Microwave welding of polymeric-microfluidic devices," *Journal of Micromechanics and Microengineering*, vol. 15, pp. 1692–1699, SEP 2005. PT: J; NR: 28; TC: 37; J9: J MICROMECH MICROENG; PG: 8; GA: 969LB; UT: WOS:000232234500024.

[77] S. Luan, R. Xing, Z. Wang, X. Yu, and Y. Han, "Solvent-assisted polymer-bonding lithography," *Journal of Vacuum Science and Technology B*, vol. 23, pp. 236–241, JAN-FEB 2005. PT: J; NR: 28; TC: 2; J9: J VAC SCI TECHNOL B; PG: 6; GA: 901RZ; UT: WOS:000227300900043.

[78] P. Gu, K. Liu, H. Chen, T. Nishida, and Z. H. Fan, "Chemical-assisted bonding of thermoplastics/elastomer for fabricating microfluidic valves," *Analytical Chemistry*, vol. 83, pp. 446–452, JAN 1 2011. PT: J; NR: 51; TC: 5; J9: ANAL CHEM; PG: 7; GA: 698DB; UT: WOS:000285570600062.

[79] R. K. Jena, C. Y. Yue, and L. Anand, "Improvement of thermal bond strength and surface properties of cyclic olefin copolymer (coc) based microfluidic device using the photo-grafting technique," *Sensors and Actuators B-Chemical*, vol. 157, pp. 518–526, OCT 20 2011. PT: J; NR: 40; TC: 1; J9: SENSOR ACTUAT B-CHEM; PG: 9; GA: 797WR; UT: WOS:000293161300026.

[80] M. Matteucci, T. L. Christiansen, S. Tanzi, P. F. Ostergaard, S. T. Larsen, and R. Taboryski, "Fabrication and characterization of injection molded multi level nano and microfluidic systems," *Microelectronic Engineering*, no. 0.

[81] R. Abdolvand and F. Ayazi, "An advanced reactive ion etching process for very high aspect-ratio sub-micron wide trenches in silicon," *Sensors and Actuators A-Physical*, vol. 144, pp. 109–116, MAY 28 2008. PT: J; NR: 13; TC: 32; J9: SENSOR ACTUAT A-PHYS; PG: 8; GA: 302TU; UT: WOS:000255993200016.

[82] N. Roxhed, P. Griss, and G. Stemme, "A method for tapered deep reactive ion etching using a modified bosch process," *Journal of Micromechanics and Microengineering*, vol. 17, pp. 1087–1092, MAY 2007. PT: J; NR: 16; TC: 9; J9: J MICROMECH MICROENG; PG: 6; GA: 168VH; UT: WOS:000246551600033.

[83] W.-L. Ong, K.-C. Tang, A. Agarwal, R. Nagarajan, L.-W. Luo, and L. Yobas, "Microfluidic integration of substantially round glass capillaries for lateral patch clamping on chip," *Lab on a Chip*, vol. 7, no. 10, pp. 1357–1366, 2007. PT: J; NR: 28; TC: 21; J9: LAB CHIP; PG: 10; GA: 214LY; UT: WOS:000249740500027.

[84] C. Chen and A. Folch, "A high-performance elastomeric patch clamp chip," *Lab on a Chip*, vol. 6, pp. 1338–1345, OCT 2006. PT: J; NR: 39; TC: 29; J9: LAB CHIP; PG: 8; GA: 101HF; UT: WOS:000241731200018.

[85] T. A. Polymers, "Cyclic olefin copolymer coc," 2006.

[86] T. Lehnert, M. Gijs, R. Netzer, and U. Bischoff, "Realization of hollow sio2 micronozzles for electrical measurements on living cells," *Applied Physics Letters*, vol. 81, pp. 5063–5065, DEC 23 2002. PT: J; NR: 10; TC: 43; J9: APPL PHYS LETT; PG: 3; GA: 628VY; UT: WOS:000180018300057.

[87] C. J. CLOPPER and E. S. PEARSON, "The use of confidence or fiducial limits illustrated in the case of the binomial," *Biometrika*, vol. 26, pp. 404–413, December 01 1934.

[88] T. Sordel, F. Kermarrec, Y. Sinquin, I. Fonteille, M. Labeau, F. Sauter-Starace, C. Pudda, F. de Crecy, F. Chatelain, M. D. Waard, C. Arnoult, and N. Picollet-D'hahan, "The development of high quality seals for silicon patch-clamp chips," *Biomaterials*, vol. 31, pp. 7398–7410, OCT 2010. PT: J; NR: 38; TC: 2; J9: BIOMATERIALS; PG: 13; GA: 642DE; UT: WOS:000281183000019.

[89] F. Sigworth and K. Klemic, "Patch clamp on a chip," *Biophysical journal*, vol. 82, pp. 2831–2832, JUN 2002. PT: J; NR: 5; TC: 39; J9: BIOPHYS J; PG: 2; GA: 555PP; UT: WOS:000175802700001.

[90] M. Malboubi, Y. Gu, and K. Jiang, "Experimental and simulation study of the effect of pipette roughness on giga-seal formation in patch clamping," *Microelectronic Engineering*, vol. 87, pp. 778–781, MAY-AUG 2010. PT: J; CT: 35th International Conference on Micro-and Nano-Engineering; CY: SEP 28-OCT 01, 2009; CL: Ghent, BELGIUM; NR: 7; TC: 2; J9: MICROELECTRON ENG; PG: 4; GA: 578NO; UT: WOS:000276300700024.

[91] F. Yu and W. Catterall, "Overview of the voltage-gated sodium channel family," *Genome biology*, vol. 4, no. 3, p. 207, 2003. PT: J; NR: 51; TC: 174; J9: GENOME BIOL; PG: 7; GA: 675KU; UT: WOS:000182694200003.

[92] B. He and D. M. Soderlund, "Human embryonic kidney (hek293) cells express endogenous voltage-gated sodium currents and nav1.7 sodium channels," *Neuroscience letters*, vol. 469, pp. 268–272, 1/22 2010.

[93] J. Dempster, *Chapter Seven - Recording and Analysis of Intracellular Electrophysiological Signals*, pp. 172–225. The Laboratory Computer, London: Academic Press, 2001.

[94] O. M. L. Sontheimer, Harald, *Chapter two - Whole-Cell Patch-Clamp Recordings*, pp. 35–68. Patch-Clamp Analysis Advanced Techniques, Totowa, New Jersey: Humana Press, second ed., 2007.

[95] F. Bezanilla and C. M. Armstrong, "Inactivation of the sodium channel. i. sodium current experiments.," *The Journal of general physiology*, vol. 70, pp. 549–566, November 01 1977.

[96] B. BEAN, C. COHEN, and R. TSIEN, "Lidocaine block of cardiac sodium-channels," *Journal of General Physiology*, vol. 81, no. 5, pp. 613–642, 1983. PT: J; NR: 85; TC: 559; J9: J GEN PHYSIOL; PG: 30; GA: QQ831; UT: WOS:A1983QQ83100001.

[97] B. Gao, S. Peigneur, J. Dalziel, J. Tytgat, and S. Zhu, "Molecular divergence of two orthologous scorpion toxins affecting potassium channels," *Comparative Biochemistry and Physiology A-Molecular and Integrative Physiology*, vol. 159, pp. 313–321, JUL 2011. PT: J; NR: 40; TC: 5; J9: COMP BIOCHEM PHYS A; PG: 9; GA: 774JM; UT: WOS:000291381500015.

[98] J. Yao, X. Chen, H. Li, Y. Zhou, L. Yao, G. Wu, X. Chen, N. Zhang, Z. Zhou, T. Xu, H. Wu, and J. Ding, "Bmp09, a "long chain" scorpion peptide blocker of bk channels," *Journal of Biological Chemistry*, vol. 280, pp. 14819–14828, APR 15 2005. PT: J; NR: 48; TC: 18; J9: J BIOL CHEM; PG: 10; GA: 914OI; UT: WOS:000228236800060.

[99] C. Miller, "An overview of the potassium channel family," *Genome Biol*, vol. 1, no. 4, pp. 1–5, 2000.

[100] J. Dalziel, S. Finch, and J. Dunlop, "The fungal neurotoxin lolitrem b inhibits the function of human large conductance calcium-activated potassium channels," *Toxicology letters*, vol. 155, pp. 421–426, MAR 15 2005. PT: J; NR: 29; TC: 18; J9: TOXICOL LETT; PG: 6; GA: 892JE; UT: WOS:000226645800010.

[101] E. Berthier, E. W. K. Young, and D. Beebe, "Engineers are from pdms-land, biologists are from polystyrenia," *Lab on a Chip*, vol. 12, no. 7, pp. 1224–1237, 2012. PT: J; NR: 140; TC: 10; J9: LAB CHIP; PG: 14; GA: 904LD; UT: WOS:000301196700002.

[102] C. D. Chin, V. Linder, and S. K. Sia, "Commercialization of microfluidic point-of-care diagnostic devices," *Lab on a Chip*, vol. 12, no. 12, pp. 2118–2134, 2012. PT: J; NR: 78; TC: 16; J9: LAB CHIP; PG: 17; GA: 947RY; UT: WOS:000304448700005.

[103] H. Becker, "It's the economy ...," *Lab on a Chip*, vol. 9, no. 19, pp. 2759–2762, 2009. PT: J; NR: 6; TC: 16; J9: LAB CHIP; PG: 4; GA: 494GM; UT: WOS:000269799800001.

[104] H. Becker, "Chips, money, industry, education and the "killer application"," *Lab on a Chip*, vol. 9, no. 12, pp. 1659–1660, 2009. PT: J; NR: 1; TC: 10; J9: LAB CHIP; PG: 2; GA: 453MZ; UT: WOS:000266616000001.

[105] D. Danchip, "Annex 1 - pricebook for dtu danchip effective: January 1st - 2013 version: 2013-1.0," 2013.

[106] J. Greener and R. Wimberger-friedl, *Precision Injection Molding: Process, Materials, And Applications-*. Munich: Hanser, 2006.

[107] "Ansi/sbs 4-2004 well positions for microplates," 2004.

List of publications

PAPER I *Fabrication of combined-scale nano- and microfluidic polymer systems using a multilevel dry etching, electroplating and molding process.* Simone Tanzi, Peter Friis Østergaard, Marco Matteucci, Thomas Lehrmann Christiansen, Jiri Cech, Rodolphe Marie, and Rafael Taboryski, J. Micromech. Microeng. 22 (2012) 115008

PAPER II *All-in-polymer injection molded device for single cell capture using multilevel silicon master fabrication.* Simone Tanzi, Simon T. Larsen, Marco Matteucci and Rafael Taboryski, Conference proceeding for NSTI-Nanotech 2012, Vol. 2, 2012

PAPER III *Fabrication and characterization of injection molded multi level nano and microfluidic systems.* Marco Matteucci, Thomas Lehrmann Christiansen, Simone Tanzi, Peter Friis Østergaard, Simon T. Larsen and Rafael Taboryski, Microelectron. Eng. (2013)

PAPER IV *High quality ion channels recordings on an injection molded polymer chip.* Simone Tanzi, Marco Matteucci, Thomas Lehrmann Christiansen, Søren Friis, Mette T. Christensen, Jørgen Gærnes, Sandra Wilson, Jonatan Kutchinsky and Rafael Taboryski, Ready to be submitted

PATENT APPLICATION I *Polymeric device for electrophysiological recordings.* European Patent Application No. EP13166109.2 (DTU ref. 95412).

PAPER I

Fabrication of combined-scale nano- and microfluidic polymer systems using a multilevel dry etching, electroplating and molding process

Simone Tanzi, Peter Friis Østergaard, Marco Matteucci, Thomas Lehrmann Christiansen, Jiri Cech, Rodolphe Marie, and Rafael Taboryski

J. Micromech. Microeng. 22 (2012) 115008

IOPscience iopscience.iop.org

Home Search Collections Journals About Contact us My IOPscience

Fabrication of combined-scale nano- and microfluidic polymer systems using a multilevel dry etching, electroplating and molding process

This article has been downloaded from IOPscience. Please scroll down to see the full text article.

2012 J. Micromech. Microeng. 22 115008

(http://iopscience.iop.org/0960-1317/22/11/115008)

View the table of contents for this issue, or go to the journal homepage for more

Download details:
IP Address: 87.60.10.232
The article was downloaded on 06/10/2012 at 08:55

Please note that terms and conditions apply.

J. Micromech. Microeng. 22 (2012) 115008 (11pp) doi:10.1088/0960-1317/22/11/115008

Fabrication of combined-scale nano- and microfluidic polymer systems using a multilevel dry etching, electroplating and molding process

Simone Tanzi[1], Peter Friis Østergaard[1], Marco Matteucci, Thomas Lehrmann Christiansen, Jiri Cech, Rodolphe Marie and Rafael Taboryski[2]

Department of Micro- and Nanotechnology, Technical University of Denmark, DTU Nanotech, Building 345E, DK-2800 Kongens Lyngby, Denmark

E-mail: rata@nanotech.dtu.dk

Received 29 May 2012, in final form 23 July 2012
Published 25 September 2012
Online at stacks.iop.org/JMM/22/115008

Abstract

Microfabricated single-cell capture and DNA stretching devices have been produced by injection molding. The fabrication scheme employed deep reactive ion etching in a silicon substrate, electroplating in nickel and molding in cyclic olefin polymer. This work proposes technical solutions to fabrication challenges associated with chip sealing and demolding of polymer high-volume replication methods. UV-assisted thermal bonding was found to ensure a strong seal of the microstructures in the molded part without altering the geometry of the channels. In the DNA stretching device, a low aspect ratio nanoslit (1/200) connecting two larger micro-channels was used to stretch a 168.5 kbp DNA molecule, while in the other device single-HeLa cells were captured against a micro-aperture connecting two larger microfluidic channels. Different dry etching processes have been investigated for the master origination of the cell-capture device. The combination of a modified Bosch process and an isotropic polysilicon etch was found to ensure the ease of demolding by resulting in slightly positively tapered sidewalls with negligible undercut at the mask interface.

(Some figures may appear in colour only in the online journal)

Introduction

In recent years, polymeric materials [1–4] have gradually replaced glass and silicon [5, 6] as the preferred production platform for the production of microfluidic devices. Polymers exhibit a broad range of appealing chemical, mechanical, electrical and optical properties [7]. Moreover, the multitude of different methods to manufacture microstructures in polymers make polymeric materials suitable for almost any given application, ranging from fast prototyping methods such as polydimethylsiloxane (PDMS) casting, laser milling or micromachining [8–10] to high volume mass production. In terms of physical parameters and thus technological pathways to fabrication, polymers can be classified into thermosets, thermoplastics and elastomers [7]. While PDMS have become a primary choice for fast prototyping and low-volume manufacturing in the academic environment [11], technical thermoplastic polymers are employed by commercial replication methods like injection molding [12, 13] and hot embossing [14]. However, polymer mass replication methods are poorly compatible with the requirements for flexibility and fast turnaround times in the research environment. Traditional injection-molding tools are expensive and very time-consuming to fabricate. We propose a technology that aims to narrow the gap between methods and materials used

[1] These two authors contributed equally to this article.
[2] Author to whom any correspondence should be addressed.

 © 2012 IOP Publishing Ltd Printed in the UK & the USA

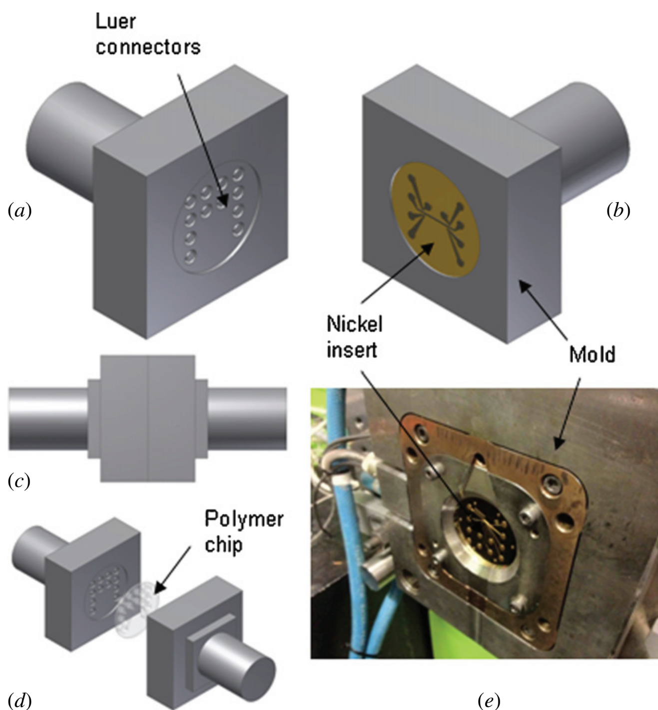

Figure 1. The figures illustrate the principle of the injection molding process. (*a*) Mold shaped with the Luer connectors. (*b*) Mold containing the microstructured nickel shim. (*c*) Mold is closed in order to form the cavity where polymer is injected. (*d*) Mold is pulled apart and the polymer chip can be removed. (*e*) Pictures of the mold with the nickel insert.

in the academic and industrial environments. This consists of a versatile prototyping technology directly applicable to mass production. A nickel electroform is produced from a microfabricated silicon master to transfer micrometer features to a substrate suitable for injection molding, as shown in figure 1. Origination of a master having the inverse structures of the final part is the underlying principle of any replication technology [7]. The relatively expensive step requiring microfabrication is only performed once on a single master and identical polymer substrates can be produced in high quantity [7]. Various techniques have been used in the past for mold insert origination such as micromachining methods and electroplating methods [15]. Among those methods, the most commonly used are LIGA[3] [16], and LIGA-like techniques, depending on the source of radiation employed [17, 18]. Although LIGA remains the best choice for high aspect ratio microstructures [19], it suffers from serious drawbacks when required facilities and the associated costs are considered. LIGA-like processes, in particular, the well-established UV-LIGA, then becomes the low-cost alternatives. Despite the fact that SU-8 is a versatile material, it suffers from technological limitations when multilevel structuring in the microrange and a silicon single-crystal polished master surface flatness are needed. Therefore, an alternative fabrication process has to be evaluated. A method where micro-channels are not made in thick photoresist but directly in silicon using wet etching was first described by McCormick *et al* [20]. Elwenspoek *et al* [21] proposed a process in which the x-ray lithography step of the LIGA process is substituted by dry etching. The process was called DEEMO, which is the acronym for dry etching, electroplating and molding [21, 22]. The state of the art in dry etching techniques makes it possible to design advanced microfluidic systems, where the intersection between channels with heights in broad ranges from nanometers or micrometers to tens of micrometers are required [23]. Moreover, this method exploits the advantages of dry etching in terms of directional freedom—the serious drawback when wet etching is used—low roughness and high selectivity with respect to the mask material [24–26]. We describe a procedure to fabricate combined microfluidic and nanofluidic systems in a thermoplastic polymer platform. Networks of microfluidic channels down to 100 nm in height are demonstrated. The performance of microfluidic systems, originated by using a multilevel DEEMO process, has been evaluated by fabricating two different devices addressing specific biological applications such as single-cell trapping and stretching of DNA molecules. A multilevel fabrication scheme has been adopted where a silicon oxide mask is employed to define the small features on the Si master. Reactive ion etching (RIE) and deep reactive ion etching (DRIE) techniques are used for etching. The parts are injection molded in cyclic olefin copolymers (COCs) [27, 28]. As reviewed by Nunes *et al* [29] COCs are increasingly popular as substrates for microfluidic applications. They have promising properties such as high chemical resistance, low water absorption, good optical transparency and ease of fabrication by injection molding [15]. Devices in COCs have already been implemented for a multitude of applications, including capillary electrophoresis [30], electrochromatography [31] and mass spectroscopy [32].

The novel feature of this work is the demonstration of DEEMO processes to fabricate combined scale microfluidic chips for cell capture and for DNA stretching. The key feature of the cell trapping chip is a few micrometer-sized side channels that connect two 50 μm deep channels, while the key feature of the DNA chip is the combined scale of a 100 nm slit connecting two micrometer-sized main channels. Both devices were fabricated by injection molding of COC Topas and sealed by UV-assisted thermal bonding to a thin polymer foil. The complete device resulted from only two parts bonded together. Figure 2 shows a 3D model of the polymer device and the molded part before bonding. The use of the thin polymer foil addresses the requirements of the short working distance for microscopy in both applications. Integrated inlet/outlet ports designed according to the Luer-fitting standard [33] for practical fluidic interconnects are defined by the traditional machined part of the injection-molding tool, figure 1(*a*). In addition, we also propose technical solutions to the fabrication challenges of any injection-molded microfluidic device such as chip sealing and part demolding.

Chip design and motivation

Two different chip designs have been studied. The first design addresses the capture of single cells, while the second one is concerned with stretching of DNA macromolecules.

[3] German acronym for lithographie (lithography), galvanoformung (electroplating), abformung (molding).

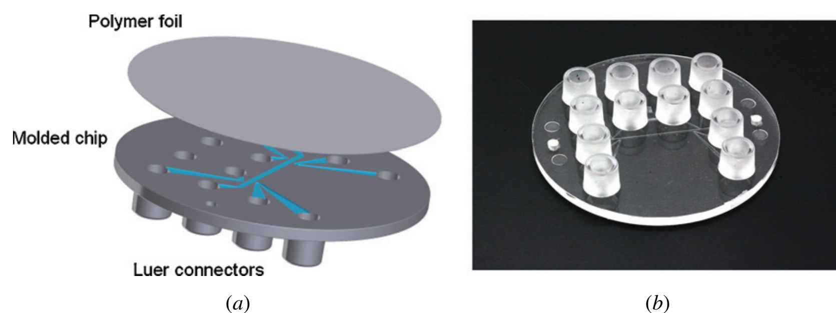

(*a*) (*b*)

Figure 2. (*a*) 3D representation of the polymer device concept. Both the final devices result from UV-assisted thermal bonding between an injection-molded polymer part and a 100 μm thick lid. The blue color shows the microfluidics open system for the cell-capture device. (*b*) Molded part for the cell-capture device.

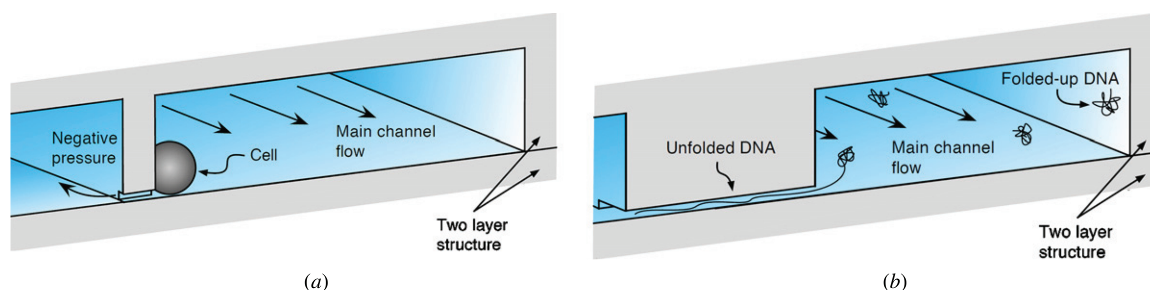

(*a*) (*b*)

Figure 3. (*a*) Concept design of the cell-capture device with 'cornered' apertures based on microfluidic junctions between a large chamber for cell delivery and a lateral capillary for cell trapping. (*b*) Concept design of DNA stretching device with intersection between a nanoslit and a large inlet channel.

Figure 3 shows the concept design for both devices. Precise manipulation of cells and DNA molecules at micro- and nanoscale are both becoming widely used techniques with a broad range of biological applications. Here we utilize these devices as examples to present solutions to specific fabrication challenges related to polymer microfluidic systems such as demolding of the polymer parts and sealing of structures with a very low aspect ratio (height over width).

Single-cell capture

Manipulation of single cells is basic for cell-related studies, such as drug screening and cell impedance analysis. The most commonly used technologies for cell trapping in microfluidic systems comprise both non-contact and contact mode trapping techniques [34–36]. Either hydrodynamic effects are used to retain cells or externally applied field gradients that induce forces on cells such as electrical [37], optical [38], magnetic [39] or acoustic [40] fields are used to enable cell trapping conditions. Among hydrodynamic cell trapping methods, the most common way consists of creating side channels in a main transport channel, where the side channel dimensions are sufficiently small to trap cells to it by suction. Seo *et al* [41] reported on lateral apertures in the PDMS microfluidic device for electrophysiology recordings. Lee *et al* [42] reported on the device for monitoring direct cell–cell communication via gap junctions between individual cell pairs. Our device enables us to capture a cell flowing in a carrier channel close to a small microhole by the application of suction. The chip comprises a 'cornered' (non-planar) aperture based on a microfluidic junction between a large chamber for cell delivery and a lateral capillary for cell trapping. Similar apertures have been reported by Zanetti *et al* [43], but for an elastomeric platform. The silicon master contains both suction channels (5 μm wide, 4 μm deep) and carrier channels (200 μm wide, 50 μm deep). The critical dimensions of the suction channels are comparable with defects associated with demolding, as will be discussed later.

DNA stretching

Stretching of DNA macromolecules through nanofluidic networks is becoming a powerful tool for direct sizing and mapping of DNA [44, 45]. Utko *et al* [46] have demonstrated DNA stretching experiments performed on individual double-stranded molecules in nanochannels on an injection-molded substrate. Rough sequencing of the genetic code of DNA can be performed by melting mapping experiments of elongated DNA, as explained by Reisner *et al* [47, 48]. Polymer systems intended for such purposes have been fabricated by the use of injection molding [46], but for long strands of DNA, narrow channels are not preferable, as the DNA can get in the way of itself, blocking the channel. Instead, nanoslits, that have a height in the nanometer regime, but a width in the micrometer regime, can be used [49, 50]. For fabricating the slit devices, the use of very expensive e-beam pattering is thus not required as the nanometer-sized dimension is defined by the oxide thickness [46]. The chip comprises nanoconducts (100 nm deep, 20 μm wide) intersecting a micro-scale channel. In this case the main challenge is the sealing of the fluidic system using UV-assisted bonding, when the extremely low aspect ratio may cause a collapse of the nanostructures.

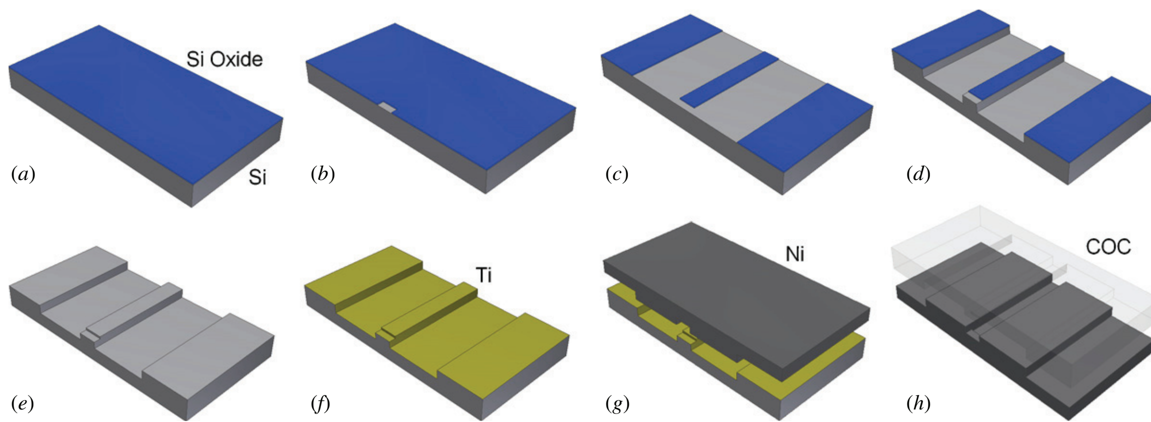

Figure 4. Schematics of the fabrication process for the cell-capture device after main steps: (*a*) oxidation with 100 nm thick silicon oxide; (*b*) oxide etching of the shallow microchannels; (*c*) oxide etching of the main chambers; (*d*) DRIE of the main chambers; (*e*) RIE of the shallow channels and oxide removal; (*f*) sputtering of 100 μm titanium seed layer; (*g*) electroplating of 340 μm nickel shim; (*h*) injection molding of COC Topas chips.

Table 1. The table shows the process parameters for the silicon master origination for both devices. For the etching of the inlet channels (called deep in the table) two different processes have been used: DRIE for the cell-capture device and RIE for the DNA stretching device.

Process	Parameters cell-capture device	Parameters DNA stretching device
Oxide deposition	1050 °C dry oxidation; $t = 90$ min + 20 min annealing	
Spin coating	HMDS vapor deposition 2.2 μm AZ5214E pre-bake: 90 °C for 90 s	HMDS vapor deposition 1.5 μm AZ5214E pre-bake: 90 °C for 90 s
Photolithography	hard contact mode, front side alignment W/A = 7 mW cm^{-2}; $t = 9$ s AZ351 developer; $t = 90$ s	hard contact mode, front side alignment W/A = 7 mW cm^{-2}; $t = 7$ s AZ351 developer; $t = 70$ s
Oxide etch (shallow channels)	CF_4/CHF_3 = 14/26 sccm; $t = 210$ s; W_{RF} = 60 W; P = 100 mTorr	
Spin coating	HMDS vapor deposition 6.2 μm AZ5214E pre-bake: 100 °C for 100 s	HMDS vapor deposition 1.5 μm AZ5214E pre-bake: 90 °C for 90 s
Photolithography	hard contact mode, front side alignment W/A = 7 mW cm^{-2}; $t = 30$ s AZ351 developer; t = 300 s	hard contact mode, front side alignment W/A = 7 mW cm^{-2}; $t = 7$ s AZ351 developer; t = 70 s
Oxide etch (deep channels)	CF_4/CHF_3 = 14/26 sccm; $t = 210$ s; W_{RF} = 60 W; P = 100 mTorr	
Si DRIE/RIE (deep channels)	$SF_6/O_2/Ar$ = 180/160/100; P = 246≫91mT, coil 2.8kW, platen (HF) 170≫215W, t = 2:40 min	SF_6/O_2 = 32/8 sccm; W_{RF} = 30 W; t = 13.5 min; P = 80 mTorr
Si RIE (shallow channels)	SF_6/O_2 = 32/8 sccm; W_{RF} = 30 W; t = 4 min; P = 80 mTorr	Not required
Oxide removal	BHF bath; t = 3 min	Not required

Experimental details

Fabrication

The fabrication scheme for the two systems is similar, as can be seen in table1. Hence, the description will be made in parallel and only substantial differences between the processes will be marked and explained. A two-step lithography process is needed to fabricate the Si master, figure 4. We start from 100 mm, ⟨1 0 0⟩, single side polished, 525 μm thick silicon wafers. Wafers are oxidized for 90 min in a Tempress horizontal furnace at 1050 °C with an oxygen flow of 5 slm[4] and 20 min annealing at the same temperature, with a nitrogen flow of 3 slm. During heating and cooling, a nitrogen flow of 3 slm is used.

While for the cell-capture device the oxide layer is used only to mask the Si along the process, for the DNA chip the 100 nm thick oxide defines the height of the nanoslits. A chemical treatment with hexamethyldisilazane (HMDS) before any spin coatings is used to promote the adhesion of the resist. The treatment is performed in a STAR2000 HMDS/vapor prime oven from IMTEC. A μm range thick layer of AZ5214E photoresist from MicroChemicals is applied to the substrates, using a SSE Maximus 804 cluster system. The desired layouts are then transferred to the wafer, using a

[4] Standard liters per minute.

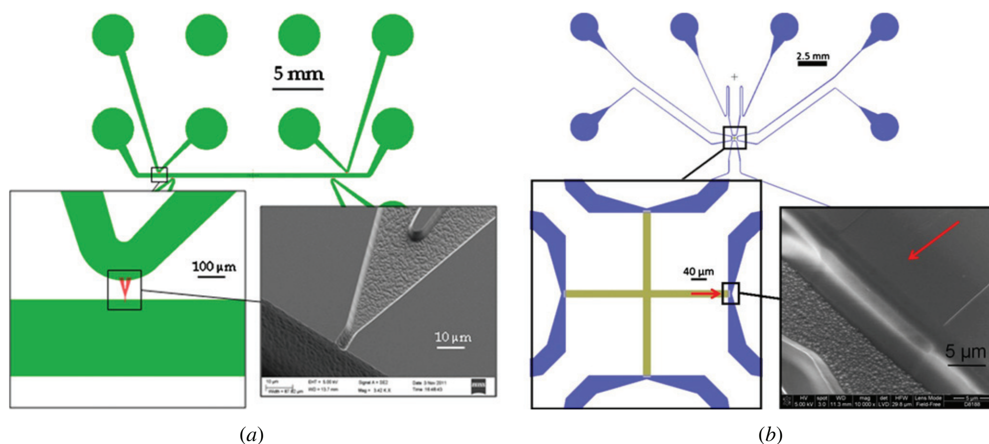

(*a*) (*b*)

Figure 5. Layout of the two devices. (*a*) Design of the cell-capture chip, with an enlargement of the suction channel and a SEM micrograph of it. (*b*) Design of the DNA stretching chip, with an enlargement of the crossing nanoslits and a SEM micrograph of the intersection.

Karl Süss Mask Aligner MA6 (exposure wavelength 365 nm) in hard contact mode and front side alignment. To obtain the nanoslits and the shallow channels, the wafers are then developed in AZ351 and exposed to a CF_4/CHF_3 plasma reactive ion etch in an STS (surface technology systems) cluster system C004. The high SiO_2/Si selectivity of this etching process ensures that the final height corresponds to the height of the oxide layer. The remaining photoresist is then removed in oxygen plasma. A second lithography step is performed for the fabrication of the carrier channels in Si, and to access the Si the oxide is etched as described above. The process for producing the carrier channels differs between the two chips; for the DNA chip an anisotropic RIE etching of Si is performed, while for the cell-capture chip a DRIE is required. A continuous process is performed with a Pegasus STS system. The $SF_6/O_2/Ar$ plasma was optimized to obtain tapered sidewalls and smooth surfaces. For the fabrication of the shallow channels in the cell-capture system, a final RIE etching into silicon is performed using the oxide left as mask. The final result gives shallow channels of 4 μm deep and 5 μm wide. The proposed scheme, in which the fabrication of the small channels is postponed, allows the use of the RIE step to eliminate the small undercut that the carrier channels exhibit after the continuous DRIE process. The removal of the oxide mask in a buffered HF completes the process. To prepare the samples for electroplating, a conductive seed layer is sputtered by a sputtering system from Lesker. For the DNA chip, a 90 nm nickel/vanadium thick layer is used, while a 100 nm thick layer of Ti is deposited for the cell-capture chip. Different seed materials are needed due to the fact that it was not possible readily to separate the Ni shim from the Si wafer for the cell-capture device, so the Si was etched away in KOH, and long etching time in KOH was found to damage the NiV. Electroplating is performed in a Technotrans Microform 200 electroplater. In this process, the current is increased linearly from 0 to 0.5 A during the first 15 min, and from 0.5 to 1.5 A for the next 15 min. Then the current is constantly raised up to 17 A. This gives a nickel shim with a thickness of about 300 μm. The silicon wafer is removed. If the wafer is loosely attached to the Ni shim, then this can be carried out by lifting it off by hand, and with stronger adhesion, the Si wafer is dissolved in KOH (figures 2 and 5). The resulting nickel-electroplated sample is punched into an 85 mm diameter shim by using a hydraulic press fitted with a customized punching tool. The shims have two flats to ensure rotational direction definition when mounted in the injection-molding tool. Standard epoxy high-temperature resistant glue is used to fill up the resultant cavities on the backside of the shim, and then manually polished with fine grade sand paper to even the backside.

Replicas of the original structures are injection molded in an ENGEL Victory 80/45 Tech injection molder, with the Ni-shim installed into the mold. The custom designed mold produces 50 mm in diameter and 2 mm in thickness polymer chips that contain 12 Luer-fittings [15] used to connect the microfluidic channels on the chip to external flow or air-pressure controls, figure 2(*b*).

Parts are molded from COC TOPAS grade 5013 from TOPAS Advanced Polymers GmbH. Topas grade 5013 has a glass transition temperature (T_g) of 135 °C and is molded using a variotherm process with a nozzle temperature of 280 °C, a mold temperature of 110 °C and a demolding temperature of 65 °C. A high holding pressure of 1300 bar was used to prevent the polymer from backflowing during the cool down period.

The molded chip is sealed against an extruded 100 μm thick TOPAS foil of the same grade, by UV-assisted thermal bonding. A 3D model of the final device is shown in figure 2.

UV-assisted thermal bonding

Both the chip and thelid were exposed to a UV radiation for 30 s. The exposure was performed using a DIMAX mercury UV bulb F/5000 lamp emitting over the full unfiltered Hg line spectrum and the bonding by using a P/O/Weber press with decoupled internal temperature control of both plates. In order to ensure uniform pressure all over the chip surface, an aluminum holder was built in which the Luer-fitting protrusions could be inserted. In addition, the top lid was covered with a combination of a 300 μm thick nickel disc and a thin PDMS layer with the purpose of compensating possible non-uniformities in flatness. Sealing of the cell-capture device employed a piston force of 10 kN applied for

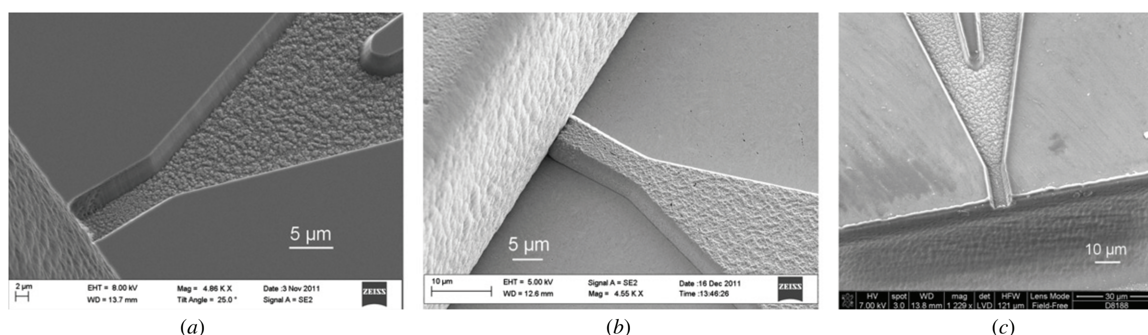

(*a*) (*b*) (*c*)

Figure 6. SEM micrographs of the capturing channel after the main steps of the DEEMO process; shaping of the silicon master (*a*), electroplating of the nickel insert (*b*) and molding of the final part (*c*).

Table 2. Sample surfaces have been evaluated using tapping mode AFM. We used DME DualScope C-21 with BS-TAP300AL probes. Probe force constant was 40 N m^{-1}. We collected topology data from three regions (10.5 μm × 10.5 μm) on each of investigated samples, selected regions have been cca 75 μm apart. Each region was scanned with resolution of 512 × 512 points.

	Silicon master			Nickel tool			TOPAS polymer		
	A	B	C	A	B	C	A	B	C
S_A(nm)	0.780	0.773	0.801	0.877	1.000	1.090	0.636	1.060	0.941
S_{RMS}(nm)	1.180	1.010	1.100	1.200	2.640	2.540	0.837	1.400	1.250
S_{SK}	6.020	1.030	2.240	1.240	19.700	18.900	0.600	−0.830	−1.460

5 min, while maintaining a temperature of 120 °C.[5] For the DNA stretching device, the force was applied for 10 min at 110 °C as the standard procedure. The timing and choice of pressure are fairly critical as the polymer begins to deform plastically as it approaches the glass transition temperature.

Validation of the cell-capture chip

HeLa cells were cultured on collagen (type 1, Sigma Aldrich) coated Nunclon T25 flasks (Nunc A/S). Cells were detached using trypsin, triturated to loosen cell clumps, centrifuged at 1200 rpm for 3 min and resuspended in phosphate-buffered saline (PBS, Lonza). The cell solution was vortexed on a vortex mixer to distribute the cells evenly. Microscope images and videos were obtained using an AxioObserver A1 microscope with Axiovision software (Carl Zeiss, GmbH). Prior to experiments, the fluidic channel system of the cell-capture chip was filled with PBS. Cells were introduced into the inlet port by using a 1 ml syringe and they slowly flowed along the carrier channel. When a targeted cell approached within 100 μm from the lateral aperture, a slight suction (<20 mbar) was applied to the side channel using a custom-made pressure controller build from a piezo-valve terminal from Festo controlled with Labview software (National Instruments).

Validation of the nanoslit chip

To ensure that the low aspect ratio nanoslit is open after the bonding, the channels are filled with ethanol. Since the COC polymer is hydrophilic toward ethanol, the filling happens by capillary forces, and no external pumps are required to do the testing. In order to verify that the slit is not collapsed, the chip was observed under a reflective microscope (Zeiss Axioskop 40), and the difference of refractive indexes between ethanol and air makes it easy to see when the nanoslit is filled. See figure 9. To further verify the functionality of the chip, preliminary experiments[6] were performed with YOYO-1 (Invitrogen) stained T4GT7-DNA, with a length of 168.5 kbp suspended in TBE buffer. The DNA was driven into the nanoslit by the application of hydrostatic pressure to relevant Luer ports of the chip and observed by fluorescence microscopy. See the bottom panel of figure 9.

Results and discussions

An overview of the two layouts of the channel patterns is shown in figure 5. In the cell-capture device, a shallow microfluidic channel works as a hydraulic connection between two of the deep inlet channels. The suction channel has a depth and a width shallower than the size of the cells at the opening for the cell capture. It has a wider opening at the other end for the reduction of the total hydraulic resistance of the suction channel for the ease of cell capture by the application of a negative pressure difference across it. A support structure has been introduced for the prevention of collapse of the channel during the bonding process. The second design shows a cross of two nanoslits connected to inlet channels. In both devices the inlet channels connect to buffer reservoirs consisting of female Luer connectors, which provide direct access to the described fluidic systems.

The intersections between inlet channels and either suction capillary or nanoslit are the key features in both the designs. The replication accuracy of those structures at the intersection gives a vital indication about the device performance after bonding. The replication quality of the injection-molded microstructures is investigated by scanning electron microscopy (SEM) and atomic force microscopy

[5] Further details on the bonding process will be reported elsewhere.

[6] Further results on the usage of the DNA devices will be reported elsewhere.

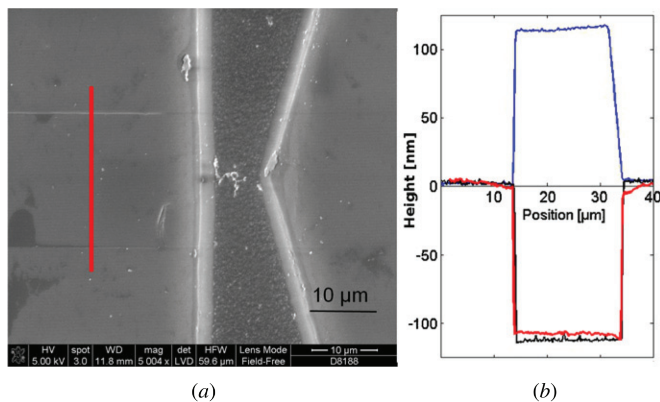

Figure 7. Detail of the intersection between nanoslits and carrier channels in the DNA-stretching chip (*a*) together with atomic force microscope (AFM) measurements of the nanoslit section (red line). (*b*) Profile across the slit measured on the silicon wafer (black line), the nickel shim (blue line) and the polymer part (red line).

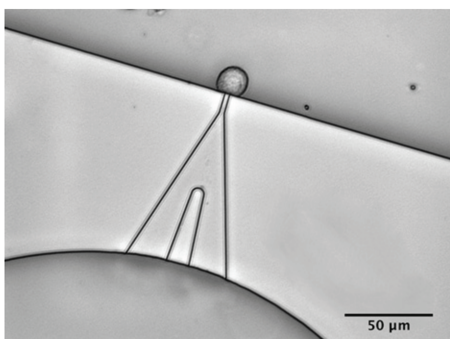

Figure 8. Optical microscope image of a single HeLa cell captured at the cornered aperture at one end of the capturing channel. This chip is a replica of a silicon master fabricated with the modified Bosch process.

(AFM). Figure 6 shows SEM micrographs of the capturing channel after the main steps of the DEEMO process. All details are faithfully replicated from the silicon to the thermoplastic chip. Moreover, the surface roughness of the three samples, respectively, silicon wafer, nickel shim and COC part was investigated by AFM. The polymer part exhibited a very low surface roughness (Sa <1 nm) comparable with the initial roughness of the silicon wafer demonstrating an optimal replication through the whole process. Topology data from the bonding surfaces are shown in table 2. The surface roughness in the channels was somewhat higher, but this was not critical for the functionality of the devices. In the DNA chip, the replication of the nanoslits was verified by the characterization of the silicon, nickel and polymer samples by AFM, results shown in figure 7.

A strong motivation for employing a DEEMO process instead of UV-LIGA is the possibility of exploiting the enormous potential of the MEMS tool box. Multilevel microfluidic systems have been realized by SU-8 [51, 52], and two level SU-8 structures have been used to fabricate high aspect ratio gear structures in plastic by the UV-LIGA process [53]. However, the very low surface flatness across the silicon wafer is easily compromised in the double-layer LIGA process making it very challenging to seal the resulting parts afterward.

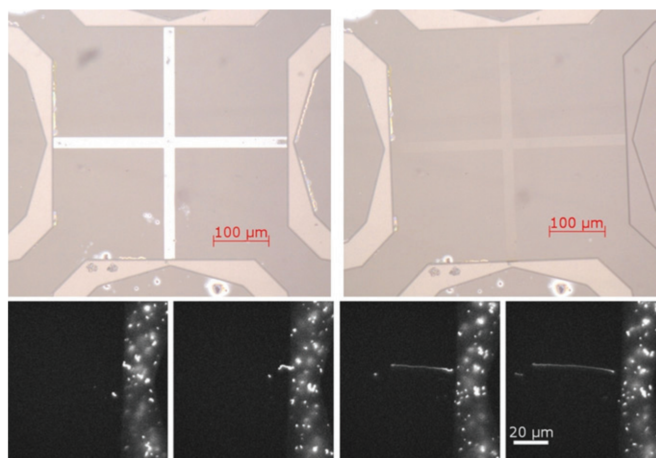

Figure 9. Bonded nanoslit. On the top image to the left, the slit is empty, on the image to the right, the slit has been filled with ethanol. In the bottom pictures, the fluorescence micrographs show a strand of T4GT7-DNA being pushed into the nanoslit. In the picture to the left, the DNA is at the inlet of the nanoslit. For each picture further to the right, it has been pushed further into the slit, until all of it has entered the slit in the picture to the far right.

In addition, the possibility of originating the positive geometry in the silicon master allows a single electroforming, where a nickel ‘mother’ electroform is not needed [20]. This results in a more robust process avoiding possible challenges when it comes to the mechanical separation of the nickel electroform ‘daughter’ from the ‘mother’.

Injection molding of micron and sub-micron scale structures is achieved through a molding process known as variotherm [7, 54], where the cavity is heated to a temperature close to the glass transition temperature of the polymer to facilitate the polymer to flow into the microfeatures of the mold insert. The part is ejected when the mold is cooled down below a suitable release temperature (in our case 60 °C) to release the molded part well after freeze of the polymer. This process substantially increases the cycle time, which was 220 s long in our case, of which the mold cool down time was 130 s. However, we believe that this time can be significantly reduced in an industrial framework by redesigning the mold for lower thermal mass, and a local cooling and heating system that does not require the whole mold to be heated and cooled. In addition, a parallelization of the molding and bonding process, using a multicavity mold for molding, and a bonding process that allows for bonding of more than one chip at a time would dramatically increase the throughput.

The efficiency of the thermal bonding on both devices was verified by filling the fluidic structures with liquid, as shown in figure 9. The DNA nanoslits with aspect ratios down to 1/200 could be successfully sealed only if great care was taken, using a special rig that allowed avoiding the direct contact between the piston and the foil in the critical slit areas of the devices. Failure modes resulting in collapse were caused by misalignment in the rig, leading to low but finite yield between 5% and 10% for the nanoslit devices. We do not see this issue as prohibitive for commercialization of the devices though, as automated precision alignment is possible on industrial scale. If the aspect ratio was increased to 1/20, the bonding occurred

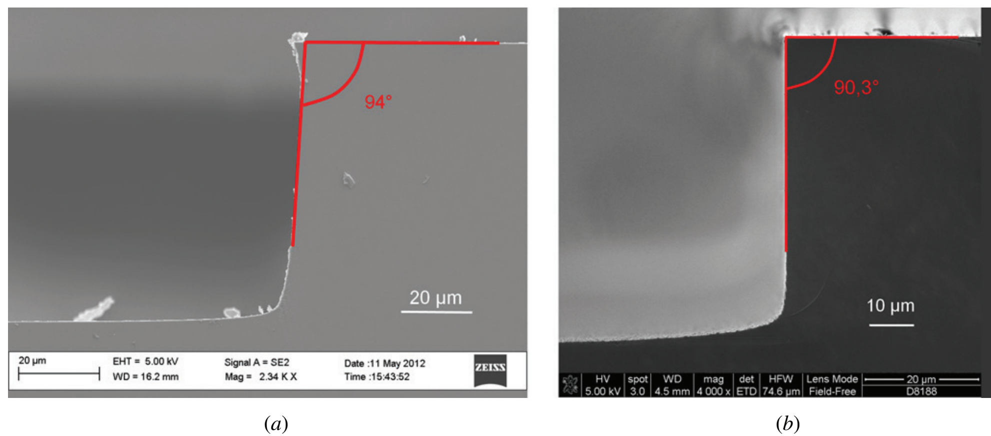

(*a*) (*b*)

Figure 10. (*a*) SEM micrograph of the cross-sectional profile of the deep channel from a cleaved wafer processed with continuous SF6/O2/Ar plasma isotropic etch process. The sidewall is positively tapered with an angle of 94°, while the underetching is about 4 μm. (*b*) SEM micrograph of the cross-sectional profile of the deep channel from a cleaved wafer processed with modified Bosch etching process. The sidewall slope is 90.3° and the underetching at the surface of the wafer is almost non-existing.

without collapse of the structures at almost all times using our standard procedure described above. Moreover, the bonding of chips for cell capture was not prone to channel collapse. When performed properly, the bonding process did not change the channel geometry significantly. This was verified by recording the electrical resistance of the channels, when those were filled with the electrolytic buffer solution. This measurement was then compared with the theoretical value calculated using the specific resistivity of the electrolyte and the detailed channel geometry. This method is very sensitive, since the electrical resistance of microfluidic channels is always dominated by the narrowest channel dimensions. Typically, correspondence within 10% was found between measured and calculated resistance. X-ray photoelectron spectroscopy (XPS) indicated that the UV treatment did not alter the surface chemistry of the parts, as opposed to plasma treatment, which is known to create O–C radicals on the surface. Rather the UV treatment seemed to have an annealing effect on the surface.

HeLa cells were used to demonstrate the functionality of the cell-capture device. Cells were introduced through the Luer ports into the inlet channel and then successfully attracted and trapped to the microopening by applying suction to the end of it. Figure 8 shows an optical micrograph of the capture of an HeLa cell at a cornered aperture. The functionality of the nanoslit system was also demonstrated by preliminary DNA stretching experiments with T4GT7 DNA molecules, as shown in figure 9.

Several dry etching processes for the silicon master origination for the cell-capture design were investigated, as this appeared to be a crucial step in the DEEMO process. Some applications can require channel depths of more than 100 μm, and the deeper the inlet channels, the larger are the challenges associated with demolding of the polymer parts in the injection-molding process. These issues occurred mainly due to undercuts at the interface with the mask in the DRIE process and caused scratching of the inlet channel sidewalls during demolding. In the worst scenario, the scratching can seal off the capture opening and make the device useless. The requirements for a proper mold are smooth and slightly positively tapered sidewalls and negligible undercut.

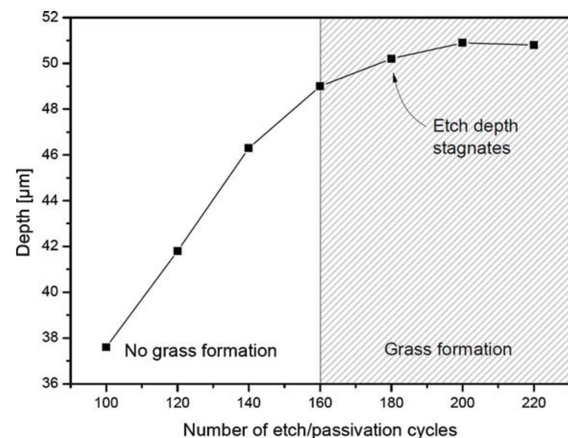

Figure 11. A plot of the etched depth as a function of the number of cycles in the modified DRIE Bosch process for the deep channel etches. It is seen that for high numbers of cycles, the etched depth stagnates, which is consistent with the observation of grass formation in the bottom of the etched channels.

Roxhed *et al* [55] reported on a method for etching tapered sidewalls in silicon using DRIE based on consecutive switching between anisotropic etching using the Bosch process and isotropic dry etching. Li *et al* [56] reported on a continuous DRIE of tapered via holes for three-dimensional integration. Jo *et al* [57] reported on a modified Bosch-type process applied to silicon mold fabrication used for structuring a microarray.

Two fabrication iterations have shown good results and they will be discussed. A continuous SF6/O2/Ar plasma isotropic etch process, as previously described in table 1, resulted in smooth tapered sidewalls (94°) with a mask undercut of about 4 μm, figure 10. The taper deviation at the interface between the oxide mask and the etched substrate is mainly caused by the difficulty of the etch gas to reach regions close below the mask [55]. This curvature generated challenges in terms of demolding when structures shallower than 4 μm have been structured. For smaller and in particular shallower (2 μm) lateral apertures, we used a modified Bosch etching process as a powerful alternative. Smaller capture holes are

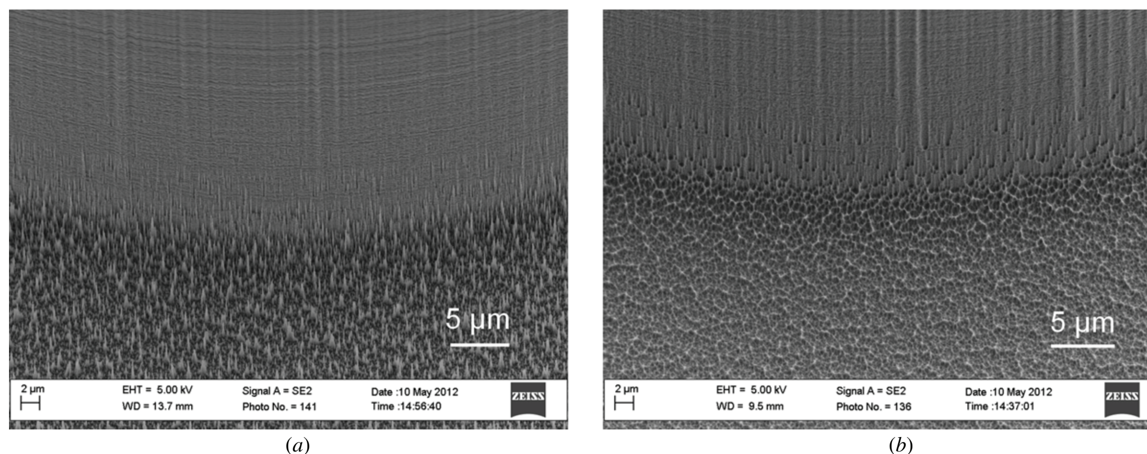

(*a*) (*b*)

Figure 12. (*a*) SEM micrograph of the grass developed in the bottom of the channel due to the high passivation to etch cycle time in the end of the etch process. (*b*) SEM micrograph of the same detail after the polysilicon (mixture of HNO_3, BHF and H_2O) wet etching process.

crucial when the device is intended for electrophysiological recordings [43]. A standard DRIE Bosch process is based on many repetitions of alternating etch and passivation cycles [58]. The etch depth is controlled by adjusting the number of cycles. This results in a scalloped sidewall with a slightly negative slope for deep etching, since ions are experiencing increased deflection from the bottom and sidewalls of the channel, thereby degrading the passivation layer and allowing slight lateral etching [59]. In order to correct this effect, the etch/passivation cycle time over the duration of the process was ramped. The slope of the ramping of the passivation cycle was set to be lower than the slope of the etch cycle time, hence resulting in an increase in the passivation to etch ratio. This was found to counteract the lateral etching and improve the sidewalls slope (90.3°) compared with a standard Bosch etching, see figure 10(*b*). The process showed almost no taper deviation ($<0.2\ \mu$m). However, the passivation layer was not sufficiently removed, due to the high passivation to etch cycle time at the end of the etch creating substantial grass formation at the bottom of the channel, figure 12(*a*). As can be seen from figure 11, showing the etched depth for varying numbers of etch/passivation cycles, the etch depth starts to stagnate around 160–180 cycles, indicating that the grass formation is dominating for higher cycle numbers. This might potentially be a problem during molding, as the polymer will fill up many small cavities in the nickel shim created by the grass, hence impeding the de-molding process. To this end, a polysilicon etch mixture of HNO_3, BHF and H_2O in the ratio 20:1:20 was found to remove the grass. Wet etching agents were previously used to smoothen rough silicon surfaces [60]. Well-known etchants such as KOH and TMAH can be used to smoothen surfaces, but both KOH and TMAH are anisotropic silicon etching agents, while polysilicon etch is a completely isotropic etch [61]. Figure 12 shows how the wet isotropic etching successfully reduced the grass and smoothened the scallops. The polymer parts injection molded from a silicon master originated with this second method showed excellent replication of the microstructures down to 2 μm in depth. The chip shown in figure 8 was fabricated with the modified Bosch process.

Conclusion

In this work, we presented a replication method for thermoplastic materials that we believe is suitable for prototyping, but also directly applicable to large-scale production. We used a standard injection-molding machine to demonstrate it. We have developed a fabrication scheme to produce multilevel all-polymer devices for biological applications. We employed the DEEMO method, which enables the direct etching of the silicon substrate, and exploits the large MEMS tool box for Si microfabrication. Using dry etching techniques, multilevel microfluidic systems can be structured in silicon and then replicated in thermoplastic polymers. This work also proposes technical solutions to typical challenges for molding of any polymer microfluidic devices such as chip sealing and chip demolding. UV-assisted thermal bonding was found to ensure strong seals of both micro- and nanostructured fluidic channels in the molded parts without altering their geometry. Two different etching processes have been demonstrated for master origination.

Acknowledgments

This work is supported by the Danish Advanced Technology Foundation through the Advanced Technology Project PILOC (grant no 061-2010-1) and by Sophion Bioscience for the part regarding the cell capture and by the Danish Council for Strategic Research through the Strategic Research Center PolyNano (grant no 10-092322/DSF) for the DNA stretching.

References

[1] Becker H and Gaertner C 2008 Polymer microfabrication technologies for microfluidic systems *Anal. Bioanal. Chem.* **390** 89–111
[2] de Mello A 2002 Plastic fantastic? *Lab Chip* **2** 31N–6N
[3] Figeys D and Pinto D 2000 Lab-on-a-chip: a revolution in biological and medical sciences *Anal. Chem.* **72** 330A–5A
[4] Curtis A and Wilkinson C 2001 Nantotechniques and approaches in biotechnology *Trends Biotechnol.* **19** 97–101

[5] Andersson H and van den Berg A 2003 Microfluidic devices for cellomics: a review *Sensors Actuator* B **92** 315–25

[6] Harrison D, Fluri K, Seiler K, Fan Z, Effenhauser C and Manz A 1993 Micromachining a miniaturized capillary electrophoresis-based chemical-analysis system on a chip *Science* **261** 895–7

[7] Becker H and Gartner C 2000 Polymer microfabrication methods for microfluidic analytical applications *Electrophoresis* **21** 12–26

[8] Becker H and Locascio L 2002 Polymer microfluidic devices *Talanta* **56** 267–87

[9] Duffy D, McDonald J, Schueller O and Whitesides G 1998 Rapid prototyping of microfluidic systems in poly(dimethylsiloxane) *Anal. Chem.* **70** 4974–84

[10] Klank H, Kutter J and Geschke O 2002 CO_2-laser micromachining and back-end processing for rapid production of PMMA-based microfluidic systems *Lab Chip* **2** 242–6

[11] McDonald J and Whitesides G 2002 Poly(dimethylsiloxane) as a material for fabricating microfluidic devices *Acc. Chem. Res.* **35** 491–9

[12] Heckele M and Schomburg W 2004 Review on micro molding of thermoplastic polymers *J. Micromech. Microeng.* **14** R1–14

[13] Giboz J, Copponnex T and Mele P 2007 Microinjection molding of thermoplastic polymers: a review *J. Micromech. Microeng.* **17** R96–109

[14] Heckele M, Bacher W and Muller K 1998 Hot embossing—The molding technique for plastic microstructures *Microsyst. Technol.* **4** 122–4

[15] Andresen K O *et al* 2010 Injection molded chips with integrated conducting polymer electrodes for electroporation of cells *J. Micromech. Microeng.* **20** 055010

[16] Becker E *et al* 1982 Production of separation-nozzle systems for uranium enrichment by a combination of x-ray-lithography and galvanoplastics *Naturwissenschaften* **69** 520–3

[17] Kupka R, Bouamrane F, Cremers C and Megtert S 2000 Microfabrication: LIGA-X and applications *Appl. Surf. Sci.* **164** 97–110

[18] Piotter V, Hanemann T, Ruprecht R and Hausselt J 1997 Injection molding and related techniques for fabrication of microstructures *Microsyst. Technol.* **3** 129–33

[19] Malek C and Saile V 2004 Applications of LIGA technology to precision manufacturing of high-aspect-ratio micro-components and -systems: a review *Microelectron. J.* **35** 131–43

[20] McCormick R, Nelson R, AlonsoAmigo M, Benvegnu J and Hooper H 1997 Microchannel electrophoretic separations of DNA in injection-molded plastic substrates *Anal. Chem.* **69** 2626–30

[21] Elders J, Jansen H, Elwenspoek M and Ehrfeld W 1995 DEEMO: A new technology for the fabrication of microstructures *IEEE Proc. Micro Electro Mechanical Systems (New York, NY)* pp 238–43

[22] Fintschenko Y and van den Berg A 1998 Silicon microtechnology and microstructures in separation science *J. Chromatogr.* A **819** 3–12

[23] Judy J 2001 Microelectromechanical systems (MEMS): fabrication, design and applications *Smart Mater. Struct.* **10** 1115–34

[24] Kastenmeier B, Matsuo P, Beulens J and Oehrlein G 1996 Chemical dry etching of silicon nitride and silicon dioxide using CF4/O-2/N-2 gas mixtures *J. Vac. Sci. Technol.* A **14** 2802–13

[25] Bondur J 1976 Dry process technology (reactive ion etching) *J. Vac. Sci. Technol.* **13** 1023–9

[26] Yih P, Saxena V and Steckl A 1997 A review of SiC reactive ion etching in fluorinated plasmas *Phys. Status Solidi* b **202** 605–42

[27] Lamonte R and McNally D 2000 Uses and processing of cyclic olefin copolymers *Plast. Eng.* **56** 51–5

[28] Shin J, Park J, Liu C, He J and Kim S 2005 Chemical structure and physical properties of cyclic olefin copolymers—(IUPAC technical report) *Pure Appl. Chem.* **77** 801–14

[29] Nunes P S, Ohlsson P D, Ordeig O and Kutter J P 2010 Cyclic olefin polymers: emerging materials for lab-on-a-chip applications RID A-7838–2012 RID E-3256–2010 *Microfluid. Nanofluid.* **9** 145–61

[30] Castano-Alvarez M, Fernandez-Abedul M and Costa-Garcia A 2005 Poly(methylmethacrylate) and topas capillary electrophoresis microchip performance with electrochemical detection *Electrophoresis* **26** 3160–8

[31] Faure K *et al* 2008 Development of an acrylate monolith in a cyclo-olefin copolymer microfluidic device for chip electrochromatography separation *Electrophoresis* **29** 4948–55

[32] Liu J, Ro K, Nayak R and Knapp D R 2007 Monolithic column plastic microfluidic device for peptide analysis using electrospray from a channel opening on the edge of the device *Int. J. Mass Spectrom.* **259** 65–72

[33] International Standard ISO 1986 1st edn 5941

[34] Di Carlo D and Lee L P 2006 Dynamic single-cell analysis for quantitative biology *Anal. Chem.* **78** 7918–25

[35] Jang L and Wang M 2007 Microfluidic device for cell capture and impedance measurement *Biomed. Microdevices* **9** 737–43

[36] Nilsson J, Evander M, Hammarstrom B and Laurell T 2009 Review of cell and particle trapping in microfluidic systems *Anal. Chem. Acta* **649** 141–57

[37] Taff B and Voldman J 2005 A scalable addressable positive-dielectrophoretic cell-sorting array *Anal. Chem.* **77** 7976–83

[38] Grier D 2003 A revolution in optical manipulation *Nature* **424** 810–6

[39] Lee H, Purdon A and Westervelt R 2004 Manipulation of biological cells using a microelectromagnet matrix *Appl. Phys. Lett.* **85** 1063–5

[40] Evander M *et al* 2007 Noninvasive acoustic cell trapping in a microfluidic perfusion system for online bioassays *Anal. Chem.* **79** 2984–91

[41] Seo J, Ionescu-Zanetti C, Diamond J, Lal R and Lee L 2004 Integrated multiple patch-clamp array chip via lateral cell trapping junctions *Appl. Phys. Lett.* **84** 1973–5

[42] Lee P, Hung P, Shaw R, Jan L and Lee L 2005 Microfluidic application-specific integrated device for monitoring direct cell-cell communication via gap junctions between individual cell pairs *Appl. Phys. Lett.* **86** 223902

[43] Ionescu-Zanetti C, Shaw R, Seo J, Jan Y, Jan L and Lee L 2005 Mammalian electrophysiology on a microfluidic platform *Proc. Natl Acad. Sci. USA* **102** 9112–7

[44] Tegenfeldt J *et al* 2004 The dynamics of genomic-length DNA molecules in 100-nm channels *Proc. Natl Acad. Sci. USA* **101** 10979–83

[45] Riehn R, Lu M, Wang Y, Lim S, Cox E and Austin R 2005 Restriction mapping in nanofluidic devices *Proc. Natl Acad. Sci. USA* **102** 10012–6

[46] Utko P, Persson F, Kristensen A and Larsen N B 2011 Injection molded nanofluidic chips: Fabrication method and functional tests using single-molecule DNA experiments RID F-3057–2011 RID C-4746-2008 *Lab Chip* **11** 303–8

[47] Reisner W *et al* 2005 Statics and dynamics of single DNA molecules confined in nanochannels *Phys. Rev. Lett.* **94** 196101

[48] Reisner W *et al* 2010 Single-molecule denaturation mapping of DNA in nanofluidic channels *Proc. Natl Acad. Sci. USA* **107** 13294–9
[49] Chantiwas R *et al* 2010 Simple replication methods for producing nanoslits in thermoplastics and the transport dynamics of double-stranded DNA through these slits *Lab Chip* **10** 3255–64
[50] Lee J, Yun Y, Kim Y and Jo K 2009 PDMS nanoslits without roof collapse *Bull. Korean Chem. Soc.* **30** 1793–7
[51] Huang S, Tan W, Tseng F and Takeuchi S 2006 A monolithically three-dimensional flow-focusing device for formation of single/double emulsions in closed/open microfluidic systems *J. Micromech. Microeng.* **16** 2336–44
[52] Steigert J *et al* 2008 A versatile and flexible low-temperature full-wafer bonding process of monolithic 3D microfluidic structures in SU-8 *J. Micromech. Microeng.* **18** 095013
[53] Lorenz H, Despont M, Fahrni N, Brugger J, Vettiger P and Renaud P 1998 High-aspect-ratio, ultrathick, negative-tone near-UV photoresist and its applications for MEMS *Sensors Actuator* A **64** 33–39
[54] Fu G, Loh N, Tor S, Tay B, Murakoshi Y and Maeda R 2005 A variotherm mold for micro metal injection molding *Microsyst. Technol.* **11** 1267–71
[55] Roxhed N, Griss P and Stemme G 2007 A method for tapered deep reactive ion etching using a modified bosch process *J. Micromech. Microeng.* **17** 1087–92
[56] Li R, Lamy Y, Besling W F A, Roozeboom F and Sarro P M 2008 Continuous deep reactive ion etching of tapered via holes for three-dimensional integration *J. Micromech. Microeng.* **18** 125023
[57] Jo S, Lee M, Lee S, Lee E, Park S and O B 2005 Characterization of a modified Bosch-type process for silicon mold fabrication *J. Vac. Sci. Technol.* A **23** 905–10
[58] Ayon A A, Braff R, Lin C C, Sawin H H and Schmidt M A 1999 Characterization of a time multiplexed inductively coupled plasma etcher *J. Electrochem. Soc.* **146** 339–49
[59] Dixit P and Miao J 2006 Effect of SF(6) flow rate on the etched surface profile and bottom grass formation in deep reactive ion etching process *J. Phys.: Conf. Ser.* **34** 577–82
[60] Tezcan D S *et al* 2006 Development of vertical and tapered via etch for 3D through wafer interconnect technology *Proc. Conf. Electron. Packaging Technol. (New York, NY)* pp 22–8
[61] Kovacs G, Maluf N and Petersen K 1998 Bulk micromachining of silicon *Proc. IEEE* **86** 1536–51

PAPER II

All-in-polymer injection molded device for single cell capture using multilevel silicon master fabrication

Simone Tanzi, Simon T. Larsen, Marco Matteucci and Rafael Taboryski

Conference proceeding for NSTI-Nanotech 2012, Vol. 2, 2012

All-in-polymer injection molded device for single cell capture using multilevel silicon master fabrication

S. Tanzi, S. T. Larsen, M. Matteucci and R. Taboryski

*Department of Micro- and Nanotechnology, Technical University of Denmark, DTU Nanotech, Building 345B, DK-2800 Kongens Lyngby – Denmark; simt@nanotech.dtu.dk

ABSTRACT

This work demonstrates a novel all-in-polymer device for single cell capture applicable for biological recordings. The chip is injection molded and comprises a “cornered” (non planar) aperture. It has been demonstrated how cornered apertures are straightforward to mold in PDMS [1,2]. In this study we demonstrate cornered apertures made in a thermoplastic polymer. One of the advantages of cornered apertures is the ease of microscopy under a standard inverted optical microscope, when using transparent materials. After the part is injection molded, the sealing of the chip is performed by thermal bonding to a polymer foil, so the complete device results from only two parts. It differs from similar devices in the novel material and fabrication platform that enables high reproducibility and inexpensive mass production. Optimization of the fabrication scheme has been carried out in order to avoid defects during demolding. Capturing of single PC12 cells has been demonstrated.

Keywords: injection molding, polymer, single cell capture, UV LIGA, dry etching

1 INTRODUCTION

For the lab-on-a-chip systems, polymers are an obvious choice of materials when cost efficiency and implementation for mass production are taken into consideration. Within all the mass replication technologies, injection molding is receiving more and more attention because of its high production efficiency, and potential to fabricate patterns of down to nanometer scale. In our case, we enroll injection molding as final step of a UV LIGA process [3]. The patterns are first transferred into a silicon sample by means of standard UV photolithography and dry etching and then replicated to a metallic shim by using electroplating. This shim is inserted into the molding tool for injection molding polymer replicas that are exact copies of the Si master. The chips are sealed by UV-assisted thermal bonding to a 100 µm thick polymer foil. The requirement for a good mold is having a positively tapered sidewall profile, which will allow an easy demolding. Therefore, it is very important to fabricate templates with a suitable etching profile. Furthermore, mask undercut, which can prevent the demolding process, should be avoided or at least controlled. Within this framework, we demonstrate an all-in-polymer chip for single-cell capture.

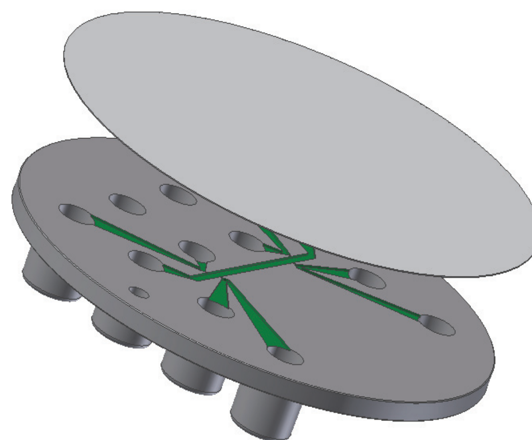

Figure 1: The figure shows a 3D representation of the device concept. The final device results from thermal bonding between an injection molded polymer part and a commercially available foil. The green colour shows the microfluidics open system.

2 CHIP DESIGN AND MOTIVATION

Reported methods of cell capture are mechanical trapping, electric trapping and optical tweezers [4]. Standard mechanical trapping uses fluids to flow through a microchannel and it utilizes either silicon [5] or PDMS [4] pillars to catch cells. Although electric trapping and optical tweezers have been demonstrated, they might alter or damage cells due to high electric field or heat generated by the laser. Therefore, mechanical trapping remains one of the most reliable and non-invasive alternatives. Our device presents a different approach for mechanical capture, where a single cell flowing in a carrier channel can be trapped to a small capturing micro hole by applying suction to it, see Fig. 2. The chip comprises a “cornered” (non planar) aperture based on a microfluidic junction between a large chamber for cell delivery and a lateral capillary for cell

trapping. Zanetti et al. have reported that mammalian cells can be trapped to a micro hole using this kind of apertures in PDMS [1, 2]. In this study we demonstrate that cornered apertures are straightforward to mold in a thermoplastic polymer. One of the advantages of cornered apertures is the ease of microscopy under a standard inverted optical microscope. The chip design combines channels with different heights in a multilevel microfluidic system. Despite such devices have been reported in PDMS, the mold fabrication and the demolding represents a challenge when injection molding is used for fabrication. The main challenge comes from combining, in the same design, channels with depths that differs in order of magnitudes. The silicon master contains both suction channels (~5 µm wide, ~4 µm deep) and carrier channels (~200 µm wide, ~50 µm deep). The critical dimensions of the suction channels are comparable with defects that can occur during the demolding. The smaller the size of the structures, the more critical this issue becomes. A multilayer fabrication scheme has been adopted here, using a silicon oxide mask to define the small features.

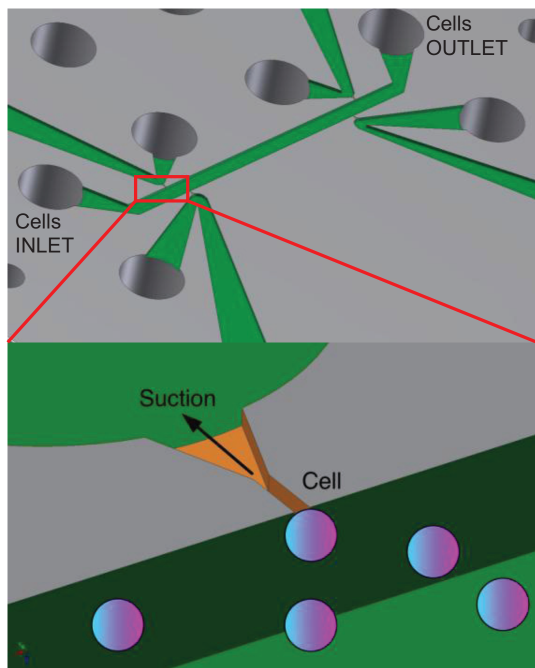

Figure 2: The figure shows chip design with “cornered” apertures based on microfluidic junctions between a large chamber for cell delivery and a lateral capillary for cell trapping.

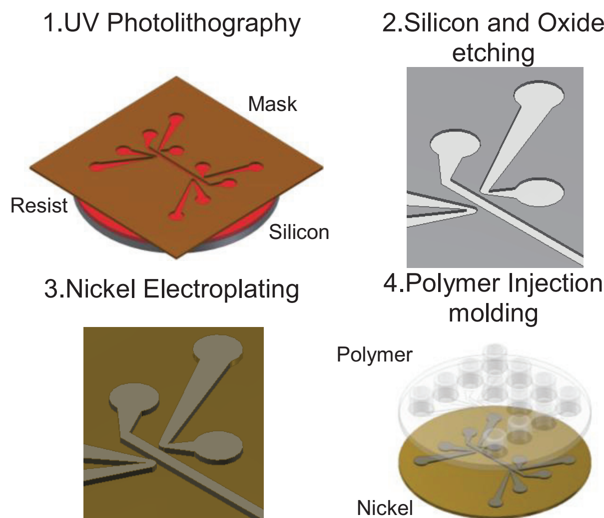

Figure 3: The figure shows the main steps in a UV-LIGA process. Photolithography and dry etching for Si master origination, Electroplating for Nickel shim fabrication and Injection molding for replication of the master.

3 FABRICATION

A two steps lithography process is needed to fabricate the Si master. We start from a 100 mm, <100>, single side polished, 525 µm thick silicon wafer. A 200 nm thick thermal SiO2 hard mask is grown at 1050°C in a Tempress horizontal furnace. A chemical treatment with Hexamethyldisilazane before both the spin coatings is used to promote the adhesion for photoresist. The photolithography process is done by Karl Suss Mask Aligner MA6 (exposure wavelength 365nm) in hard contact mode, front side alignment at 7 mW/cm2. A 2,2 µm thick AZ5214E positive resist is spun on the top side of the wafer using a Maximus 804 SEE Sister Semiconductor Equipment spinning system, baked at 90°C for 90 seconds and patterned by the first lithography step in order to define the smaller features that will originate the lateral apertures. A silicon oxide etch process is conducted to transfer the mask design into the oxide layer by using RIE (reactive ion etching) from Surface Technology Systems STS. Then, a 6,2µm thick AZ4562 positive resist is spun on the top side of the wafer using the same spinning system, baked at 100°C for 100 seconds and patterned by the second lithography step in order to define the carrier channels. A RIE oxide etch process is therefore conducted to transfer also the second mask design into the oxide layer and a DRIE (deep reactive ion etching) etching is performed by a Pegasus STS (Surface Technology Systems) system to etch the deep features into silicon wafer. A continuous process of silicon etching using a SF6/O2 plasma tapered sidewalls and smooth surface. A final RIE silicon etch process is conducted to etch the shallow channels into silicon wafer. This silicon master, which is an exact copy of the final chip, needs to be electroplated in order to fabricate a Ni insert to

Process	Parameters
Oxide deposition	1050°C dry oxidation ; t = 100 min
Spin coating	- HMDS vapor deposition - 2,2 µm AZ5214E - pre-bake: 90 °C for 90 sec
Photolithography	- hard contact mode, front side alignment W/A= 7 mW/cm^2 ; t = 9 sec - AZ351 developer; t = 90 sec
Oxide etch (shallow channels)	CF_4/CHF_3= 14/26 sccm; t = 4 min
Spin coating	- HMDS vapor deposition - 6,2 µm AZ5214E - pre-bake: 100 °C for 100 sec
Photolithography	- hard contact mode, front side alignment W/A= 7 mW/cm^2 ; t = 30 sec - AZ351 developer;t = 300 sec
Oxide etch (deep channels)	CF_4/CHF_3= 14/26 sccm; t = 4 min
Si etch (deep channels)	$SF_6/O_2/Ar$ = 180/160/100; t = 2:40 min
Si etch (shallow channels)	SF_6/ O_2 = 32/8 sccm; t = 4 min
Oxide removal	BHF bath; t = 3 min

Table 1: The table shows the process parameters for the Silicon master creation.

be used in the injection molding machine. A 100 nm thick Ti seed layer is sputtered on the wafer by a Lesker CMS 18 sputter system. This is intended to increase the conductivity of the silicon wafer and facilitate the Nickel plating. An electrochemical deposition of Nickel is conducted on the silicon master by using Technotrans Microform 200, to obtain a final thickness 340 µm. Standard 28 wt% KOH silicon etch at 80°C for 7 hours is performed to dissolve the silicon wafer completely. The advantage of using this procedure is to exploit the flatness of the silicon wafer to define the flatness of the final polymer parts [6], since this is particularly important for the bonding with the top lid.
The resulting Nickel electroform is punched into an 85 mm diameter shim by using a customized hydraulic press. A standard epoxy glue resistant to high temperature is used to fill up the resultant cavities in the back side of the shim, and sand paper to polish it. The shim is inserted into a copper-based alloy mold, which defines the backside of the chip. Injection molding was done with an Engel Victory 80/45 Tech hydraulic injection molding machine equipped with an Engel pick up robot. Parts are molded from Cyclic Olefin Copolymer (COC) TOPAS grade 5013 from TOPAS Advanced Polymers GmbH with a glass transition temperature of 135° C. The parts were produced using a mold temperature at 110° C with a clamp force of 50 kN. Parts were released when mold was cooled down to 60°C. Chips are then bonded against a 100 µm thick TOPAS film using UV-assisted thermal bonding, as described by Matteucci et al. [7]

4 METHODS

Passage 12 rat pheochromocytoma (PC 12) cells were cultured on Collagen (type 1, SigmaAldrich) coated Nunclon T25 flasks (Nunc A/S). Cells were detached using trypsin, triturated to loosen cell clumps, centrifuged and resuspended in phosphate-buffered saline (PBS, Lonza). The cell solution was vortexed on a vortex mixer to distribute the cells evenly. Microscope images and videos were obtained using an AxioObserver A1 microscope with Axiovision software (Carl Zeiss GmbH).
Prior to experiments the fluidic channel system of the chip was filled with PBS, starting from the capillaries. Cells were introduced into the inlet port by using a 1ml syringe and they slowly flowed along the carrier channel. When a targeted cell was found within 100µm of the lateral aperture, it was attracted to it and trapped by applying a gentle suction (< 20 mbar) to the side channel using a VEMA piezo valve terminal (Festo) controlled with Labview software (National Instruments), see Fig. 4.

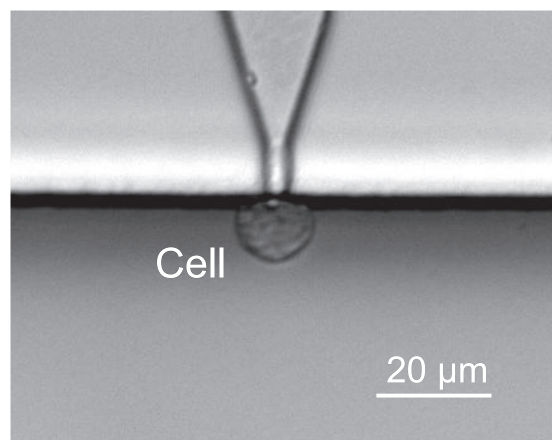

Figure 4: The figure shows a single PC12 cell being captured in the lateral aperture by by applying a gentle suction (< 20 mbar) to the side channel.

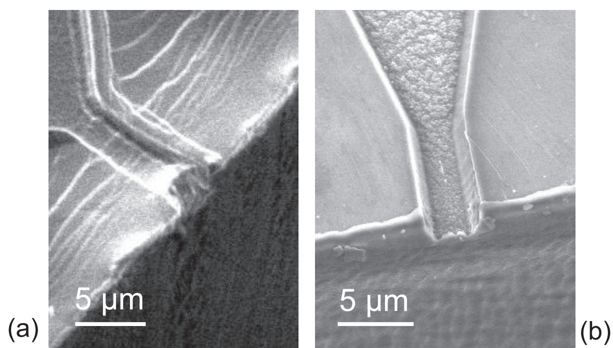

Figure 5: The figure shows SEM micrographs of lateral aperture in the final polymer part. To the left, a polymer part molded from a Si master etched with a standard Bosch process (a). To the right, a polymer part molded from a Si master etched with a continuous etching process enrolling Oxide hard mask (b).

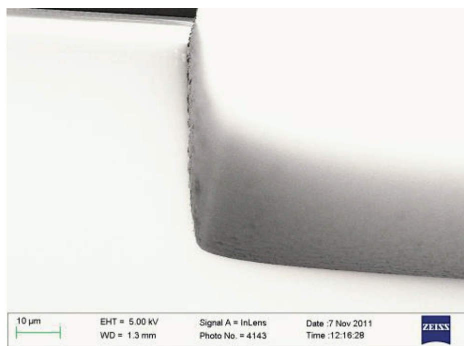

Figure 6: The figure shows SEM micrographs of lateral tapered sidewalls in the Silicon master during the fabrication. It shows a mask undercut smaller than 4 µm.

5 RESULTS AND CONCLUSION

Initially the fabrication process was designed to be as simple as possible and it enrolled a standard Bosch process optimized to realize vertical sidewall. Photo resist could be used as masking material and no hard masks were required, making the process flexible and faster. The polymer parts showed scratches of material from the sidewalls of the carrier channels that blocked the lateral apertures, see Fig. 5. We then performed the etching experiments with a continuous process by using the gases SF6, O2 and Ar, using an additional oxide layer for masking the Si.
This gave smooth tapered sidewall (>90°) and a mask undercut lower than the depth of the suction channel, see Fig. 6. The result was a perfect replica of the microstructures without any damages during the molding.
Experiments show that PC12 cells can be trapped to the lateral aperture simply by applying a slight negative pressure (< 20 mbar) to the small features.
In the future, this kind of device might be suitable for impedance measurements on a chip, where implementation with an electrode material will be required. This could be accomplished using Pedot:tosylate conductive polymer microelectrodes, which are integratable in the chip system presented here and exhibit good electrochemical properties [8]. Furthermore a reduction of the lateral aperture size, by means of etching process giving no undercut, will make the device suitable for electrophysiological recordings on single cells.

6 ACKNOWLEDGEMENTS

This work is supported by the Danish Advanced Technology Foundation through the Advanced Technology Project PILOC (grant no. 061-2010-1).

REFERENCES

[1] Seo, J. et al. (2004) *Appl. Phys. Lett.,* **84** , 1973-1975
[2] Ionescu-Zanetti et al. (2005) *PNAS,* **102**, 9112-9117
[3] E. W. Becker et al. (1982) *Naturwissenschaften* 69, 520–3
[4] Ling-Sheng Jang, Min-How Wang (2007) *Biomed Microdevices*, **9**, 737-743
[5] Andersson,H. et al. (2000) *Sens. Actuators,* **67**, *203–208*
[6] Taboryski, R. et al. (2010) *J. Micromech. Microeng.,* **20**, 055010
[7] M. Matteucci et al. *Submitted for publication*
[8] S. T. Larsen et al. (2012) *Analyst.*, **137**, 1831–1836

PAPER III

Fabrication and characterization of injection molded multi level nano and microfluidic systems

Marco Matteucci, Thomas Lehrmann Christiansen, Simone Tanzi, Peter Friis Østergaard,
Simon T. Larsen and Rafael Taboryski

Microelectron. Eng. (2013)

Microelectronic Engineering xxx (2013) xxx–xxx

Contents lists available at SciVerse ScienceDirect

Microelectronic Engineering

journal homepage: www.elsevier.com/locate/mee

Fabrication and characterization of injection molded multi level nano and microfluidic systems

Marco Matteucci [*,1], Thomas Lehrmann Christiansen [1], Simone Tanzi,
Peter Friis Østergaard, Simon Tylsgaard Larsen, Rafael Taboryski

Department of Micro- and Nanotechnology, Technical University of Denmark, DTU Nanotech, Building 345E, DK-2800 Kongens Lyngby, Denmark

ARTICLE INFO

Article history:
Available online xxxx

Keywords:
Dry etching
Electroplating
Injection molding
Thermal bonding
Lab-on-chip
Microfluidics

ABSTRACT

We here present a method for fabrication of multi-level all-polymer chips by means of silicon dry etching, electroplating and injection molding. This method was used for successful fabrication of microfluidic chips for applications in the fields of electrochemistry, cell trapping and DNA elongation. These chips incorporate channel depths in the range between 100 nm and 100 μm and depth to width aspect ratios between 1/200 and 2. Optimization of the sealing process of all-polymer COC microfluidic chips by means of thermal bonding is also presented. The latter includes comparing the bonding strength of UV-treated foils and presentation of a simple model for estimating the delamination pressure. With UV surface treatments, foils of 100 μm thickness were found to withstand pressures up to 9 atm in Ø4 mm cylindrical inlets when thermally bonded to micropatterned substrates of 2 mm thickness.

© 2013 Elsevier B.V. All rights reserved.

1. Introduction

For the fabrication of micro- and nano-machined systems for as Lab-on-chip (LoC) applications polymers are gaining at present more and more consideration over materials used for standard IC fabrication like Silicon and glass [1,2].

Polymer manufacturing is performed mostly by means of rapid prototyping methods such as polydimethylsiloxane (PDMS) casting, laser milling, or micromachining [3–5].

Although such fabrication methods are quite mature, they suffer from serious drawbacks when it comes to industrial production and cost efficiency. While the feasibility of more and more applications has been successfully demonstrated, only a few of the presented prototypes have reached the market. For large scale fabrication of polymer chips for Lab-on-Chip (LoC) applications, the most common methods for micro- and nanopatterning are LiGA (German acronym for Lithography, Electroplating and Molding) [6] or LiGA-like processes that involve, for example, the use of UV lithography [7]. In order to avoid the use of expensive synchrotron sources necessary for LiGA, obtain extremely flat and smooth sample surfaces and at the same time avoid the double inversion of stamp polarity [8], it is possible to carve the structures into the Si wafers in a so-called DEEMO (acronym for Dry Etching, Electroplating and Molding) process as first proposed by Elders et al. [9].

The procedure we here present is a variation of the DEEMO process performed using multiple and overlapped Si dry etching steps described in detail elsewhere [10]. This process enables high spatial resolution both in the width and the depth of the channels. The patterned Si wafers are then used to make nickel multi-level stamps (hereby referred to as shims) that are used for the fabrication of all-polymer chips by means of injection molding of Cyclic Olefin Copolymer (COC) 5013L10 from Topas™. Although a large number of polymers can be used for injection molding purposes, Topas is optimal when a material with low autofluorescence (for optical detection) and high chemical and thermal resistance are required.

Sealing of the devices was performed by thermal bonding with Topas foils of the same grade with thickness ranging from 100 μm to 2 mm. We focused on two methods based on previous works [11–14]: Plasma assisted and UV assisted thermal bonding. Of these, the UV bonding was superior and less time-consuming and is presented here. Data on the plasma method is given in Supplementary material S1.

The bonding procedure should be optimized for maximum bonding strength while still preserving the integrity of the channel geometry. We here report on such an optimization by applying the so-called razor blade test to measure the bonding strength [15], as this method can be applied while still maintaining the functionality of the device. In addition, we have deduced and experimentally verified that the crack length measured in the razor blade test can

* Corresponding author.
E-mail address: mamat@nanotech.dtu.dk (M. Matteucci).
[1] These two authors contributed equally to this research.

0167-9317/$ - see front matter © 2013 Elsevier B.V. All rights reserved.
http://dx.doi.org/10.1016/j.mee.2013.01.060

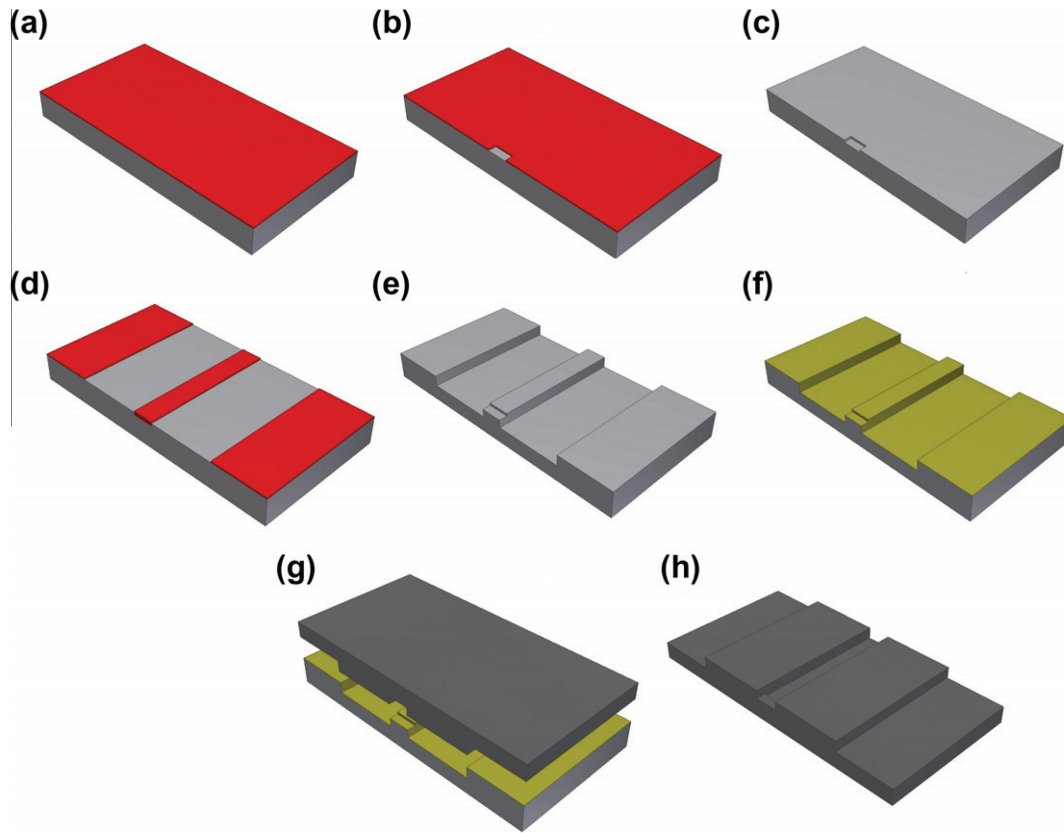

Fig. 1. Fabrication procedure for Ni shims: Spin coating (a), UV lithography (b), RIE etching of shallow channels and resist removal (c), spin coating and UV lithography (d), DRIE of Si for deep channels and resist removal (e), sputtering (f), Ni electroplating (g) and KOH etching of Si (h).

be directly related to the critical delamination pressure in a microfluidic channel by means of a simple model, see Supplementary material S2 for details. In this model, the delamination pressure in a circular inlet is given by:

$$P_{\max} = \frac{2E'\delta\tau^3}{a^2L^2} \quad (1)$$

where a is the inlet radius, τ the lid thickness, $E' = E/(1-\nu^2)$ E being Young's modulus and ν the Poisson ratio of the lid material, δ the blade thickness, and L the measured crack length.

Regarding the shim fabrication, we here describe a simplified version of a multi-level etching process presented in detail elsewhere [10].

The modified process is sketched in Fig. 1.

In respect to the one previously used, we here simplify the procedure by substituting an oxide etch mask with a spin coated resist layer of 2.2 µm thickness during both RIE and DRIE processing. The use of a resist mask was made possible by using only the modified BOSCH process described in [10]. As in previous work [10], the shim thickess was tuned to be around 300 µm. Using this process, chips equipped with luer fittings were injection molded with an ENGEL Victory 80/45 with a maximum clamping force of 450 Tons. Mold temperatures between 110 and 130 °C as well as an injection pressure of 1700 Bars were used for sample molding. Samples having features ranging in width from 5 to 50 µm and in depth between 100 nm and 50 µm and with aspect ratios as low as 1/200 without channel collapse. The cycle times of the injection molding were noticeably reduced compared to the process described in [10] to about 1 min by inserting a system for localized heating and cooling of the sample area.

For the bonding, commercially available TOPAS 5013L10 foils (T_g = 134 °C) of thickness between 100 and 500 µm purchased from TOPAS Advanced Polymers GmbH were used as sealing lids. The foils are obtained by extrusion of the same material provided for injection molding. All bonding experiments here described were performed with 100 µm thick foils. Such thickness was chosen because a large number of bio-applications use thin lids in order to have small working distances and allow on-chip optical detection. To test also the bonding of thicker substrates, 2 mm thick flat disks, similar to the patterned ones were injection molded to be used as sealing lids. An example of a bonded chip is shown in Fig. 2. Before thermal bonding, the surfaces of both the foil and the 2 mm thick sample were exposed to a UV lamp (DYMAX mercury UV-bulb F/5000) emitting over the full unfiltered Hg line spectrum with a power of 44.5 W/cm^2 measured at the wavelength 365 nm. All samples were kept under the UV light for 30 s.

After bonding samples at temperatures between 110 and 125 °C, we concluded that at higher temperatures the main issue is the partial filling of the channels with lower aspect ratios. In particular, at T = 125 °C it was not possible to separate the thin 100 µm thick folis from the 2 mm thick substrates. For this reason we kept a maximum bonding temperature of 120 °C.

Bonding (further details in Supplementary material S3) was therefore performed applying forces between 2 and 15 kN at temperatures of 115 and 120 °C. In order to assess the influence of bonding time, samples were bonded at 115 °C for both 5 min and 10 min. The razor blade test was then performed as shown in Fig. 3. To obtain the crack length L the horizontal projection of the blade slope L' was added to the distance L_0 between the blade tip and the last fringe. The blades used (Millarco) were of rectangular shape 39.5 × 20 mm. After the measurement of the crack length, a measurement of the delamination pressure was performed on the same samples by inserting a liquid dye into the microchannels and then applying pressure until delamination

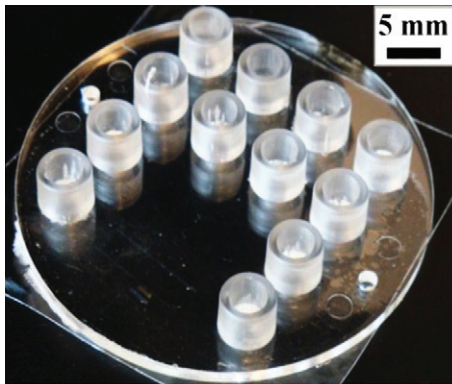

Fig. 2. An injection molded TOPAS 5013 microchip with Luer fittings bonded to a 100 μm thick TOPAS 5013 foil.

occured, acting as a reference for validating the delamination model. The critical pressure was considered to be the one at which the area near the Luer fittings started to delaminate.

During optimization, we observed that, as can be seen in Fig. 4, the samples bonded at 120 °C showed a much better bonding strength than the ones bonded at 115 °C for the same time. The data in Fig. 4 also show how bonding time plays a major role: Samples bonded for 10 min at 115 °C exhibit crack lengths comparable with the ones obtained at 120 °C and more than a factor of three shorter than the samples bonded at the same temperature for 5 min. This suggests that samples with critical dimensions could be bonded at lower temperatures for a longer time with the drawback of a more time consuming process.

Tuning of temperature and pressure is also fundamental to avoid microchannel deformation. Although no evident effects were found on micron-sized structures after optimization of bonding parameters (see SEM micrographs on Fig. 6) and functionality was assured in nanochannels, optical methods are at study at the moment to verify micro and nanochannel dimensions without having to cleave the samples.

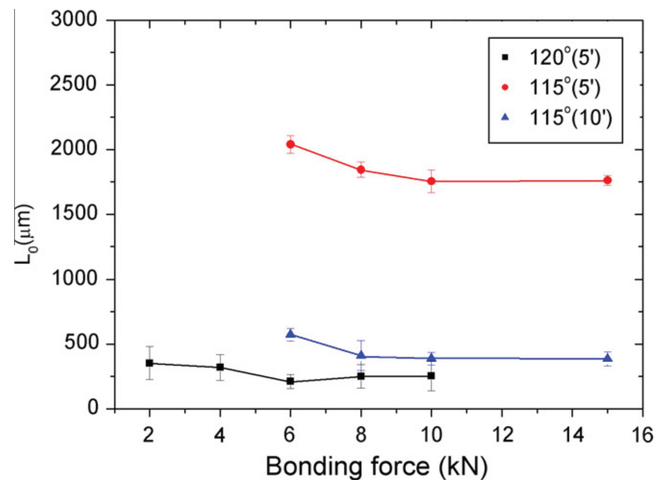

Fig. 4. L_0 values for UV-treated samples as a function of bonding force at both 115 and 120 °C.

In order to study the surface modifications that cause the bonding strength enhancement after UV treatment, XPS measurements of treated and untreated surfaces were performed. Since no surface modifications were recorded, the bonding enhancement was believed to be caused by thermal reordering of surface molecules (further details in Supplementary material S4).

The comparison between the delamination pressures calculated with Eq. (1) and the measured values is shown in Fig. 5. The theory shows very good correspondence with the experimental data for both longer and shorter crack lengths. SEM micrographs illustrating the quality of the bonding are also inserted in Fig. 5, showing un-collapsed polymer microchannels after bonding.

For values of L around 250 microns, the maximum reachable pressure was 9 atmospheres, equivalent to a binding energy of 61 μJ/m^2, and a mode I fracture toughness of $K_I = 425$ Pam$^{1/2}$. Such values are up to two orders of magnitude higher than the ones

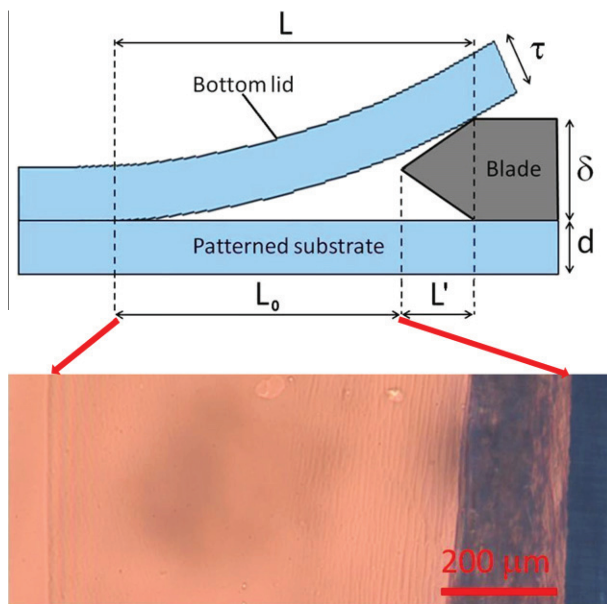

Fig. 3. Illustration of the razor blade test between two polymer sheets of thickness τ and d (top) together with the optical measurement of the distance L_0 between the blade tip and the fringes that indicate the detachment of the polymer sheet (bottom). The crack length L is obtained by adding the horizontal projection of the blade slope L' to L_0. The area near the blade tip is darker because of the high stress released by the stiffer plate during blade insertion.

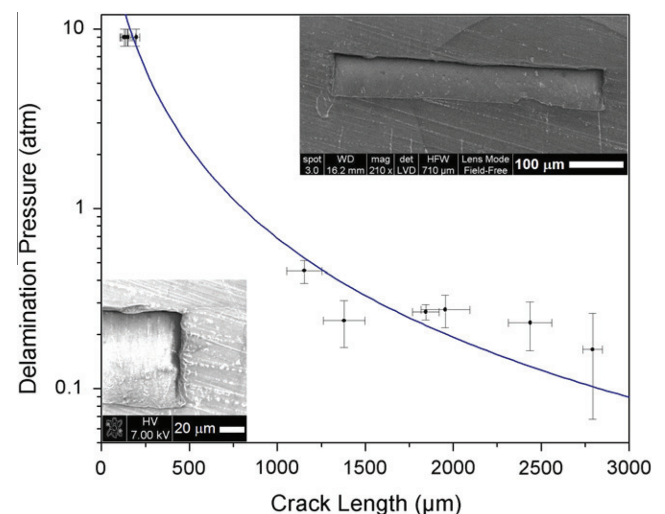

Fig. 5. Delamination pressure as a function of crack length. The pressure curve is calculated with the measured values a = 2 mm, δ = 60.3 μm, L' = 134 μm. For Topas 5013 a Young's modulus of 2550 MPa and a Poisson's ratio of 0.37 were used. The small panels show SEM details of a microchannel cross-section obtained by cleaving a sample after UV-enhanced bonding.

Please cite this article in press as: M. Matteucci et al., Microelectron. Eng. (2013), http://dx.doi.org/10.1016/j.mee.2013.01.060

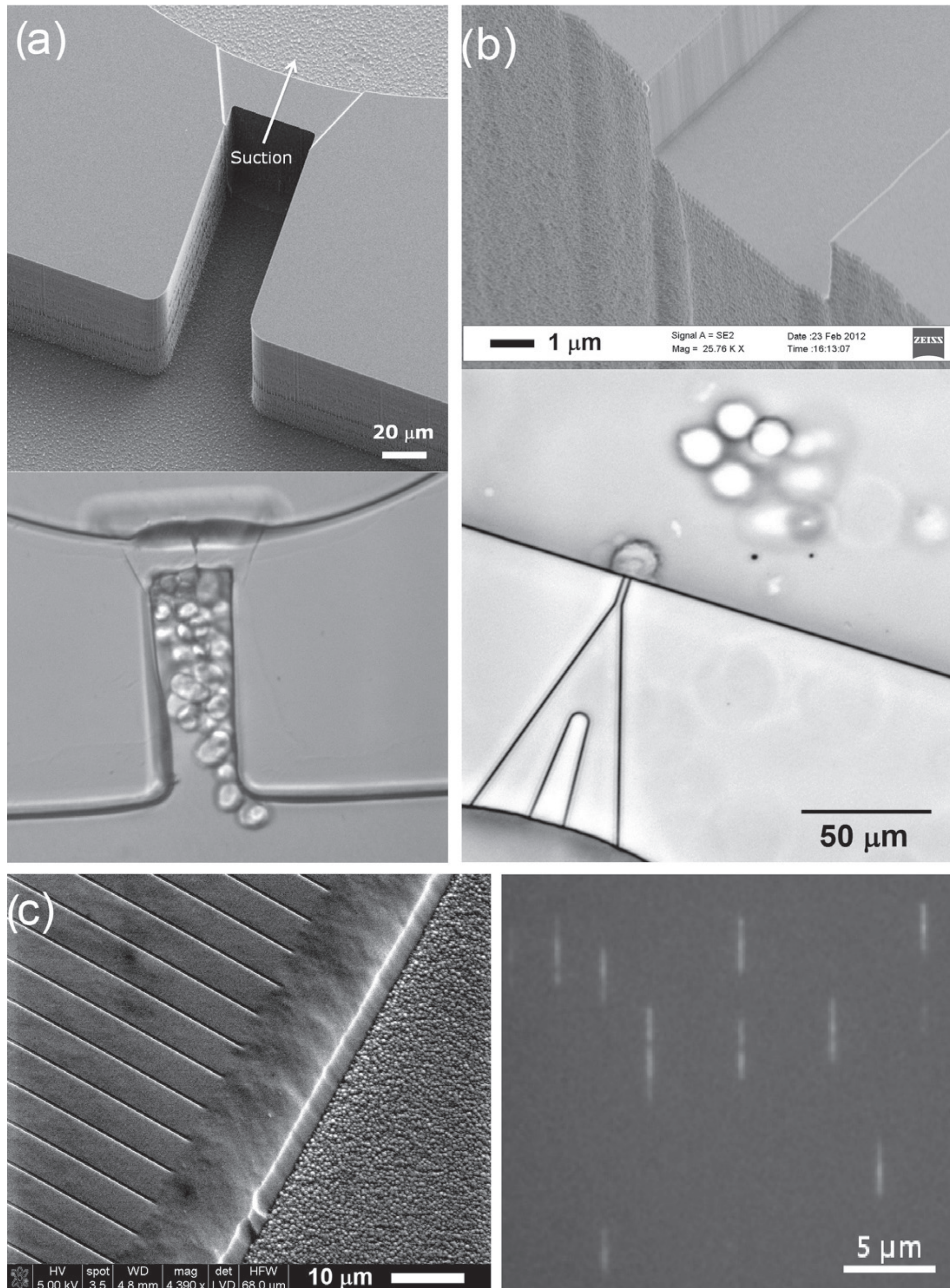

Fig. 6. Silicon master and final polymer chips for capture of PC 12 cells (a), and single HeLa cells (b). Detail of the polymer chip with nanochannels for λ-DNA elongation and fluorescence microscopy measurements (c).

obtained with UV/O_3 treated COC and PMMA substrates [8]. After such value, the polymer foil in most cases exceeded its yield strength and fractured at the Luer edges without delaminating, emphasizing the fact that after optimization, the bonding was no longer the limiting factor in high-pressure applications such as nanochannels with high hydraulic resistance.

In order to demonstrate the capabilities of the presented fabrication process, LoC chips with different functionalities have been successfully tested as can be seen in Fig. 6.

Neurotransmitter detection with microfabricated Pedot:Tosylate electrodes was previously demonstrated in [16,17], and as an extension to this, LoCs for multi (6a) and single (6b) cell capture have been fabricated and tested for cell capture. Both these chips will be combined with electrodes to perform "on chip" neurotransmitter detection.

Devices for single (6b) and multi (6a) cells capture has been successfully tested with respectively PC12 and HeLa cells [10]. Manipulation of single cells is basic for many cell-related studies

Please cite this article in press as: M. Matteucci et al., Microelectron. Eng. (2013), http://dx.doi.org/10.1016/j.mee.2013.01.060

ARTICLE IN PRESS

such as drug screening and impedance analysis, while capture of large groups of cells is relevant when studying detection of neurotransmitter release.

Stretching of DNA macromolecules through nanofluidic networks is also considered a powerful tool for direct sizing and mapping of DNA [18,19].

Fig. 6c shows a device with nanochannels enables to perform barcoding of DNA macromolecules by means of fluorescence microscopy measurements [20]. Fluorescent intensity variations from extended macromolecules have been demonstrated via chemical counterstaining against a cell-impermeant stain.

In conclusion, a platform for fabrication of all-polymer LoCs by means of silicon dry etching, electroplating and injection molding was here described. Moreover, the thermal bonding of injection molded TOPAS 5013 chips to commercially available TOPAS foils of 100 μm thickness and the same grade was optimized. The characterization of bonding strength was performed by measuring the bonding strength with the razor blade test. UV-treatment of surfaces was performed in order to enhance surface bonding. A simple method that is able to predict the delamination pressure of microchannels as a function of crack length was also verified: in optimized bonding conditions, the reached pressures was as high as 9 atm, equivalent to a binding energy of 53 $\mu J/m^2$, and a mode I fracture toughness of $K_I = 375\ Pam^{1/2}$. Finally, examples of applications were given in the fields of single/multi cell capture and DNA elongation.

Acknowledgements

This work is supported by the Danish Council for Strategic Research through the Strategic Research Center PolyNano (Grant No. 10-092322/DSF).

Appendix A. Supplementary data

Supplementary data associated with this article can be found, in the online version, at http://dx.doi.org/10.1016/j.mee.2013.01.060.

References

[1] A. de Mello, Lab Chip 2 (2002) 31N–36N.
[2] H. Andersson, A. van den Berg, Sens. Actuators B 92 (2003) 315–325.
[3] T. Hanemann, W. Bauer, R. Knitter, P. Woias (Eds.), MEMS/NEMS Handbook, Springer, 2006. pp. 801–869.
[4] J. Zhou, A.V. Ellis, N.H. Voelcker, Electrophoresis 31 (2010) 2–16.
[5] P.S. Nunes, P.D. Ohlsson, O. Ordeig, J.P. Kutter, Microfluid. Nanofluid. 9 (2010) 145–161.
[6] E. Becker, W. Ehrfeld, D. Munchmeyer, H. Betz, A. Heuberger, S. Pongratz, et al., Naturwissenschaften 69 (11) (1982) 520–523.
[7] R. Kupka, F. Bouamrane, C. Cremers, S. Megtert, Appl. Surf. Sci. 164 (2000) 97–110.
[8] K.Ø. Andersen, M. Hansen, M. Matschuk, S.T. Jepsen, H.S. Sørensen, P. Utko, D. Selmeczi, T.S. Hansen, N.B. Larsen, N. Rozlosnik, R. Taboryski, J. Micromech. Microeng. 20 (2010) 055010 (9pp.).
[9] J. Elders, H. Jansen, M. Elwenspoek, W. Ehrfeld, DEEMO: A New Technology for the Fabrication of Microstructures, IEEE, 345 E 47th St., NY 10017, New York, 1995.
[10] Simone Tanzi, Peter Østergaard, Marco Matteucci, Thomas Christiansen, Jiri Cech, Rodolphe Marie, J. Micromech. Microeng. 22 (2012) 115008.
[11] K. Cho, Y. Setsuhara, K. Takenaka, M. Shiratani, M. Sekine, M. Hori, Thin Solid Films 519 (2011) 6810–6814.
[12] R. Truckenmüller, P. Henzi, D. Herrmann, V. Saile, Microsyst. Technol. 10 (2004) 372–374.
[13] C.W. Tsao, L. Hromada, J. Liu, P. Kumar, D.L. DeVoe, Lab Chip 7 (2007) 499–505.
[14] A. Bhattacharyya, C.M. Klapperich, Lab Chip 7 (2007) 876–882.
[15] H. Taylor, D. Boning, C. Iliescu, J. Micromech. Microeng. 21 (2011) 067002.
[16] S.T. Larsen, R. Taboryski, Analyst 137 (2012) 5057–5061.
[17] S.T. Larsen, R.F. Vreeland, M.L. Heien, R. Taboryski, Analyst 137 (2012) 1831–1836.
[18] J. Tegenfeldt et al., Proc. Natl Acad. Sci. USA 101 (2004) 10979–10983.
[19] R. Riehn, M. Lu, Y. Wang, S. Lim, E. Cox, R. Austin, Proc. Natl. Acad. Sci. USA 102 (2005) 10012–10016.
[20] Peter Friis Østergaard, Macro Matteucci, Walter Reisner, Rafael Taboryski, Analyst 138 (2013) 1249.

PAPER IV

High quality ion channels recordings on an injection molded polymer chip

Simone Tanzi, Marco Matteucci, Thomas Lehrmann Christiansen, Søren Friis, Mette Thylstrup Christensen, Jørgen Gærnes, Sandra Wilson, Jonatan Kutchinsky, and Rafael Taboryski

Ready to be submitted

High quality ion channels recordings on an injection molded polymer chip

Simone Tanzi, Marco Matteucci*, Thomas Lehrmann Christiansen*, Søren Friis‡, Mette Thylstrup Christensen‡, Jørgen Gærnes§, Sandra Wilson‡, Jonatan Kutchinsky‡, and Rafael Taboryski**

*Department of Micro- and Nanotechnology, Technical University of Denmark,

Building 345E, DK-2800 Kongens Lyngby, Denmark

‡Sophion Bioscience A/S, Baltorpvej 154, DK-2750 Ballerup, Denmark

§Danish Fundamental Metrology, Matematiktorvet, Building 307, DK-2800 Kongens Lyngby, Denmark

Address correspondence to: rata@nanotech.dtu.dk

ABSTRACT

In this paper we demonstrate high quality recordings of the ion channel activity across the cell membrane in a biological cell by employing the so called patch clamping technique on an injection molded polymer microfluidic device. The findings will allow direct recordings of ion channel activity to be made using the cheapest materials and production platform to date, and with the potential for very high throughput. The employment of cornered apertures for cell capture allowed the fabrication of devices without through holes and *via* a scheme comprising of master origination by dry etching in a silicon substrate, electroplating in nickel and injection molding of the final part. The most critical device parameters were identified as the length of the patching capillary and the very low surface roughness inside of the capillary. The cross-sectional shape of the orifice was found to be less critical, as both rectangular and semicircular profiles seemed to have almost the same ability to form tight seals with cells with negligible leak currents. The devices were functionally tested with Human Embryonic Kidney cells expressing voltage-gated sodium channels ($Na_v1.7$), and benchmarked against a commercial state-of-the-art system for automated ion channel recordings. These experiments considered current-voltage (IV) relationships for activation and inactivation of the $Na_v1.7$ channels and their sensitivity to a local anesthetic, lidocaine. Both IVs and lidocaine dose response curves obtained from the injection molded polymer device were in excellent agreement with data obtained from the commercial system.

KEYWORDS: automated patch clamping · lateral patch clamping · injection molding · thermoplastic polymers · voltage gated sodium channels · lidocaine

The patch clamping technique was introduced in 1976 by Neher and Sakmann,[1] and has become the accepted standard for fundamental studies of ion channel proteins and the discovery of drugs that affect them. Ion channels play a central role in the excitability of nerves and muscles; they underlie the heartbeat, muscle contractions and brain activity as well as many other basic physiological actions.[2] Ion channels are macromolecular pores with the ability to regulate the movement of ions across the otherwise impermeable cell membrane.[2] Ion channels are also involved in a diverse range of disorders and pathological conditions, called channelopathies.[3,4] Mutations in ion channel genes have been associated with diseases such as cystic fibrosis, hypertension, ataxia, arrhythmia and several types of epilepsy.[4,5] In pharmacology, ion channels represent highly attractive targets for drug discovery with an estimated market of US$12 billion.[6,7]

Despite their enormous potential as druggable targets, the use of ion channels for drug discovery has been well behind the expectation, mainly due to the lack of adequate screening technology.[8] Conventional manual patch clamping delivers high information content but it is a complex technique that requires skilled personnel and suffers from extremely low throughput; while on the other hand all indirect screening methods suffer from low specificity and thus the associated risk of generating false negative or positive results.[8,9] With the promise of removing this trade-off, the first automated parallel patch clamping system (APC) was made available in 2003.[10] Since then, 5 companies (Molecular Devices, Sophion Bioscience, Nanion, Cytocentric, and Fluxion) have entered the market, establishing APC as an essential technology for secondary screening, lead optimization and cardiac safety testing.[11] Performances of the different systems have been discussed in a few reviews.[11-14] APC systems replace the use of conventional glass micropipettes with single-use, disposable devices fabricated in materials such as quartz[15] and silicon/silicon-dioxide.[16] The majority of the available platforms share the so- called planar approach, where cells in suspension are blindly positioned by suction onto micro apertures made

as through holes in thin membranes.[15] Alternatively, a lateral approach has been proposed, where suspended cells are trapped at lateral apertures generated at the junction of two microfluidic channels.[17]

The ability to form a high electrical resistance seal, preferably in the order of GΩ (the so-called gigaseal) between the aperture and the biological cell membrane, and the fabrication of such micro sized through holes in thin substrates (10-20 µm) are the two most relevant benchmarks. These constraints have traditionally narrowed the range of usable materials and technologies to almost exclusively micromachining of silicon and glass, at least for commercial use.

The use of polymeric substrates has also been widely investigated, and planar microfluidic chips have been demonstrated in hybrid poly(dimethylsiloxane)-polyimide (PDMS-PI)[18], polyimide[19], oxygen plasma treated PDMS[20-22] and poly(ethylene glycol) (PEG)/SU-8 mixture.[23] Unfortunately, all the afore-mentioned polymer devices have so far failed to deliver relevant electrophysiological results. It has been more or less implicitly believed in the community that silicon oxide surfaces possess a unique surface chemistry for forming gigaseals, essentially through van der Waals interactions.[24-26] The interaction between lipid membranes and other surfaces is, however, complicated and only poorly understood, and thus leaves some leverage for challenging the uniqueness of these surfaces[27-31] by employing polymers. Zanetti *et al* implemented lateral junctions into a microfluidic device fabricated by casting of polydimethylsiloxane (PDMS).[17,32] In 2009, this device was eventually commercialized by Fluxion, and it remains the only APC system relying on cornered apertures to date.[33]

Looking at all of the commercially available APC systems, the manufacturing cost per device is still prohibitive for establishing APC as a routine technique.[34] Of the two materials employed nowadays, silicon remains extremely costly to purchase and machine, while PDMS is less suitable for mass production. Moreover, PDMS has issues when used for biological applications such as high permeability for small molecules, non-crosslinked oligomers, and surface diffusion of low molecular weight chains.[35]

The aim of this work is to propose a method for massive production of extremely cheap APC systems without compromising functionality. The trick lies in understanding the requirements to form tight seals between thermoplastic polymers and the cells. By shaping apertures that allow for a considerably larger effective interface area between low energy polymer surfaces and the cell membrane, we demonstrate the formation of gigaseals, enabling high quality ion channel recordings. The proposed device consists of only two parts: an injection molded part in Topas cyclic olefin copolymer (COC) comprising the microfluidics, and a polymer film of the same polymer grade, which is thermally bonded to the injection molded part.[36] For comparison, the commercially available QPlate^{TM} from Sophion Bioscience comprises several materials, thermoplastic polymer, elastomer, ceramic, glass, and silicon. Moreover, Topas has none of the previously mentioned limitations of PDMS. Furthermore, the materials and fabrication platform fulfills all the requirements for cheap manufacturing in terms of "design for manufacturability", "economy of scale" and production yield and it avoids all drawbacks typical of prototyping methods.[37] After an initial investment in master mold origination, injection molding delivers a cost per part that exponentially decreases with the number of parts, becoming the cheapest technology when production is greater than ~10k units.[37] After assembly into chips, the systems were tested with HEK cells expressing $Na_v1.7$, a voltage-gated sodium channel appropriate for benchmarking studies. Experiments were designed to explore current-voltage (IV) relationships for activation and inactivation of $Na_v1.7$ channels and their sensitivity to a local anesthetic, lidocaine. Both IVs and lidocaine dose response curves obtained from the injection molded polymer device were benchmarked against the commercially available QPatch^{TM} system from Sophion Bioscience. In the following section, we provide the details of the device layout and functionality, benchmarking tests against existing state-of-the-art methods, and finally a surface topology characterization of the patching capillaries.

RESULTS AND DISCUSSION

The chip design contains four independent lateral apertures 600 µm apart, which are aligned along a straight channel reserved for extracellular electrolyte solution, as shown in Figure 1a-c. The side channels are connected at the other end to four separate inlet channels which contain intracellular electrolyte solution. The patching channel is Y shaped and consists of a straight capillary with a rectangular profile and rounded corners (approximately 2 µm × 2 µm) at the end where the cell is captured and a wider opening at the opposing end for the reduction of the total hydraulic resistance. In addition, a second type of device with a semicircular profile was molded and tested. The two groups of devices will be called type A (rectangular profile) and type B (semicircular profile). A cell trapped to one of the patching orifices is shown in Figure 1d. It was observed that the cell membrane tends to protrude a long distance into the patching capillary, as also previously reported for PDMS devices.[17,38] In order to find the optimal length of the patching channels, we made all four channels with different lengths. The optimal length of the straight capillary fraction appeared to be the largest we had (45 µm), while shorter capillaries did not show good sealing properties. This indicates that the gigaseal formation must occur due to interaction between the cell membrane and the polymer along the whole length of the patching capillary and not only in the proximity of the orifice.

Our customized polymer chip, 50 mm in diameter and 2 mm in thickness, contained 12 Luer-fittings[39] used to interface the microfluidic network. A single use injection molded device is shown in Figure 1e. Prior to experiments; the device was primed with the electrolyte solutions. First, the capillary was filled with intracellular solution and then the cell carrier channel was filled with extracellular solution. The recording channel was connected to an external pressure controller and reservoirs with intracellular solution were employed to prevent formation of air bubbles when applying suction. Ag/AgCl electrodes positioned across the recording channel and connected to the amplifier ensured electrical connection, as shown in Figure 1f-g.

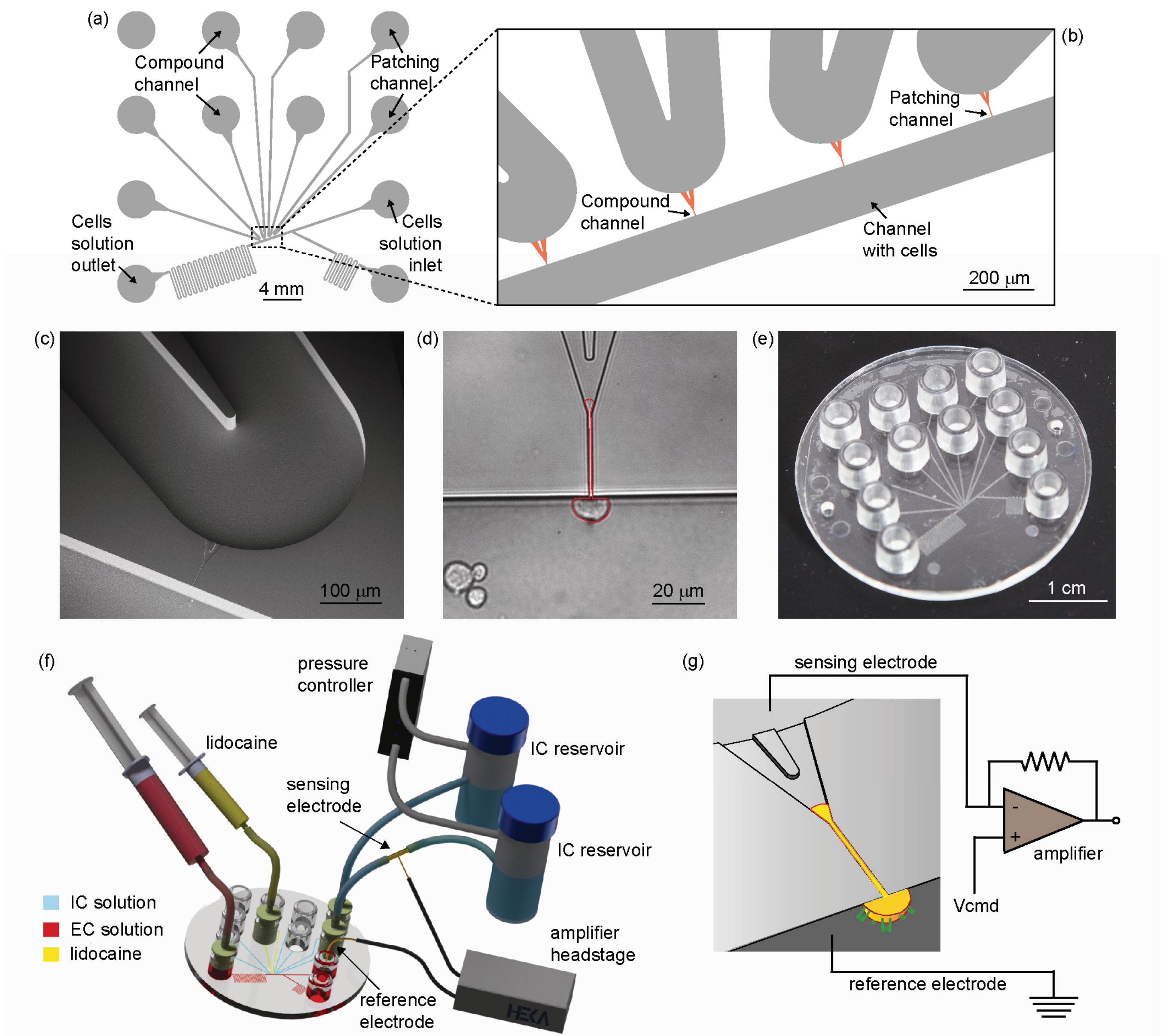

Figure 1. (a) Layout of the microfluidic device. (b) Close-up of the key part of the design with patching channel, channel for compound perfusion and channel for cell loading. (c) SEM micrograph of the Y shaped patching channel connecting extra and intra cellular channels. (d) Optical microscope image of a captured HEK cell. Highlighted in red, the cell membrane is seen to protrude a distance of about 50 µm into the patching capillary shortly after being captured. (e) A single use injection molded device used for the experiments. (f) Illustration of the set-up used for the recordings. The polymer device is connected to two intracellular solution reservoirs and then to the pressure controller. Ag/Cl electrodes are connected

to the headstage of the amplifier. Syringes are used to transport cells by convective flow from the inlet to the patch zone and to perfuse lidocaine through one of the lateral apertures respectively. (g) Schematic of the patch clamping recording: a cell trapped to a lateral aperture. Electrodes are located across the orifice.

Cells were introduced into the inlet port and transported by the convective flow induced by a syringe. Before trapping one of the cells, a slight positive pressure was applied to the patching channel to prevent contamination of the aperture. Conveniently, one of the unused patching capillaries could be used for perfusion of lidocaine by using a syringe connected to the corresponding Luer port. During perfusion, the estimated average flow velocity in the carrier channel was approximately 1 mm/s, and the average flow rate in the perfusion channel was estimated to be about 20 % higher than the flow rate in the carrier channel. The lateral flow was applied for less than 10 seconds. A COMSOL® simulation, shown in Figure 2, supports the premise that 100 % of the lidocaine in solution was successfully delivered to the cell. The simulation considered a worst case scenario of lidocaine diffusion when a high lidocaine concentration of 1 mM was perfused.

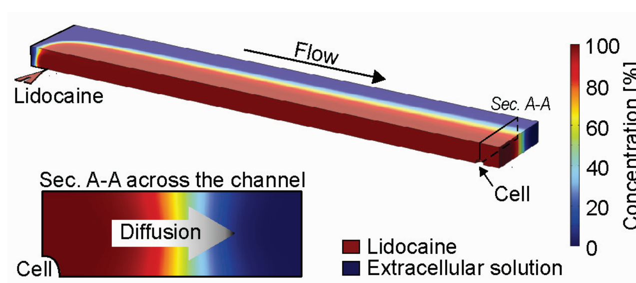

Figure 2. Lidocane (1mM) delivery to the cell being patched simulated in COMSOL®. A lateral flow (in red) perfused into the flow in the carrier channel (in blue). The simulation accounted for lidocaine diffusion in the extrallular solution. A sectional view across the channel shows how the concentration corresponds to 100% in the proximity of the cell.

As previously reported,[40] injection molding enables high replication accuracy of micro and nano features. Figure 3a-c show SEM micrographs of the orifice formed at the junction between the patching channel and the carrier channel of a polymer device after the three main steps of the fabrication process; etching, electroplating and molding. The uniformity of the patching channels was confirmed for several devices by the narrow range of chip resistances, the resistances were measured across the 45 µm long patching capillaries with the presence of only the electrolyte solutions. This was 9.4 ± 0.2 MΩ (mean ± Standard Error of the Mean, n = 33) for type A devices and 10.5 ± 0.2 MΩ (n = 14) for type B devices. The devices with semicircular profile (type B) had a slightly larger chip resistance as expected from their smaller cross-sectional area. Both devices showed exactly the same resistance variation. Since the chip resistance is mainly a function of the capillary geometry, its variation is a good indication of variations in channel geometry.[41] The chip resistances are comparable to those reported by Zanetti[17] and Chen[38], however the variation is significantly smaller, indicating a better reproducibility of the present method. However, the chip resistance is significantly higher than the typical 2-4 MΩ access resistance reported for planar patch clamping devices where the holes are tapered on the back side.[42]

Device	*Total of cells tested*	*R < 100 MΩ*	*R > 100 MΩ*	*R > 250 MΩ*	*R > 1000 MΩ*	*Gigaseal frequency*	*Confidence interval for gigaseal*
Rectangular profile (A)	33	14 (9)	20 (13)	8 (8)	5 (5)	15%	6% - 29%
Semicircular profile (B)	14	6 (4)	8 (6)	3 (3)	2 (2)	14%	3% - 38%

Table 1. The table shows the number of cells that were successfully sealed and perforated into whole-cell configuration. The numbers include the cells with higher seals. In parenthesis, the number of cells that were successfully perforated into whole-cell configuration. The exact confidence interval for the gigaseal frequency was calculated at a confidence level of 90% .

In order to test the devices, whole-cell recordings were performed with Human Embryonic Kidney HEK cells. Of 47 cells captured, 19 cells (40 % of the total) allowed for whole-cell access with seal resistance of at least 100 MΩ and of those 7 (15 %) were gigaseals. A success rate of 15% is thus attributed to our experiments. The rest of the cells showed either no whole-cell achievement or seal resistance below 100 MΩ. More precisely, tests were carried out on devices both having patching capillaries with rectangular (type A, n=33) and semicircular (type B, n=14) profiles. As shown in Table 1, both device types showed very similar sealing capability and ability to achieve the whole-cell configuration in a range of seal resistances. Both profiles also have similar gigaseal frequency. The exact confidence interval for gigaseal frequency was calculated with the Clopper-Pearson method[43] and is given at a confidence level of 90%. The confidence intervals for gigaseal frequency were also comparable for the two profiles. During cell experiments it was noted that high resistance seals could only be achieved on longer channels, shorter channels were also tested with cells, but they all failed to deliver quality seals (data not reported). Importantly, for the 45 μm long channels each cell showing a seal resistance above 250 MΩ also allowed for whole-cell recordings. It was observed that tight seals appeared gradually after the whole-cell configuration was established, eventually reaching gigaseal during a period of 10-20 minutes. Achievement of the whole-cell configuration was verified by activation of sodium currents through a depolarization of the cell membrane. Seals had an average lifetime of 30 minutes. Furthermore, it was also observed that whole cell configuration with rupture of the patched cell membrane was obtained spontaneously upon cell capture without an intermediate cell attached state, where electrical access to the interior of the cell goes through the patched piece of cell membrane inside the pipette in traditional patch clamping experiments. This seems to differ from other systems, both those using traditional pipettes and planar chips, where a drop in resistance when breaking the cell membrane is normally observed.

In the literature numerous discussions regarding the importance of various device parameters for high quality seal formation exist, such as the aperture diameter,[20] length of membrane protrusion into the microhole,[44] smooth edges of the microholes,[45] and hydrophilicity of the substrate.[20] Additionally these evaluations were done with different substrate materials and capturing geometries and none with thermoplastic polymers. Our experiments indicate that long and smooth patching channels and apertures of approximately 4 μm^2 with clean and smooth orifice edges allow for good seal quality. Furthermore, these parameters contribute to an increase in total contact area between the cell membrane and the polymer surface and therefore the effective contact area seems to be the most critical prerequisite to look at. To support this hypothesis, the topography of the orifices and the inside of the patching capillaries were thoroughly characterized by atomic force microscopy (AFM). AFM data from channels with rectangular and semicircular profiles are compared in Table 2 and discussed here. The profiles across the patching channels revealed the presence of scallops with an average periodicity of approximately 180 nm for type A profile chips with scallops generated by Bosch type reactive ion etching process employed for master mold origination.[46] The amplitude and periodicity of the scallops defines the waviness of the surface and dominates the calculated roughness value. To overcome the dominating effect of the scallops and evaluate the surface roughness Rq between the scallops, images were filtered with a cut-off wavelength shorter than the average periodicity between the scallops. After filtering the surface roughness of the sidewall of the rectangular and semicircular channel are comparable and in the range of 1 to 2 nm. Therefore, the surface roughness Rq of the sidewall for both samples seems to be determined primarily by the smoothening steps that were the same for both. In general, the inside of the patching channel, including the bottom of the channel and the foil, exhibits very low surface roughness Rq of 1 to 2 nm, and it is also here, between the cell membrane and the polymer, the seal is assumed to form. These findings suggest that the surface roughness inside the patching channel is a second prerequisite for good seal formation. On the contrary, the waviness originating from the scallops does

not seem to influence the seal quality. The cell membrane, which has a thickness of only 5-10 nm, is likely to conform to the shape of the surface waviness, which has a periodicity much larger than the thickness of the cell membrane. This effect has been studied before for pipette tip roughness.[47] Hence, one can hypothesize that low surface roughness in addition to the patch channel length increases the effective contact area between the cell membrane and the polymer surface and thus facilitates the formation of tight seals. The shape of the cross section, either rectangular or semicircular, did not influence the capability of seal formation.

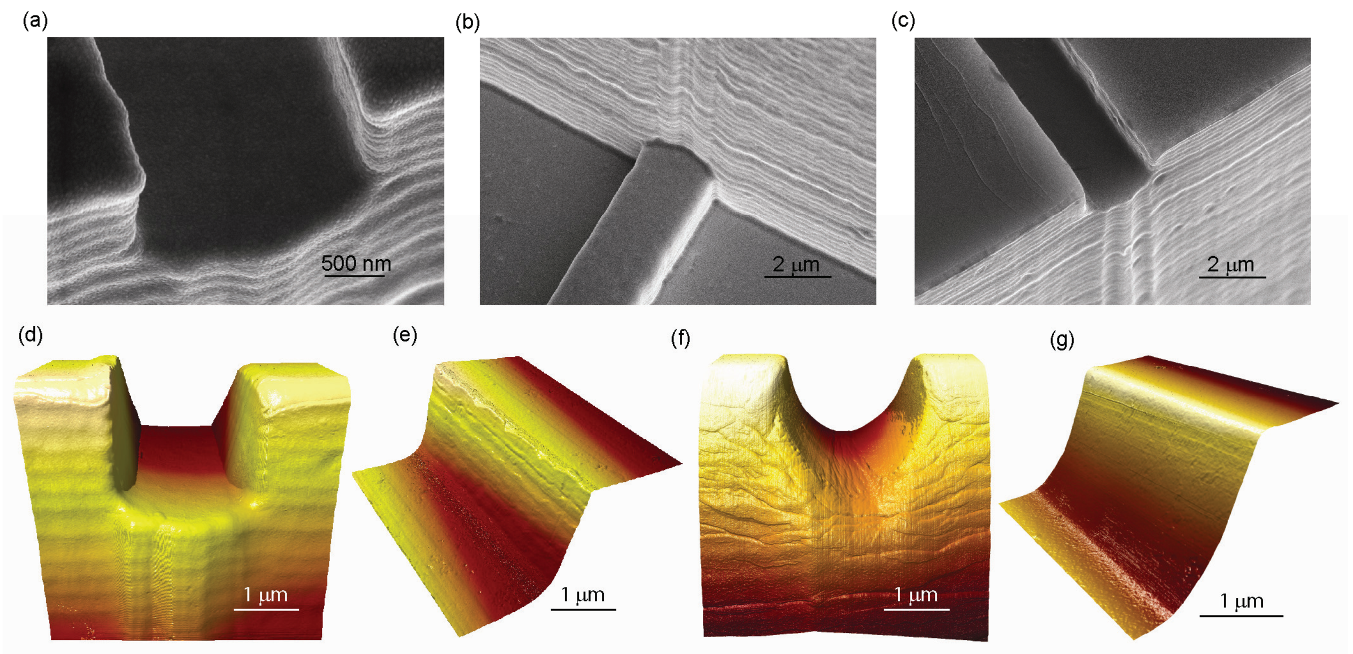

Figure 3. (a-c) SEM micrographs of the patching orifice after the main three steps of the fabrication process for type A devices: silicon master, nickel insert, and replicated polymer part (from left to the right). (d) 3D AFM image of the patching orifice (type A). (e) 3D AFM image of the sidewall of the patching capillary (type A). (f) 3D AFM image of the semicircular patching orifice (type B). (g) 3D AFM image of the sidewall of the semicircular patching capillary (type B).

Device	*Rq[nn]* *Bottom of patching capillary*	*Rq[nn]* *Sidewall patching capillary*	*Rq[nn]* *Foil*
Rectangular profile	2.0 ± 0.3	6.5 ± 1.3[(a)] (2.4 ± 0.4)[(b)]	1.2 ± 0.2
Semicircular profile	0.7 ± 0.2	1.0 ± 0.2 [(a)] (0.8 ± 0.1) [(b)]	1.2 ± 0.2

Table 2. The root mean square deviation Rq of the assessed profiles for injection molded polymer parts inside the patching capillaries for the two geometries. The image side length was 1.3 µm. The standard uncertainty is given at a confidence level of 68%. All measurements were carried out with a MultiMode 8 atomic force miscroscope from Bruker in intermittent contact mode using single crystal silicon cantilevers with spring constants of approximately 40 mN and radius of curvature of 5 nm to 10 nm. [(a)] The image was line wise corrected by a second order least mean squares fit in order to remove the (semicircular) shape of the profile. [(b)] The surface roughness Rq was calculated from an image after it was filtered so that only short wave profile components with a cut-off wavelength of λ=0.18 µm is included. The filtering was done to avoid the influence of the Bosch process induced scallops on the calculated surface roughness (only relevant for profile A devices).

Electrophysiological cell experiments were designed to record activation and inactivation currents in whole-cell voltage clamp mode from voltage-gated sodium ion channels $Na_v1.7$. Sodium channels play an essential role for the generation of action potentials in excitable cells and they have a key role in pain perception.[48] In order to benchmark the performance of the polymer devices, electrophysiology data taken on the devices were compared with data taken with the commercially available QPatch™ system. The cells, the electrolyte solutions and the compounds used for the QPatch™ recordings, and for the

polymer chip recordings were exactly the same. Raw data were collected and subsequently leak subtracted in order to compensate for the capacitance; Figure 4 shows an example of a family of sodium activation currents. A +10 mV square pulse of 10 ms from -90 mV prior to depolarization was used to calculate the leak current that was subtracted from the recorded data.[49] A description of leak subtraction is provided in the supplementary material. Automated P/n leak subtraction[50] was employed in the QPatch™ system. Activation currents were obtained after the start of depolarization pulses from -90 mV to 70 mV while the holding potential was kept at -90 mV for all the experiments. Steady state inactivation currents were investigated at +10 mV after conditioning-potentials ranging from -90 mV to 70 mV were applied for 1000 ms. The resulting current amplitude represents the portion of sodium channels in the activated and inactivated state respectively. For the polymer devices, the activation threshold was found to be between -50 and -40 mV, and the maximal current amplitude was obtained for voltages between -30 and -20 mV. At positive potentials the current amplitude gradually decreased as the electrochemical driving force disappeared. The IV curves show good agreement with those obtained with the QPatch™ system. However IV curves from the polymer device had a tendency to shift towards more negative potentials. Figure 4c shows two representative IV curves for both systems. The inactivation graph in Figure 4d shows the gradual transition from a state where the sodium channels were predominantly closed to a state where they were predominantly inactivated; above -50 mV for the polymer devices. The cut off at -90 mV does not show at which potential the transition starts, but is presumed to be at about -100 mV. As mentioned for the activation currents, the IV relationships obtained for the polymer devices, when compared to IV's from the QPatch™ system, had the tendency to shift towards more negative potentials. This shift was attributed to voltage drops across the higher access resistance of the polymer device, which was not compensated for. As we shall see in the following, this difference did not influence the pharmacology studies.

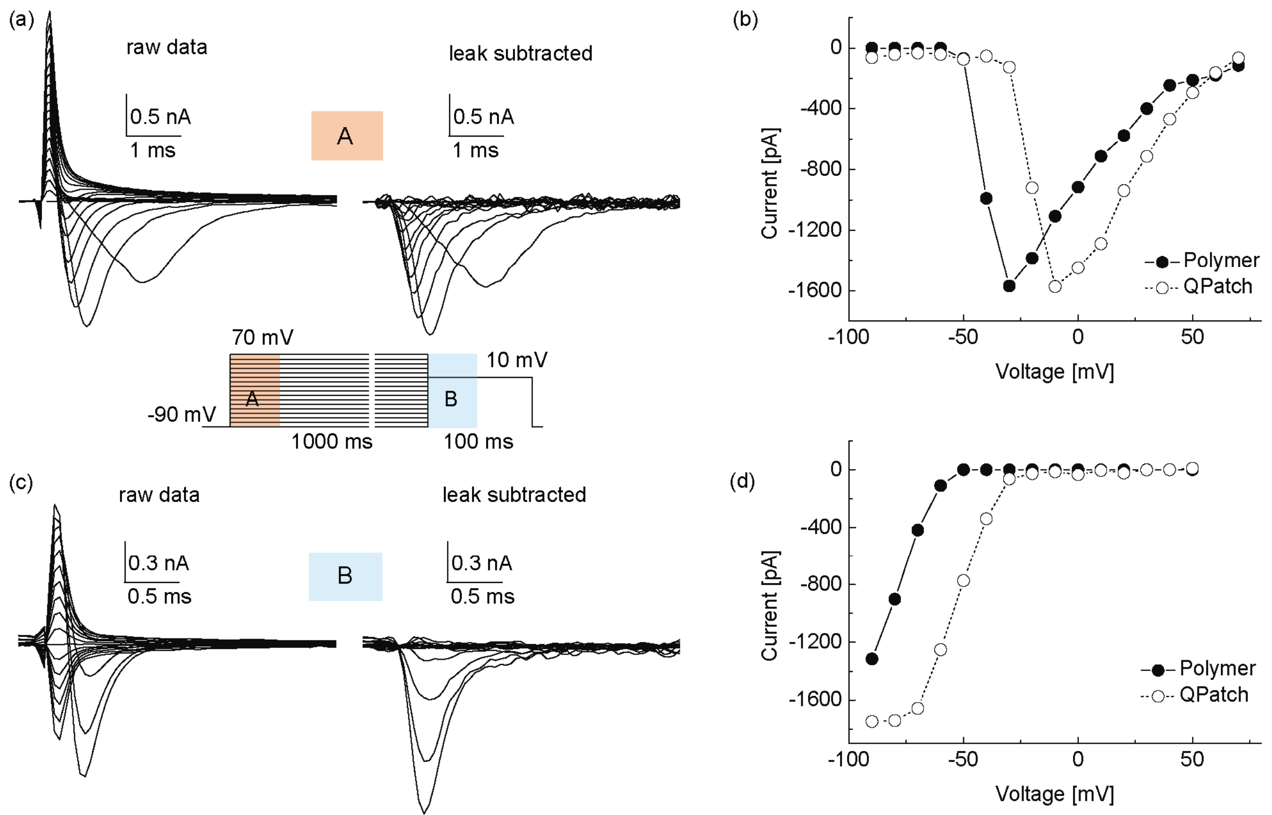

Figure 4. (a) A family of Na+ activation currents in response to depolarization pulses from -90 mV to 70 mV, measured on the polymer device. The protocol used for determining both activation and inactivation is also shown. The membrane potential was held at a holding potential of -90 mV, subsequently shifted to potentials ranging from -90 to 70 mV for 1000 ms, and finally to 10 mV. To the left, the raw current responses are shown, and to the right the data after leak subtraction. (b) A family of Na+ inactivation currents from the same recording upon the step to 10 mV. To the left, the raw current responses are shown, and to the right the data after leak subtraction. (c) The resulting IV relationship for peak Na+ channel currents. The activation threshold was -50 mV, and the maximal current amplitude was obtained at -30 mV for the polymer device. The threshold was -30 mV with a maximum at -10 mV for the QPatch^{TM}. (d) The inactivation graph for the Na+ channel. At potentials more negative than -80mV the channels were predominantly closed, whereas at potentials above -30 mV they were

predominantly inactivated for the QPatch™. For the polymer device, the channels were predominantly inactivated at potentials above -50 mV.

Dose–response experiments were carried out to further benchmark the polymer device with a pharmacological application. Lidocaine inhibition of whole-cell sodium currents was explored in voltage-clamped mode by application of lidocaine concentrations ranging from 30 μM to 1 mM. The ability of lidocaine to bind to sodium channels is state dependent, as lidocaine binds to the sodium channel in the inactivated state only.[51] To explore state-dependency, the cell was depolarized twice at 0 mV for 100 ms and 20 ms, respectively, from a holding potential of −100 mV with a temporal separation of 15 ms, see Figure 5a. Depolarization was repeated every 5 seconds. Lidocaine response was studied at the start of the second pulse after the resting interval, during which only a portion of the sodium channels were able to recover from inactivation. Figure 5b shows a typical recording in the absence of compound where the activation peak 2 was about 80 % of the size of the activation peak 1, used as a reference. When lidocaine was applied, reference peak 1 exhibited a current that was almost unchanged, while peak 2 was substantially reduced. Figure 5c shows activation currents from the same cell before and after 100 μM lidocaine was delivered to the cell. The current-time relationship for the peak sodium currents recorded in response to the first (empty circle) and the second (full circle) depolarization is shown in Figure 5d. Inhibition is plotted against lidocaine concentration in Figure 5e. The amplitudes of sodium currents immediately prior to lidocaine application were set to 100 %. Complete inhibition was observed at 1mM lidocaine, while the inhibition was only 20% at 30 μM lidocaine which was also the lowest concentration applied. From Figure 5d it can be observed that the inhibition produced by lidocaine was reversible within 60 seconds after its perfusion was stopped. For the polymer device, the half-blocking concentration IC_{50} was 119 ± 11 μM. This value is in excellent agreement with the IC_{50} of 152 ± 11 μM found with the QPatch™. The Hill coefficients were also very similar for the two systems.

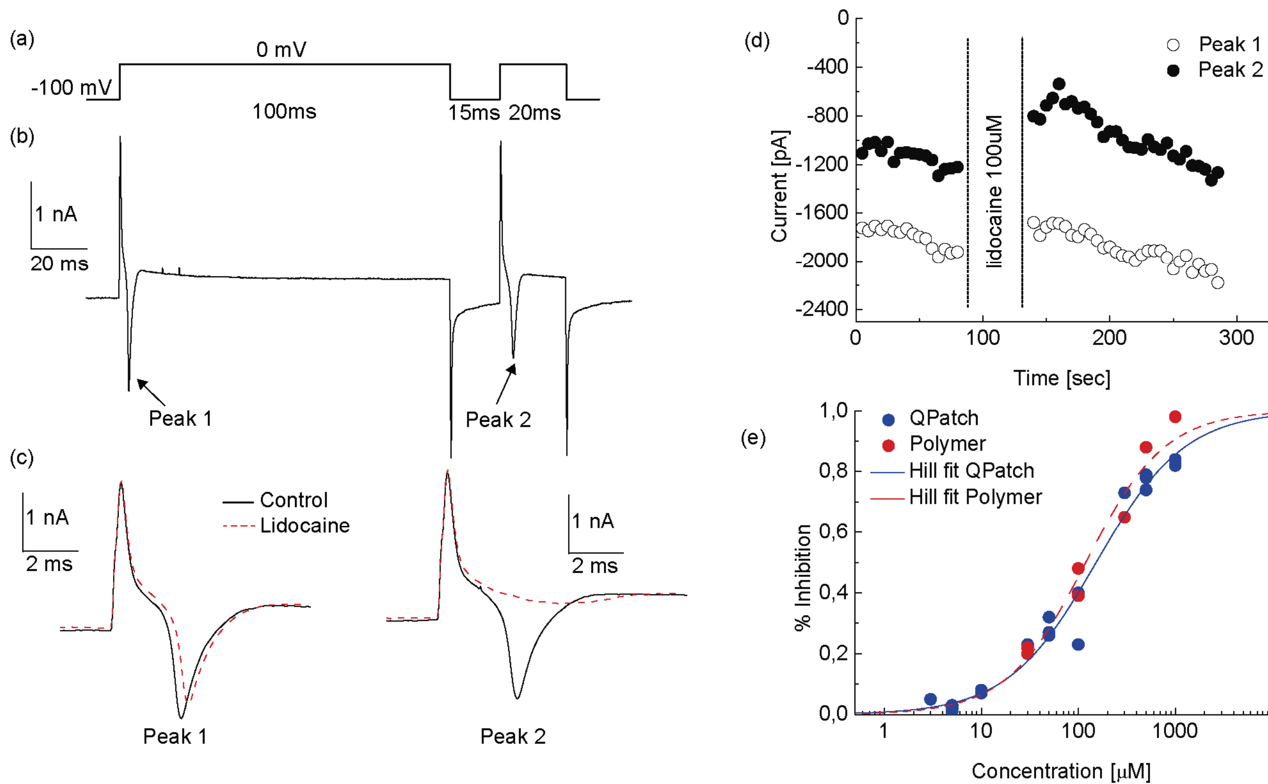

Figure 5. (a) Protocol used for determining the concentration–response relationship of lidocaine inhibition on $Na_v1.7$ channels consisting of two depolarizations to 0 mV from a holding potential of −100 mV with an interval of 15 ms. (b) Raw current response from a recording on the polymer device before lidocaine application. Amplitude of peak 2 is about 80 % of the amplitude of peak 1. (c) Raw current response for peak 1 and peak 2 before (black) and after (red) 100 µM lidocaine was applied to the cell. (d) Activation currents for $Na_v1.7$ channels for determining the lidocaine inhibition on $Na_v1.7$ channels. The graph shows values of the current amplitudes of peak 1 and 2 before and after 100 µM lidocaine was applied to the cell. Peak 1 is not affected and peak 2 is reduced by 50 %. (e) Concentration–response relationships of lidocaine inhibition on $Na_v1.7$ channels. Data were fitted with a Hill type equation. IC_{50} was 119 ±11 µM (Hill coefficient n = 1) for the polymer device and 152 ±12 µM (Hill coefficient n = 0.9) for the QPatch^{TM}.

CONCLUSIONS

We have demonstrated high-quality electrophysiological recordings on an injection molded polymer device platform for the first time. The results demonstrate that polymer APC devices can provide whole-cell current responses from voltage gated sodium channels and permit accurate analysis of drug potency for state-dependent inhibitors such as for the local anesthetic lidocaine. Moreover, the devices exhibit excellent data quality when benchmarked against the commercially available QPatch^{TM} system. Formation of gigaseals (15% of the total cells) between the polymer surfaces and the cell membranes was achieved by making patching capillaries that allowed for a large sealing area. The length of the patching channel together with the low surface roughness on the inside of the patching capillaries were identified as the most important parameters for good seal formation. We attribute this observation to indicate that a large effective sealing area between the cell membrane and the polymer surface is required to obtain tight seals. Most likely, the exceptionally large sealing area required for the polymer patching channels when compared to silica based channels is necessary to assist sealing due to slow van der Waals type interactions between the relatively low energy polymer surface and the cell membrane. Finally, we have successfully combined the simplicity of lateral cornered apertures with the use of injection molding to demonstrate the most cost effective production and materials platform for APC systems to date. The technological readiness level of the reported material and production platform is high, while the specific design of the intra- and extracellular channels (Figure 1a) is only aimed at prototyping. Thus the Y shaped patching channel constitutes the only essential feature of our microfluidic design and channels for extra and intracellular electrolyte solutions could be designed differently for a much smaller unit footprint. For maintaining exactly the same functionality per functional chip unit, six inlet/outlet wells would still be required. However, if shared cell and compound inlets are employed, one chip unit will require only four ports.

MATERIALS AND METHODS

Device fabrication. Chips were manufactured according to the methods recently reported by some of the same authors,[40] which in brief consist of lithography, dry etching of the silicon, electroplating in nickel and injection molding of the polymer parts. Two etching processes were employed to form the patching capillaries: Bosch reactive ion etching for sample A and a continuous reactive ion etching for sample B. This was to obtain respectively rectangular and semicircular profiles. However, in order to replicate patch clamping orifices smaller than the lateral apertures demonstrated for cell trapping,[40] the overall process was partially modified. Silicon oxide used as masking material was replaced by standard photoresist, while a thin layer of oxide was applied after the first etching step to prevent damage to the patching channels during the rest of the process. Fabrication was then completed by alternating wet etching steps and oxidation in order to smooth the surfaces around the patching orifices. Details of the full process are given in the supplementary material. Parts were molded from COC (TOPAS 5013, Advanced Polymers GmbH). A 100 μm thick extruded polymer film (TOPAS 5013F-04, Advanced Polymers Extrusion Lab) was used as cover lid. The two parts were bonded by UV-assisted thermal bonding.[36]

Cell culture. Human Embryonic Kidney 293 cells (HEK293) expressing the subtype of the voltage gated sodium channel Na_v 1.7 were provided by Scottish Biomedical Ltd. The cells were grown and maintained under standard culture conditions at 37 °C and 5 % CO_2. The cells were cultured in T175 culture flasks (Nunc A/S) to maximum 80 % confluence in high glucose Dulbecco's Modified Eagle Medium (DMEM, Sigma-Aldrich D0819) supplemented with 10 % fetal bovine serum (FBS, Sigma-Aldrich F2442), 2 μg/ml blasticidin S (Sigma-Aldrich 15205) and 600 μg/ml geneticin (Sigma-Aldrich G8168). The cells were sub-cultured for two weeks before reaching a stable growth pattern and then used in the experiments. For sub-culture, the culture medium was removed and the cells washed with

phosphate buffered saline (PBS) without calcium chloride and magnesium chloride (Sigma-Aldrich D8537). Trypsin/EDTA (Sigma-Aldrich T4174) was added to the culture flask and the flask incubated at 37 °C for 2 minutes. Medium was added to the flask and the cells re-suspended and placed in a new mother flask. Directly before experiments the culture medium was removed and the cells washed with PBS without calcium chloride and magnesium chloride. Detachin (VWR) was added to the culture flask and the flask incubated at 37 °C for 5 minutes or until the cells show a round shape indicating detachment from the flask surfaces. The cells were re-suspended in serum-free CHO medium (Sigma-Aldrich C5467) supplemented with 25 mM HEPES (Sigma-Aldrich H0887), 100 ug/ml penicillin/streptomycin (Sigma-Aldrich P4333) and 0.04 mg/ml soy bean trypsin inhibitor (Sigma-Aldrich T6522). Cell density and viability was determined by diluting an aliquot 1:2 in Trypan Blue (Sigma-Aldrich T8154) and performing a cell countusing the dye exclusion method in a hemocytometer. Cell concentration in the suspension was 2-3 M/ml.

Solutions and compounds. The intracellular electrolyte solution contained (in mM): 135 CsF, 1/5 ethylene glycol tetraacetic acid (EGTA)/CsOH, 10 mM HEPES and 10 NaCl. The pH was adjusted to 7.3 with KOH and osmolarity to 320 mOsm with sucrose. The extracellular electrolyte solution contained (in mM): 1 CaCl2, 1 MgCl2, 5 HEPES, 3 KCl, 140 NaCl, 0.1 CdCl2 and 20 TEA-Cl. The pH was adjusted to 7.3 with NaOH and osmolarity to 320 mOsm with sucrose. All chemicals were purchased from Sigma Aldrich. Both solutions were stored in the fridge at 4 °C and vacuum degassed for 20 minutes before use. Lidocaine hydrochloride monohydrate (Sigma Aldrich L5647) was dissolved in dimethyl sulfoxide (DMSO) to give a 100 mM stock solution kept in the freezer. Subsequent dilutions were performed in extracellular electrolyte solution.

Instrumentation. Recordings were carried out using a HEKA Patch Clamp EPC 9 amplifier (HEKA Electronics) at room temperature. Pulse software (v 8.53, HEKA Electronics) was used for data

acquisition. The device was mounted into a customized aluminum box and positioned on the stage of an Olympus IX70 inverted microscope. The two Luer ports connected to the recording patching channel were connected to two reservoirs filled with electrolyte solution and from them to a custom-made pressure controller and controlled with Labview software (National Instruments). Electrodes were electrically connected to the EPC9 head stage mounted on the customized aluminum box and the chip resistance could be monitored by applying a 10 mV test square pulse for 10 ms. Before cell trapping, a positive pressure of 3-5 mbar was applied to the patching channel to prevent aperture contamination. A cell was captured at the hole after applying suction (negative pressure of 400 mbar) to the patching channel. The amplifier offset potential was zeroed prior to patching the cell and the holding potential held at -90mV. Response currents were sampled at 10 kHz and filtered at 2,9 kHz with a 4 pole Bessel filter. The experiments on the QPatch™ were set up using standard assay settings. In brief, cells were positioned with a negative pressure of -100 mbar until a gigaseal was formed. The cell membrane was then ruptured with a negative pressure pulse of -250 mbar in order to get electrical access to the cell membrane. During this process the offset potential, the chip capacitance and the cell capacitance were canceled out. The actual experiment protocol with the relevant voltage protocols and compound additions was programmed in the Sophion Assay Software and it was executed after whole cell formation was established. QPatch™ data were sampled at 10 kHz and filtered with an 8 pole Bessel filter at 3 kHz.

Whole cell recordings. Once the cells were trapped, a suction of -400 mbar was applied for about 20 seconds and then reduced to -30 mbar. The resistance across the aperture was continuously monitored by applying a 10 mV pulse for 10 ms. At this stage, the resistance was typically between 100 and 200 MΩ. Some of the cells showed whole-cell configuration immediately after patching. Otherwise the whole-cell configuration was achieved by applying suction pulses (from -30 mbar to -400 mbar) and electrical pulses combined. Achievement of whole-cell configuration was verified by depolarizing the cell.

Eventually the cells reached whole-cell configuration and the resistance gradually increased over minutes during the experiments.

Voltage protocols. For IV relationships experiments, a protocol with incremental steps of +10 mV from -90 mV to +70 mV of 1000 ms duration was used. Steady-state inactivation was investigated at +10 mV for 100 ms after the 1000 ms pre-pulse. Each incremental sweep took place with 5 second intervals. For concentration-response experiments, two consecutive depolarizations to +0 mV respectively of 100 ms and 20 ms duration from a holding potential of -100 mV were used. The two depolarizations were spaced out by 15 ms at holding potential.

Conflict of interest: The authors declare that the present work is made primarily for the benefit of science; however some of the authors are affiliated with Sophion Bioscience, which develops, manufactures and sells APC systems on a commercial basis. A patent application relating to aspects of the device was filed by Technical University of Denmark (DTU ref. 95412) with S.Tanzi and R.Taboryski as the inventors.

Acknowledgement. We gratefully acknowledge financial support from the Danish Advanced Technology Foundation through the Advanced Technology Project PILOC (grant no 061-2010-1) and from the Danish Council for Strategic Research through the Strategic Research Center PolyNano (grant no 10-092322/DSF).

Supporting Information Available: Description of the leak current subtraction applied to the raw data obtained from the polymer devices; description of the simulation for the perfusion of lidocaine from one of the lateral channels into the deep channel during the dose response experiments; description of the fabrication process (table and illustrations); description of the challenges faced during the development of the presented polymer device (and figures). This material is available free of charge *via* the Internet http://pubs.acs.org.

REFERENCES:

1. NEHER, E.; SAKMANN, B. Single-Channel Currents Recorded from Membrane of Denervated Frog Muscle-Fibers. *Nature* **1976**, *260*, 799-802.

2. Hille, B. *Ion Channel of Exitable Membranes;* null; Sinauer Associates, Inc.: Sunderland, MA U.S.A, 2001; .

3. Lehmann-Horn, F.; Jurkat-Rott, K. Voltage-gated ion channels and hereditary disease. *Physiol. Rev.* **1999**, *79*, 1317-1372.

4. Ackerman, M.; Clapham, D. Mechanisms of disease - Ion channels - Basic science and clinical disease. *N. Engl. J. Med.* **1997**, *336*, 1575-1586.

5. Ashcroft, F. From molecule to malady. *Nature* **2006**, *440*, 440-447.

6. Overington, J. P.; Al-Lazikani, B.; Hopkins, A. L. Opinion - How many drug targets are there? *Nat. Rev. Drug Discov.* **2006**, *5*, 993-996.

7. Wickenden, A.; Priest, B.; Erdemli, G. Ion channel drug discovery: challenges and future directions. *Future Med. Chem.* **2012**, *4*, 661-679.

8. Xu, J.; Wang, X.; Ensign, B.; Li, M.; Wu, L.; Guia, A.; Xu, J. Ion-channel assay technologies: quo vadis? *Drug Discov. Today* **2001**, *6*, 1278-1287.

9. Zheng, W.; Spencer, R.; Kiss, L. High throughput assay technologies for ion channel drug discovery. *Assay Drug Dev. Technol.* **2004**, *2*, 543-552.

10. Xu, J.; Guia, A.; Rothwarf, D.; Huang, M.; Sithiphong, K.; Ouang, J.; Tao, G.; Wang, X.; Wu, L. A benchmark study with SealChip (TM) planar patch-clamp technology. *Assay Drug Dev. Technol.* **2003***, 1*, 675-684.

11. Dunlop, J.; Bowlby, M.; Peri, R.; Vasilyev, D.; Arias, R. High-throughput electrophysiology: an emerging paradigm for ion-channel screening and physiology. *Nat. Rev. Drug Discov.* **2008***, 7*, 358-368.

12. Wood, C.; Williams, C.; Waldron, G. Patch clamping by numbers. *Drug Discov. Today* **2004***, 9*, 434-441.

13. Farre, C.; George, M.; Brüggemann, A.; Fertig, N. Ion channel screening – automated patch clamp on the rise. *Drug Discovery Today: Technologies* **2008***, 5*, e23-e28.

14. Farre, C.; Fertig, N. HTS techniques for patch clamp-based ion channel screening - advances and economy. *Expert. Opin. Drug Discov.* **2012***, 7*, 515-524.

15. Fertig, N.; Blick, R.; Behrends, J. Whole cell patch clamp recording performed on a planar glass chip. *Biophys. J.* **2002***, 82*, 3056-3062.

16. Asmild, M.; Oswald, N.; Krzywkowski, K.; Friis, S.; Jacobsen, R.; Reuter, D.; Taboryski, R.; Kutchinsky, J.; Vestergaard, R.; Schroder, R.; Sorensen, C.; Bech, M.; Korsgaard, M.; Willumsen, N. Upscaling and automation of electrophysiology: Toward high throughput screening in ion channel drug discovery. *Recept. Channels* **2003***, 9*, 49-58.

17. Ionescu-Zanetti, C.; Shaw, R.; Seo, J.; Jan, Y.; Jan, L.; Lee, L. Mammalian electrophysiology on a microfluidic platform. *Proc. Natl. Acad. Sci. U. S. A.* **2005***, 102*, 9112-9117.

18. Martinez, D.; Py, C.; Denhoff, M. W.; Martina, M.; Monette, R.; Comas, T.; Luk, C.; Syed, N.; Mealing, G. High-fidelity patch-clamp recordings from neurons cultured on a polymer microchip. *Biomed. Microdevices* **2010**, *12*, 977-985.

19. Stett, A.; Bucher, V.; Burkhardt, C.; Weber, U.; Nisch, W. Patch-clamping of primary cardiac cells with micro-openings in polyimide films. *Med. Biol. Eng. Comput.* **2003**, *41*, 233-240.

20. Klemic, K.; Klemic, J.; Reed, M.; Sigworth, F. Micromolded PDMS planar electrode allows patch clamp electrical recordings from cells. *Biosens. Bioelectron.* **2002**, *17*, 597-604.

21. Klemic, K.; Klemic, J.; Sigworth, F. An air-molding technique for fabricating PDMS planar patch-clamp electrodes. *Pflugers Arch.* **2005**, *449*, 564-572.

22. Li, X.; Klemic, K.; Reed, M.; Sigworth, F. Microfluidic system for planar patch clamp electrode arrays. *Nano Lett.* **2006**, *6*, 815-819.

23. Xu, B.; Liu, Z.; Lee, Y.; Mak, A.; Yang, M. A PDMS microfluidic system with poly(ethylene glycol)/SU-8 based apertures for planar whole cell-patch-clamp recordings. *Sens. Actuator A-Phys.* **2011**, *166*, 219-225.

24. Suchyna, T. M.; Markin, V. S.; Sachs, F. Biophysics and Structure of the Patch and the Gigaseal. *Biophys. J.* **2009**, *97*, 738-747.

25. Miller, C. Everything You Always Wanted to Know about Sachs' Seals. *Biophys. J.* **2009**, *97*, 687-687.

26. Priel, A.; Gil, Z.; Moy, V. T.; Magleby, K. L.; Silberberg, S. D. Ionic requirements for membrane-glass adhesion and giga seal formation in patch-clamp recording. *Biophys. J.* **2007**, *92*, 3893-3900.

27. Israelachvili, J.; Wennerstrom, H. Role of hydration and water structure in biological and colloidal interactions. *Nature* **1996**, *379*, 219-225.

28. Schulz, M.; Olubummo, A.; Binder, W. H. Beyond the lipid-bilayer: interaction of polymers and nanoparticles with membranes. *Soft Matter* **2012**, *8*, 4849-4864.

29. Tandon, V.; Bhagavatula, S. K.; Kirby, B. J. Transient ?-potential measurements in hydrophobic, TOPAS microfluidic substrates. *Electrophoresis* **2009**, *30*, 2656-2667.

30. Tandon, V.; Bhagavatula, S. K.; Nelson, W. C.; Kirby, B. J. Zeta potential and electroosmotic mobility in microfluidic devices fabricated from hydrophobic polymers: 1. The origins of charge. *Electrophoresis* **2008**, *29*, 1092-1101.

31. Tandon, V.; Kirby, B. J. zeta potential and electroosmotic mobility in microfluidic devices fabricated from hydrophobic polymers: 2. Slip and interfacial water structure. *Electrophoresis* **2008**, *29*, 1102-1114.

32. Seo, J.; Ionescu-Zanetti, C.; Diamond, J.; Lal, R.; Lee, L. Integrated multiple patch-clamp array chip via lateral cell trapping junctions. *Appl. Phys. Lett.* **2004**, *84*, 1973-1975.

33. Golden, A. P.; Li, N.; Chen, Q.; Lee, T.; Nevill, T.; Cao, X.; Johnson, J.; Erdemli, G.; Ionescu-Zanetti, C.; Urban, L.; Holmqvist, M. IonFlux: A Microfluidic Patch Clamp System Evaluated with Human Ether-a-go-go Related Gene Channel Physiology and Pharmacology. *Assay Drug Dev. Technol.* **2011**, *9*, 608-619.

34. Fermini, B. Recent Advances in Ion Channel Screening Technologies. *Topics in Medicinal Chemistry* **2008**, *3*, 1-25.

35. Berthier, E.; Young, E. W. K.; Beebe, D. Engineers are from PDMS-land, Biologists are from Polystyrenia. *Lab Chip* **2012***, 12*, 1224-1237.

36. Matteucci, M.; Christiansen, T. L.; Tanzi, S.; Østergaard, P. F.; Larsen, S. T.; Taboryski, R. Fabrication and characterization of injection molded multi level nano and microfluidic systems. *Microelectronic Engineering* .

37. Becker, H. It's the economy ... *Lab Chip* **2009***, 9*, 2759-2762.

38. Chen, C.; Folch, A. A high-performance elastomeric patch clamp chip. *Lab Chip* **2006***, 6*, 1338-1345.

39. Andresen, K. O.; Hansen, M.; Matschuk, M.; Jepsen, S. T.; Sorensen, H. S.; Utko, P.; Selmeczi, D.; Hansen, T. S.; Larsen, N. B.; Rozlosnik, N.; Taboryski, R. Injection molded chips with integrated conducting polymer electrodes for electroporation of cells. *J Micromech Microengineering* **2010***, 20*, 055010.

40. Tanzi, S.; Ostergaard, P. F.; Matteucci, M.; Christiansen, T. L.; Cech, J.; Marie, R.; Taboryski, R. Fabrication of combined-scale nano- and microfluidic polymer systems using a multilevel dry etching, electroplating and molding process. *J Micromech Microengineering* **2012***, 22*, 115008.

41. Ong, W.; Tang, K.; Agarwal, A.; Nagarajan, R.; Luo, L.; Yobas, L. Microfluidic integration of substantially round glass capillaries for lateral patch clamping on chip. *Lab Chip* **2007***, 7*, 1357-1366.

42. Kutchinsky, J.; Friis, S.; Asmild, M.; Taboryski, R.; Pedersen, S.; Vestergaard, R.; Jacobsen, R.; Krzywkowski, K.; Schroder, R.; Ljungstrom, T.; Helix, N.; Sorensen, C.; Bech, M.; Willumsen, N. Characterization of potassium channel modulators with QPatch (TM) automated patch-clamp

technology: System characteristics and performance. *Assay and Drug Development Technologies* **2003***, 1*, 685-693.

43. Clopper, C. J.; Pearson, E. S. The use of confidence or fiducial limits illustrated in the case of the binomial. *Biometrika* **1934***, 26*, 404-413.

44. Sordel, T.; Kermarrec, F.; Sinquin, Y.; Fonteille, I.; Labeau, M.; Sauter-Starace, F.; Pudda, C.; de Crecy, F.; Chatelain, F.; De Waard, M.; Arnoult, C.; Picollet-D'hahan, N. The development of high quality seals for silicon patch-clamp chips. *Biomaterials* **2010***, 31*, 7398-7410.

45. Sigworth, F.; Klemic, K. Patch clamp on a chip. *Biophys. J.* **2002***, 82*, 2831-2832.

46. Abdolvand, R.; Ayazi, F. An advanced reactive ion etching process for very high aspect-ratio sub-micron wide trenches in silicon. *Sens. Actuator A-Phys.* **2008***, 144*, 109-116.

47. Malboubi, M.; Gu, Y.; Jiang, K. Experimental and simulation study of the effect of pipette roughness on giga-seal formation in patch clamping. *Microelectron. Eng.* **2010***, 87*, 778-781.

48. Yu, F.; Catterall, W. Overview of the voltage-gated sodium channel family. *Genome Biol.* **2003***, 4*, 207.

49. Dempster, J. In *Chapter Seven - Recording and Analysis of Intracellular Electrophysiological Signals;* The Laboratory Computer; Academic Press: London, 2001; pp 172-225.

50. Bezanilla, F.; Armstrong, C. M. Inactivation of the sodium channel. I. Sodium current experiments. *The Journal of General Physiology* **1977***, 70*, 549-566.

51. Bean, B.; Cohen, C.; Tsien, R. Lidocaine Block of Cardiac Sodium-Channels. *J. Gen. Physiol.* **1983***, 81*, 613-642.

Table of Contents Graphics

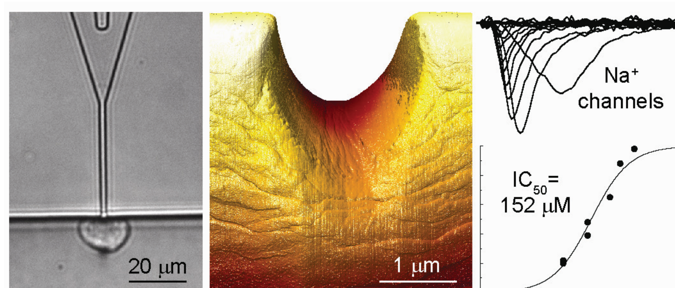

PATENT APPLICATION I

Polymeric device for electrophysiological recordings

European Patent Application No. EP13166109.2’

(DTU ref. 95412)

Europäisches Patentamt
European Patent Office
Office européen des brevets

Acknowledgement of receipt

We hereby acknowledge receipt of your request for grant of a European patent as follows:

Submission number	2110311
Application number	EP13166109.2
File No. to be used for priority declarations	EP13166109
Date of receipt	01 May 2013
Your reference	19038EP00
Applicant	DANMARKS TEKNISKE UNIVERSITET
Country	DK
Title	Polymeric device for electro-physiological recordings
Documents submitted	package-data.xml ep-request.xml application-body.xml ep-request.pdf (4 p.) SPECEPO-1.pdf\19038YY00 - FINAL DRAFT 2.pdf (31 p.) OLF-ARCHIVE.zip\19038YY00 - Application.zip f1002-1.pdf (1 p.) f1002-2.pdf (1 p.)
Submitted by	CN=E. Farrington 23973,O=Inspicos A/S,C=DK
Method of submission	Online
Date and time receipt generated	01 May 2013, 13:55 (CEST)
Message Digest	52:15:EE:F4:58:CD:5D:33:43:C1:D5:D5:70:E3:F1:E1:8C:8C:D1:15

Correction by the EPO of errors in debit instructions filed by eOLF
Errors in debit instructions filed by eOLF that are caused by the editing of Form 1038E entries or the continued use of outdated software (all forms) may be corrected automatically by the EPO, leaving the payment date unchanged (see decision T 152/82, OJ EPO 1984, 301 and point 6.3 ff ADA, Supplement to OJ EPO 10/2007).

/European Patent Office/